WP2 – Deliverable 2.7 Conceptual Geological Models

Release Status: Public
Date: 25 July 2023
Filename and Version: v. 1.0
Project ID Number: 101022664

PilotSTRATEGY (H2020- Topic LC-SC3-NZE-6-2020 - RIA)

Editor: Mark Wilkinson

Contributing authors:

France: Aurélien Bordenave, Benoit Issautier

Portugal: Daniel Marques da Silva, Maria Helena Caeiro, Pedro Pereira, Carlos Ribeiro, Júlio Carneiro, João Casacão, Bruno Pina

Spain: I. Moreno, J. García, J. F. Mediato, P. Fernández-Canteli, B. Benjumea, F. Rubio, C. Ayala, D. M. García, J. Martínez, C. Rey, P. Clariana, B. del Moral, E. R. Berrezueta, B. Ordóñez, E. Fernández de Arévalo, R. Soto, J. López, A. García, J. M. Llorente, M. Castillo, E. Pueyo

1. Document History

1.1 Location

This document is stored in the following location:

Filename	D2.7_ConceptualGeolModels
Location	www.pilotstrategy.eu

1.2 Revision History

This document has been through the following revisions:

Version No.	Delivered Date	Filename/Location stored:	Brief Summary of Changes
Region's Annexes	01/06/2023		
Region's Summaries	30/06/2023		
Compiled draft file	11/07/2023		
Reviewed draft by WP lead	15/07/2023		Missing FR References and ES authors
Reviewed draft by coordinator	23/07/2023		

1.3 Authorisation

This document requires the following approvals:

AUTHORISATION	Name	Signature	Date
WP Leader	Mark Wilkinson	MW	25/07/23
Project Coordinator	Fernanda de Mesquita Lobo Veloso	FMLV	26/07/23

1.4 Distribution

document has been distributed to:

Name	Title	Version Issued	Date of Issue
		Public	July 2023

The PilotSTRATEGY project has received funding from the European Union's Horizon 2020 research and innovation programme under grant agreement No. 101022664

Disclaimer

The information and views set out in this report are those of the author(s) and do not necessarily reflect the official opinion of the European Union. Neither the European Union institutions and bodies nor any person acting on their behalf may be held responsible for the use which may be made of the information contained therein.

The PilotSTRATEGY project has received funding from the European Union's Horizon 2020 research and innovation programme under grant agreement No. 101022664

Table of Contents

The PilotSTRATEGY project has received funding from the European Union's Horizon 2020 research and innovation programme under grant agreement No. 101022664

The PilotSTRATEGY project has received funding from the European Union's Horizon 2020 research and innovation programme under grant agreement No. 101022664

The PilotSTRATEGY project has received funding from the European Union's Horizon 2020 research and innovation programme under grant agreement No. 101022664

The PilotSTRATEGY project has received funding from the European Union's Horizon 2020 research and innovation programme under grant agreement No. 101022664

2. Executive Summary

This report summarises the work conducted as part of work package 2, task 2.3 (Conceptual Geological Models) of the PilotSTRATEGY project that contributed to this Deliverable 2.7, Geological Models of the 3 areas. Much of the data collected in WP2.3 is not included here, but has been passed to PilotSTRATEGY work package 3, for the construction of static and dynamic digital reservoir models for the modelling of CO_2 injection and CO_2 behaviour in the storage complex. The 3 areas concerned in this report (Portugal, Spain, France) have worked semi-independently on this WP, but with most collaboration between the 2 Iberian countries as the areas share some characteristics. All 3 areas use similar types of subsurface data (though of widely varying vintages and quality), and have utilised analytical techniques that are largely derived from the oil and gas exploration and production industry. With one offshore area, 2 onshore ones, and 1 carbonate reservoir and 2 clastic ones, the challenges of the areas vary considerably. Hence, each area is described separately, though similarities in methods will be seen. The report has a relatively short summary of each area, which is intended to be relatively easily read, followed by a more detailed Annex with a full description of data, methods and a summary of the results.

The Portuguese offshore area of the northern Lusitanian Basin was characterized using 2D and 3D seismic datasets, 13 wells, and rock samples collected at outcrops of onshore analogue formations. Existing aeromagnetic data and a new passive seismic survey were integrated into the interpretation. These data were used to map 6 stratigraphic horizons, defining the tectono-stratigraphic units that characterize the storage complex.

The maps generated from this allowed the characterization and capacity estimation of four target structures. Ranking and selection identified prospect Q4-TV1, in the northern part of the study area as the most promising location for the pilot storage. The trap is a four-way dip closure of 25 km^2 (P50) - 250 km^2 (P10) though this larger structure is partially bounded by faults of uncertain properties.

The Early Cretaceous Torres Vedras Group is the selected reservoir target, deposited in a fluvio-deltaic-shoreline environment with primarily sandstones and intra-reservoir claystones. The storage complex is capped by a seal unit of the Cacém Formation (Cenomanian-Turonian), composed of limestones, marls, and clays, and is continuous and homogeneous over the area of interest. The Aveiro Group (Late Cretaceous) forms a potential secondary seal.

For the onshore Ebro Basin (Spain), the target area is the Lopín structure. Here, poor to moderate quality seismic data and poor and scarce well log data were combined with passive seismic data (interpreted using the H/V method and autocorrelation; H/V is the spectral ratio of the horizontal component to the vertical component of the passive seismic noise signal), petrophysical data and gravity data. To the best of our knowledge, this is the first time the H/V method has been used in this way. Individual structural cross sections based on seismic data were adjusted within the uncertainty of interpretation to fit observed gravity profiles. Excellent matches were obtained between modelled and observed data, defining the Lopín structure.

Detailed sedimentological analysis using borehole data; analogue outcrops within Spain; and analogues from western Europe have resulted in a detailed, multi-layered reservoir model that will be the basis of the static and dynamic models to be built in WP3.

The PilotSTRATEGY project has received funding from the European Union's Horizon 2020 research and innovation programme under grant agreement No. 101022664

The study area in the Paris Basin (France) is divided into two zones. The first is defined by the new 3D seismic survey that was shot as part of the PilotSTRATEGY project, and includes the prospect pilot site. The second and larger area surrounds this and is termed the extended area of interest.

Seismic interpretation and isochron / isochore maps indicate two small geological structures in the restricted AOI, named the Charmotte and Clos-Fontaines folds. However, the storage concept is an open aquifer where CO_2 migrates slowly vertically and then in the reservoir layer.

372 meters cores have been described and sampled for the characterisation of reservoir properties. Well logs from the 47 wells in the extended area have been used to classify rock types in wells. Electro-facies defined by cross plots of density and neutron porosity logs appears to give the best correlation to rock-type classified from cores. 12 well correlations has been interpreted in the extended area.

The conceptual geological model for the depositional of the sequence is a typical carbonate ramp profile with the development of shallow oolite-dominated barrier in the mid-ramp position. This latter separates an open-marine domain dominated by fair-weather and storm waves (respectively lower shoreface and offshore) from a restricted lagoon.

3. Introduction

This document aims to complete the deliverable 2.7, task 2.3 of work package 2 (WP2, Geocharacterization) of the PilotSTRATEGY Project. Detailed description of the regional geological framework, including sedimentological, structural, and stratigraphical characterization is presented in section 6 – Regional Geological Characterization. The characterization of the storage complex is presented in section 7- Storage Complex Characterization with a comprehensive facies analysis of the reservoir and the seal. Section 7 includes the analysis of some outcrops, and in section 8 – Depositional Environemnts and Geological Concept, as a conclusion, the main deposition environments of the area of interest and some notes on the conceptual geological model, are stated.

3.1 Objectives

The objectives of PilotSTRATEGY Task 2.3 (Conceptual Geological Models), of which this report is deliverable D2.7, are, for the 3 study regions:

1) To synthesise existing knowledge to create the background needed for new work;

2) To collate existing (legacy) data from the 3 regions, mostly well and seismic data;

3) To collect new data where required to enhance the confidence and accuracy of interpretation e.g. passive seismic surveys;

4) To synthesise existing and new data into the most detailed and accurate interpretations possible of the sedimentology, geometry, reservoir and seal characteristics of the target horizons;

5) To pass the data to PilotSTRATEGY WP3 for the construction of static and dynamic reservoir models.

The PilotSTRATEGY project has received funding from the European Union's Horizon 2020 research and innovation programme under grant agreement No. 101022664

4. Methodology

The methodology used by the 3 regions has many common elements. However, different data types; vintages; rock types (carbonates versus siliciclastics); structural settings and geographic setting (onshore versus offshore) mean that the 3 regional teams used different methods in detail. These are hence described in each regional section.

5. Dataset per region

5.1 Dataset: Portugal

The location of the dataset used for the seismic interpretation of the Lusitanian Basin (LB) offshore area is illustrated in the map of Figure 5-1, composed by the 3D Cabo Mondego & São Pedro de Moel seismic volume, several 2D seismic data profiles and ten offshore wells used to tie with the seismic data. The offshore area of interest is delimited by the solid black line, corresponding to the main focus of the study, although some work was conducted onshore, including the analysis of three onshore petroleum exploration wells (Figure 5-1Figure 1-6) whenever knowledge could be gained about the same storage complex found offshore.

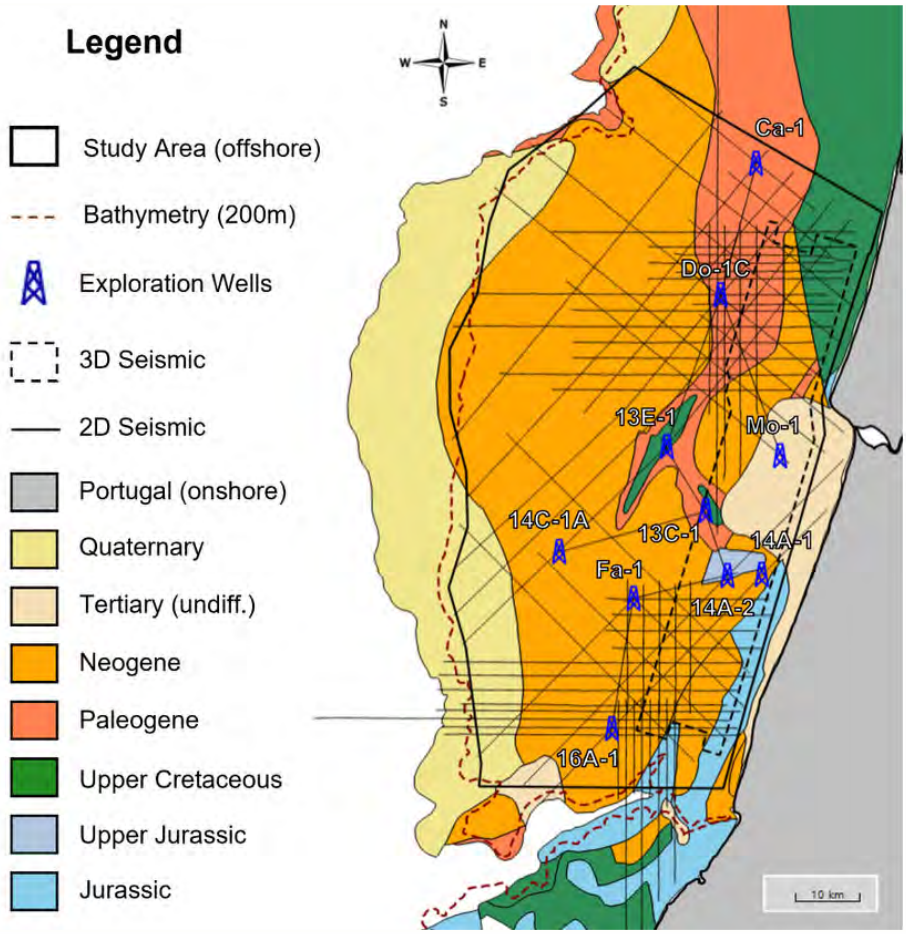

Figure 5-1: Dataset used to characterize the subsurface geology of the offshore study area. The illustrated geological units correspond to the seabed geology.

The PilotSTRATEGY project has received funding from the European Union's Horizon 2020 research and innovation programme under grant agreement No. 101022664

For well log analysis and petrophysical evaluation, 12 vertical wells were considered, 7 offshore and 5 onshore (Figure 5-2). The wells were drilled for petroleum exploration purposes and most of them spudded in the 1970s (offshore wells), with exception of the onshore wells: Alc-1, that was drilled in 2012, MRW-5, MRW-8, and MRW-9, that were drilled in the 1960s, and Alj-2, that was drilled in the 1990s. As such, they have limited data acquisition and generally poor borehole quality, which is confirmed by the identification of several washouts recorded in some of the most interesting formation targets. For more detailed information on the petrophysical analysis conducted in the LB in the aim of this project, please refer to PiloSTRATEGY Deliverable 2.6.

Additionally, the dataset includes several rock samples from the reservoirs (Torres Vedras Group and the potential Alcobaça Formation) and primary seal (Cacém Formation) collected onshore, at outcrops, and used for mineralogical, petrographic, petrophysical and geomechanical analyses.

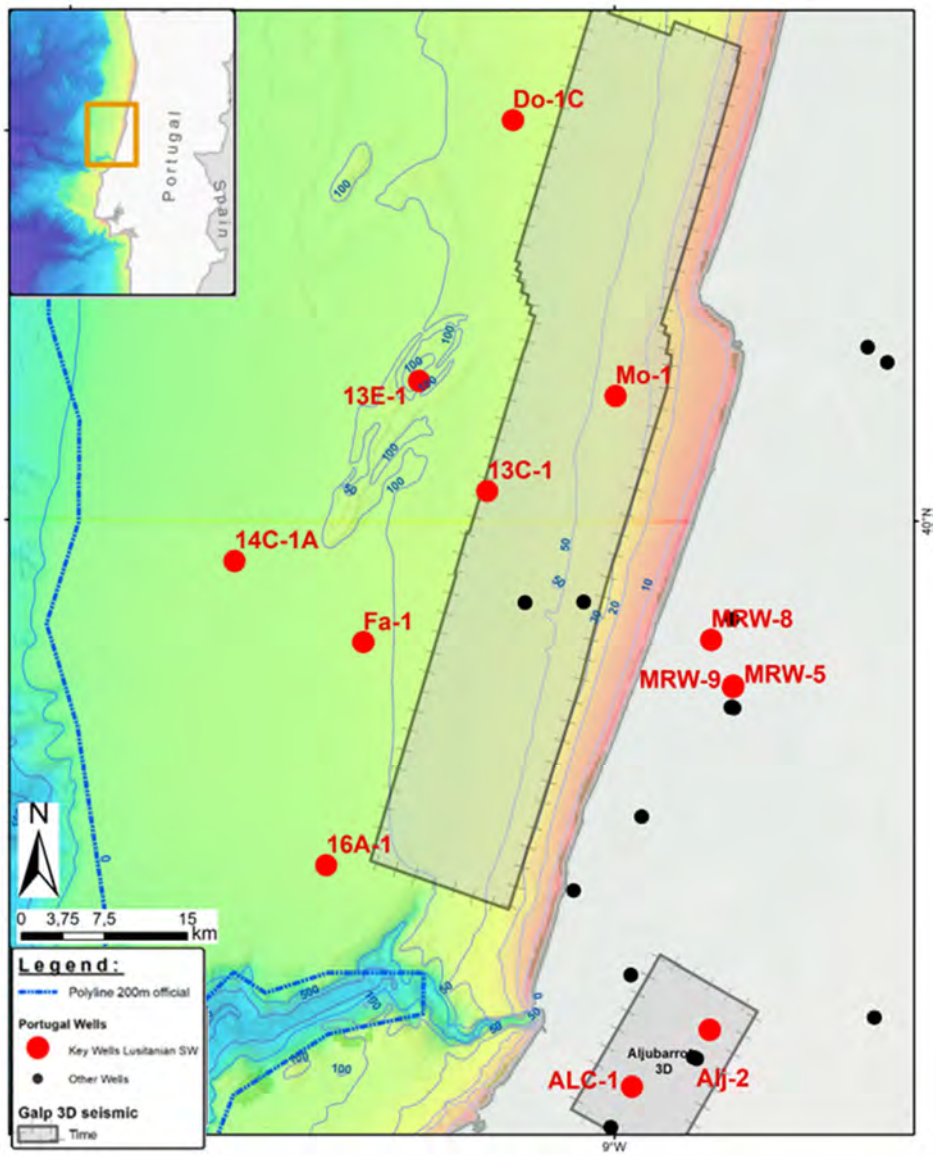

Figure 5-2: Basemap of the study area illustrating the location of the wells (highlighted in red) that were included in the petrophysical analysis.

5.2 Dataset: Spain

The data used to generate the geological model mainly come from legacy seismic lines and former exploratory well data. New data were acquired from outcrops, one borehole core (Chiprana-1 core), gravimetric and passive seismic surveys. See the following table for a summary.

Method	Data input	comments
Active Seismic Lines	9 lines (SW-NE and NW-SE). 10 horizons analysed. (Figure 7-6)	SEG-Y format files vectorised from a TIFF file (old seismic profiles).
Well data close to AOI	Lopín-1 well (Seismic Line ZA-27) (Figure 7-6)	Well logs = depth correction = horizons interpretation. Reports and Log data
Other Wells data	12 wells (Figure 7-6)	14 to 94 Km from Lopín-1 Reports and Log data
Gravimetric Modelling	(1) 10 sections = reinterpretation of vintage seismic sections. (2) 3 new sections = specifically to constrain the SE end of the model.	D2.2 ID number 101022664, https://pilotstrategy.eu/about-the-project/work-packages/geo-characterisation. Bouguer anomaly and residual anomaly maps.
Passive Seismic Survey	(1) 32 seismic stations (2) 12 seismic stations, along the ZA27 profile	(1) 120 s 3-component Trillium Compact sensors and Spyder digitizers) (2) 5 s 3-component sensor (Tellus by Lunitek) and Centaur Nanometric digitizer
Samples	44 samples Torre-Arcas 21 samples Peñas-Royas 10 samples Chiprana-1 core	Laboratory analysis
Photogrammetry with Drone	High density data point clouds, 3D. LAS format. Two outcrops 60Km SW from AOI.	Survey on Buntsandstein sandbodies geometries and amalgamation.

9 out 13 wellbores have some information of the reservoir that has been used in this report analysis.

5.3 Dataset: France

The Paris Basin has been the target of intense oil and gas exploration, thus a large amount of well and seismic data (2D / 3D) is available. These data permit reservoir characterization at several scales: from general architecture using seismic data to reservoir scale facies using well logs, cores, thin sections and petrophysical measurements. For an efficient analysis of these data, the study area is divided into two specific zone. The first one corresponds to the extension of the 3D seismic area and is the area in which the pilot-scale prospect is located. The second one is an extended area of interest the objective of which is to understand the influence of the surrounding regional on the pilot prospect. The map presented below (Figure 5-3) indicates the position of all data used in this project and the extent of areas defined above.

The PilotSTRATEGY project has received funding from the European Union's Horizon 2020 research and innovation programme under grant agreement No. 101022664

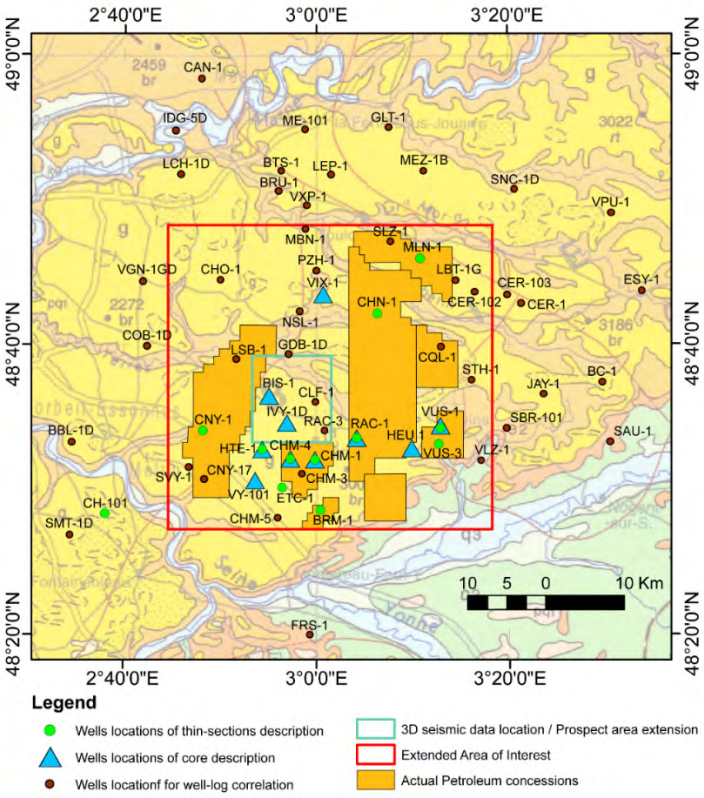

Figure 5-3: Location map of dataset used in the French region.

5.3.1 Seismic data

A newly acquired 3D seismic cube has been used to characterisation the structure of the reservoir. Details concerning this data acquisition, processing and QA/QC has been presented in Deliverable 2.3 of PilotSTRATEGY (Bordenave & Wallendorff, 2023).

5.3.2 Well data

46 wells (42 in the extended AOI) are used to characterize the large-scale geometry of the reservoir complex, depositional environments and electrofacies / facies variations along the area (Figure 5-3). These wells have basics well log measurements: sonic; gamma ray; neutron porosity; bulk density; resistivity medium; resistivity and spontaneous potential. See Annex (France) Appendix I for well characteristics and available data.

In the prospect/seismic area, 4 wells are utilized for seismic interpretation and facies calibration (Figure 5-4). Only one well has checkshot calibration and a velocity-depth law. Using this relationship allows for accurate seismic / well tie picking of the horizons.

The PilotSTRATEGY project has received funding from the European Union's Horizon 2020 research and innovation programme under grant agreement No. 101022664

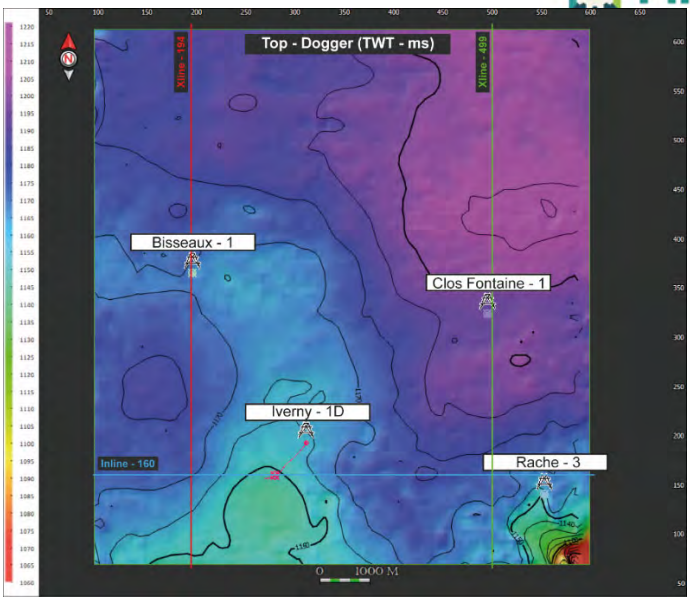

Figure 5-4: Well's locationn and their path in the prospected area. The extent of the area is presented in Figure 5-3.

Futhermore, specific petrophysical logs have been processed on wells CLF-1, IVY-1D and RAC-3 (Figure 5-5). They generate to: (i) total and effective porosity, (ii) oil, gas and water saturation, (iii) shale volume from gamma ray and density neutron, (iv) reservoir flag and (v) mineralogical volume (Calcite, Dolomite, Illite, Quartz, Kaolinite, Anhydrite). However, no previous reports mention these data, thus no critical review and QA/QC revision were done, hence utilization of these results was done with caution.

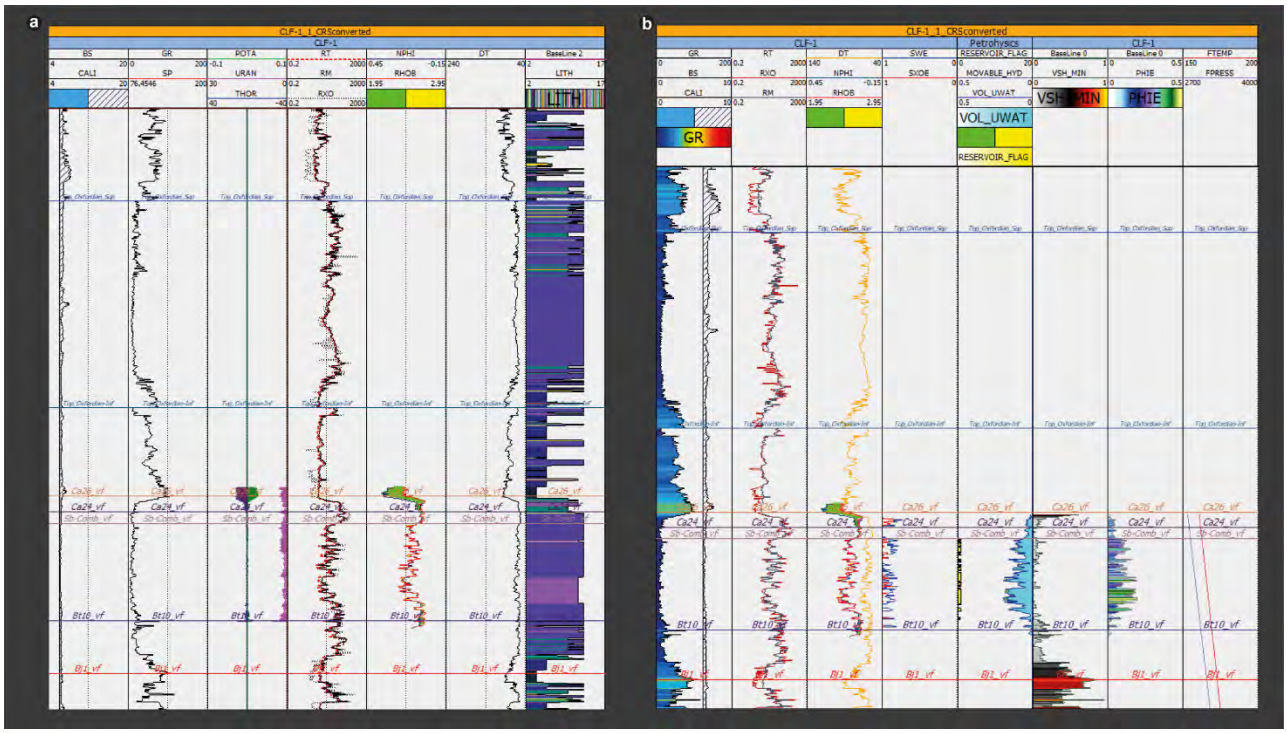

Figure 5-5: Examples of well logs a) acquired well logs and b) processed logs

The PilotSTRATEGY project has received funding from the European Union's Horizon 2020 research and innovation programme under grant agreement No. 101022664

6. Regional Geological Characterisation

6.1 Regional Geological Characterisation: Portugal

The Lusitanian Basin (LB) is a Meso-Cenozoic basin that was developed as a multiphase rift throughout much of the Mesozoic (Figure 6-1). The basin begins its evolution during the Late Triassic – Early Jurassic with the onset of the first rifting event. Other two rifting events occurred during the Late Jurassic and Early Cretaceous. Continental break-up occurred close to the transition between Early and Late Cretaceous. Mesozoic sedimentation in the LB alternated between deposits with continental influence and marine deposits, hence siliciclastics and carbonates are the most common sedimentary infill of the basin.

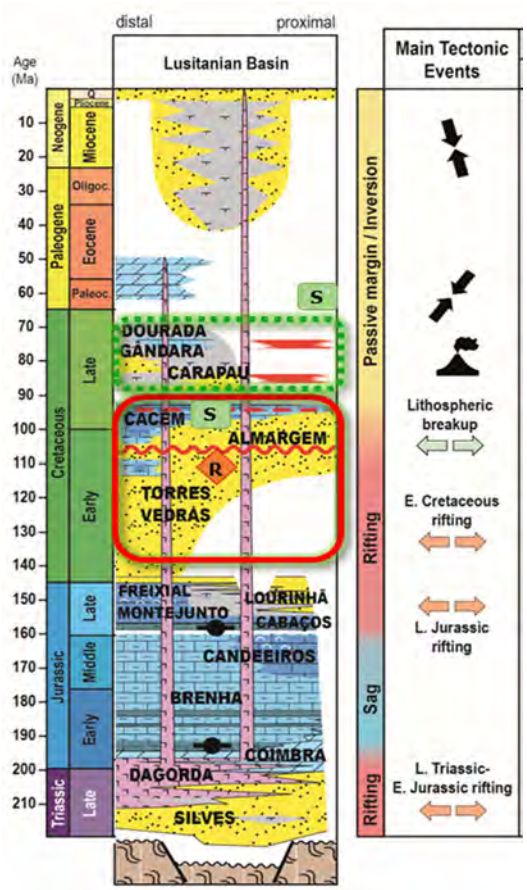

Figure 6-1: Simplified lithostratigraphic chart of the Lusitanian Basin (adapted from Casacão et al., 2023), including the main tectonic events that impacted the basin's evolution. Here it is highlighted the storage complex play that is being considered, formed by the Torres Vedras Group (reservoir unit) and Cacém Formation (seal), and the secondary seal formed by the Aveiro Group (Carapau, Gândara and Dourada formations).

Following the sequence deposited during the first rifting event, the transition to the Late Jurassic succession is made through a regional angular unconformity that resulted from tectono-eustatic

The PilotSTRATEGY project has received funding from the European Union's Horizon 2020 research and innovation programme under grant agreement No. 101022664

controls also recognized in other circum-North Atlantic basins (Rasmussen et al., 1998; Azerêdo et al., 2002). Rifting resumed after this Callovian basin-wide event that endured until the Early Cretaceous, associated with mild crustal extension in the LB. This rift episode corresponds to a period of continued extension, with reactivation of basement structures, erosion of rift shoulders, and deposition of transitional carbonates (Cabaços Formation), followed by open-marine limestones (Montejunto Formation) and fluvial, fluvio-deltaic to turbidite accumulations (Leinfelder & Wilson, 1989; Pena dos Reis, 2000; Azerêdo et al., 2003).

The later rift stage during the Early Cretaceous ultimately lead to the lithospheric breakup and the onset of seafloor spreading between the West Iberian margin (WIM) and the Canadian Grand Banks since the Late Aptian (Pinheiro et al., 1996; Dinis et al., 2008). This interval corresponds to the deposition of shallow marine to fluvial sandstones with abundant coarse-grained to fine-grained siliciclastic sediments. The Albian to Cenomanian/Turonian lithospheric breakup final sequence is particularly recognized in the LB, reflecting fluvial sedimentation (Wilson et al., 1989; Rey et al., 2006; Dinis et al., 2008) capped by shallow-marine carbonates associated to the Cenomanian-Turonian transgression (Witt, 1977), forming a unit commonly known as the Cacém Formation (Figure 6-1).

Following lithospheric breakup, west Iberia underwent the continental drift stage, with prograding siliciclastics deposited in the Northern LB, while the southern sector was emergent (Rey et al., 2006; Pimentel & Pena dos Reis, 2016). During the latest Cretaceous, a regional-scale magmatic event affected some Mesozoic basins of West Iberia, although there is no evidence of this episode within the study area.

Sedimentation continued throughout the Cenozoic in West Iberia, despite experiencing two main inversion events (e.g. Ribeiro et al., 1990). These are associated with 1) the Alpine orogeny, with basin-wide tectonic uplifts that impacted the stratigraphic record, and 2) a second inversion episode, during the Betic phase (NNW-SSE Eurasia-Africa convergence), considered as the main phase of compression in the western and southern edges of the Iberian plate (where the LB lies), causing the reactivation of ENE-WSW and NE-SW Late-Hercynian basement-cutting lineaments as reverse faults, and NW- and SE-verging thrusts (Ribeiro et al., 1990).

The geometry and structural configuration of the study area can be observed in the cross-section of Figure 6-2, where the main storage elements are also highlighted. The Dagorda salt unit (Hettangian) is seen to control Jurassic, Cretaceous and Cenozoic *strata* thickness, as well as imposing a structural component that controls trap definition.

The PilotSTRATEGY project has received funding from the European Union's Horizon 2020 research and innovation programme under grant agreement No. 101022664

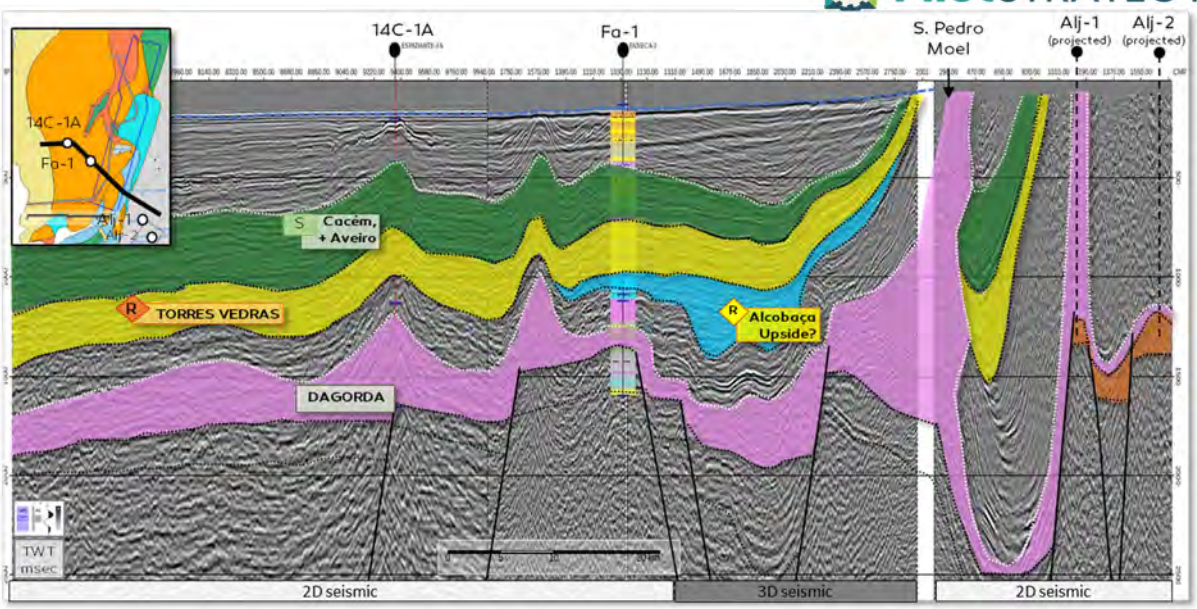

Figure 6-2: Structural configuration of the study area, resulting from the interpretation of a E-W seismic line. Main storage elements comprise the Torres Vedras Group (primary reservoir), the Cacém & Aveiro units (primary and secondary seals) and the Alcobaça Formation (secondary reservoir target). It is also interpreted the Dagorda salt unit (in pink), and the impact of diapirism in the creation of anticlines (structural traps)

The architecture of the LB reflects a continuous syn- to post-rift sedimentary record in a proximal margin with mild subsidence. The geometry and lithostratigraphic record of sedimentary packages were largely influenced by salt diapirism and normal faulting throughout the Mesozoic, and later subjected to a major episode of magmatism during the Late Cretaceous and, lastly, a regional-scale tectonic uplift controlled by the Pyrenean and Betic phases of the Alpine orogeny. This Cenozoic basin inversion resulted in the reactivation of post-Hercynian faults, and in an interplay between thick Hettangian evaporites that were already developed at that time, which caused the reactivation of salt diapirs throughout different compression phases (Ribeiro et al., 1990; Wilson et al., 1989; Pinheiro et al., 1996; Alves et al., 2002).

The relationship between salt diapirism and deep basement faulting during the Jurassic extensional phases has been widely addressed in the LB (Zbyszewski, 1959; Wilson et al., 1989; Ribeiro et al., 1990; Pinheiro et al., 1996; Rasmussen et al., 1998; Alves et al., 2002). One of the examples of known salt diapirism is illustrated by salt pillow inflation on top of relative footwalls and relative basement highs controlled by Late Hercynian lineaments, associated with the salt withdrawal from the subsident hanging-walls, leading to the creation of broad sub-basins. The Late Jurassic rifting corresponded to the period of increased fault-controlled subsidence associated with salt movement, with development of sub-basins with distinct characteristics.

Sedimentation throughout the Lower Cretaceous was locally impacted by the existence of salt diapirs that constrained the sediment transport routes implying variations in thickness and lithological types of the fluvial-deltaic deposits.

As crustal stretching progressed throughout the Early Cretaceous, a basin-ward migration of the rift locus was recorded (Murillas et al., 1990; Alves et al., 2009), in the Upper Barremian, followed by exhumation and thinning of the upper mantle until the Aptian-Albian boundary (Soares et al., 2012).

The PilotSTRATEGY project has received funding from the European Union's Horizon 2020 research and innovation programme under grant agreement No. 101022664

The Albian to Cenomanian/Turonian lithospheric breakup final stage is developed on top of the Aptian breakup unconformity, which is particularly recognized in the LB.

After the drift stage following the continental break-up, two tectonic inversion pulses affected LB – the Pyrenean phase, during the Eocene, and the Betic phase, during the Miocene, that played a critical role in salt diapirism, which resulted in the current configuration of the studied area, through 1) rejuvenation of pre-existing salt pillows and domes over basement-related faults (Alves et al., 2003); 2) Hettangian salt acting as a décollement for thin-skinned tectonics (Ribeiro et al., 1990); 3) rejuvenation and increased salt wall piercement, causing extrusion (Rasmussen et al., 1998).

Two potential storage complexes exist at the LB (Figure 6-1): i) the Triassic-Lower Jurassic Silves Group (reservoir) and Dagorda Formation (seal); and ii) the Cretaceous Torres Vedras Group (reservoir) and Cacém Formation (seal). New data from PilotSTRATEGY WP2 and re-interpreted data acquired for petroleum exploration dismissed the Triassic-Lower Jurassic storage complex in favour of the Cretaceous one (see deliverable D2.6).

The storage complex includes the main siliciclastic reservoir "Torres Vedras Group" (TVG) and the carbonate seal "Cacém Formation" (CF); sedimentation dated from the Early Cretaceous TGV to Late Cretaceous CF. A potential secondary seal composed mainly by fine grained siliciclastics sediments (part of Aveiro Group), of Upper Cretaceous age, overlies the storage complex. The Late Jurassic Alcobaça Formation, composed by fluvial to shallow marine siliciclastic sediments, has the potential to be another possible reservoir, underneath the TVG and in hydraulic connection with it (no seal separates the two formations). However, it was only characterized as a theoretical reservoir candidate due to the lack of robust data, such as the availability of more comprehensive direct geophysical measurements (i.e., well data) intercepting this geological formation to clearly confirm its potential for CO_2 storage.

6.2 Regional Geological Characterisation: Spain

6.2.1 Sedimentological and Structural Review (Spain)

The study area is situated near the southern edge of the Ebro basin (Figure 6-3 a and b). The formation of the foreland basin commenced during the Paleocene (e.g. Pardo et al., 2004). Towards the central part of the Ebro Basin, the structure corresponds to a gentle syncline (the Ebro syncline; Quirantes, 1978) (Figure 6-3 b). This fold accommodated the slight reactivation of WNW-ESE basement faults formed during Mesozoic extension (Arlegui and Simón, 2001).

The Variscan Orogeny in northeast Iberia took place in the Middle-Late Carboniferous (Vera, 2004). During the Mesozoic, general extension took place in two rifting stages: a first rifting stage during the Permian and Triassic and a second one during the Late Jurassic and Early Cretaceous (e.g. Sopeña et al., 1988; Salas et al., 2001). The collision between the Iberian and European plates from the Late Cretaceous to Miocene during the Alpine Orogeny caused the inversion of previous Variscan and Mesozoic structures (e.g. Casas-Sainz and Faccenna, 2001). This last compressional period formed the foreland Ebro basin (e.g. Arlegui and Simón, 2001).

Subsurface data reveal the presence of several structures inside the Ebro basin that affect the Paleozoic and Mesozoic rocks below the sub-horizontal Cenozoic deposits. These structures are aligned parallel to the Iberian and Catalan deformation fronts, oriented NW–SE and NE–SW,

The PilotSTRATEGY project has received funding from the European Union's Horizon 2020 research and innovation programme under grant agreement No. 101022664

respectively (Arlegui and Simón, 2001; Butillé et al., 2012; Mediato et al., 2017; Izquierdo-Llaval et al., 2019).

The underlying basement is formed of Paleozoic rocks with some degree of metamorphism. Above the basement, Triassic sediments display typical Germanic facies, including Buntsandstein red beds, Muschelkalk dolostones, limestones, and evaporites and Keuper evaporites and shales. Three different Triassic evaporitic sequences characterize the sedimentary pile at this sector: (i) a thin basal evaporite layer (Röt facies), (ii) a thick succession of Middle Triassic evaporites (M2, middle Muschelkalk facies), and (iii) a thick succession of continental evaporites and fine grained clastics of Late Triassic age (Keuper facies; Jurado, 1990; Ortí et al., 2017). The oldest Jurassic rocks of the Ebro Basin are 50 m of dolomites overlain by a cyclic anhydrite unit bearing dolomitic interbeds (Lécera Fm) with a total thickness of 200 – 450 m (Jurado, 1990; Gómez et al., 2007).

This oldest sequence is overlaid by a maximum of 300 m of multiple shallow platform carbonate sequences (dolomites, limestones and limestones with interbedded marls). This is overlain by continental carbonate and detrital Cretaceous deposits. The base of the Cenozoic continental evaporitic and detrital rocks is unconformable. This erosional surface cuts the Cretaceous and Jurassic deposits.

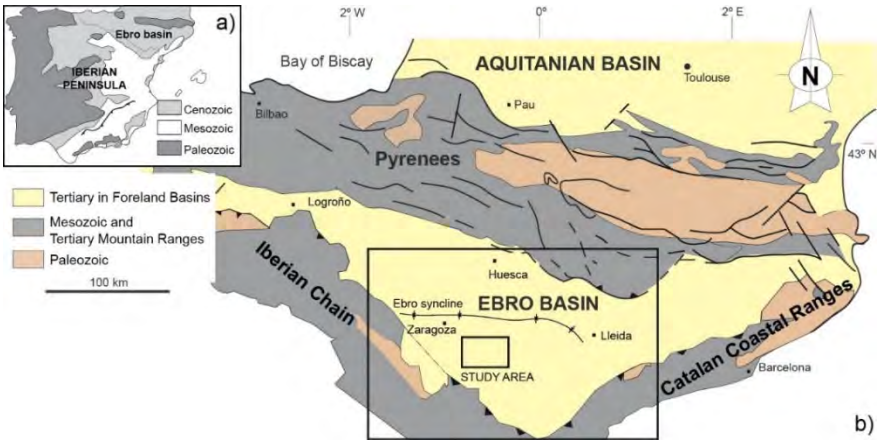

Figure 6-3 a) Simplified geological sketch of the Iberian Peninsula (from Soto et al., 2009). b) Geological sketch of the northeastern part of Iberia showing the study area in the central part of the Ebro basin and the Alpine ranges (modified from Soto et al., 2016).

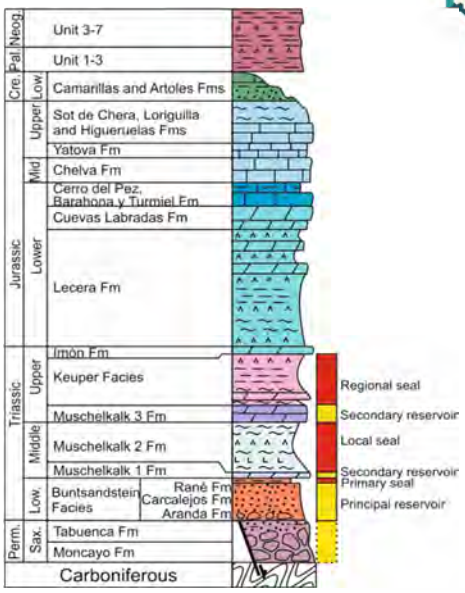

Figure 6-4 Simplified lithostratigraphic column of the area (modified from Ayala et al., 2022).

6.2.2 Storage Stratigraphy (Spain)

The Buntsandstein (main reservoir) contact with the Permian is clear and slightly discordant. Arche et al., 2004 described three formations, from bottom to top (Figure 6-4):

- **Aranda Fm.** (Lower Triassic): Sandstone, interbedded with thin (centimetre) shales, red and, occasionally, green (Díez et al., 2007).
- **Carcalejos Fm.** (Anisian age - Díez et al., 2007), it is formed by alternating red coloured sandstones and shales, and sometimes contains levels of microconglomerates.
- **Rané Fm**. (Anisian age - Díez et al., 2007), it is formed by alternating shales and fine-grained red sandstones.

In log analysis Aranda formation is unit B-1, unit B-2 corresponds to Carcalejos formation, as they are usually named in the oil and gas industry in this area (Aurell et al., 2001) (Figure 6-5). B-2 unit pass upwards gradually to Rané formation so no clear marker has been used to define this formation boundaries.

The PilotSTRATEGY project has received funding from the European Union's Horizon 2020 research and innovation programme under grant agreement No. 101022664

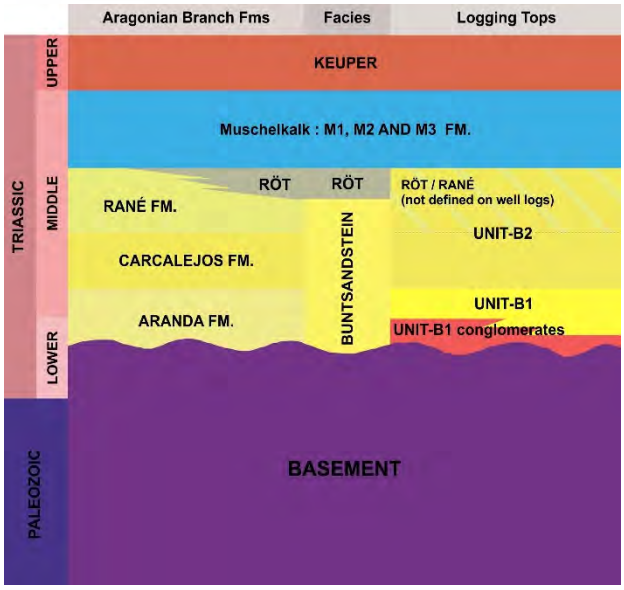

Figure 6-5 Correlation table between formations defined from outcrops in this area and units set in this report. Triassic Formations from Arche et al., 2004.

6.3 Regional Geological Characterisation: France

6.3.1 The Paris Basin: its structuration and tectono-stratigraphic history

The Mesozoic / Cenozoic Paris Basin is an intracratonic sag-type sedimentary basin lying unconformably over a Paleozoic basement (Figure 6-6). The tectono-sedimentary evolution of this basin is mainly influenced by regional geodynamical events associated with extensional stages of the Mesozoic opening of the Alpine Tethys, Atlantic Ocean and Bay of Biscay, and compressive event of the Late Cretaceous-Cenozoic Pyrenean and Alpine orogenies. This long-term geological evolution is represented by eleven major tectono-sedimentary cycles from the Triassic to the Tertiary (Guillocheau et al., 2000; Figure 6-6)

The PilotSTRATEGY project has received funding from the European Union's Horizon 2020 research and innovation programme under grant agreement No. 101022664

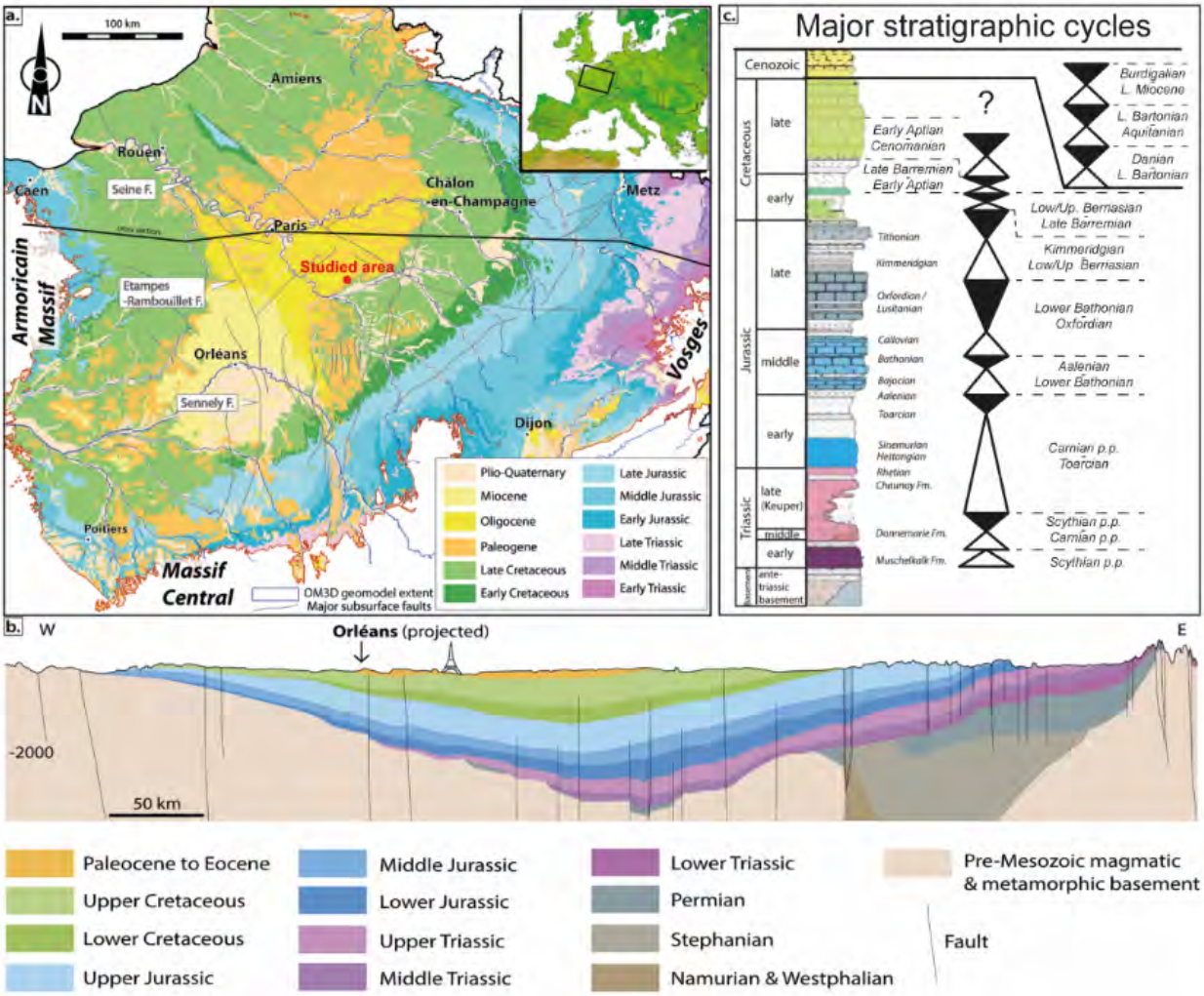

Figure 6-6: a) Geological map of the Paris basin and location of the geological section. c) Mains sequence stratigraphic cycles of the Paris Basin, proposed by Guillocheau et al., 2000. Mas et al., 2022

6.3.1.1 Tectono-stratigraphic evolution of the Paris Basin:

After the strong compressive event that resulting in the formation of the Variscan mountain belt, the Paris Basin only suffered from far field deformation related to major geodynamic events affecting the western European plate (Pyrenean and Alpine orogenies, the Atlantic opening...). These events induced local reactivation of Variscan faults and slight deformation with initiation of gentle folding and occasionally fault inversion. The Early Jurassic shows evidence of extensional setting with the development of syn-sedimentary normal faults, while the mid to late Jurassic is considered as tectonically quiescent. Recent work demonstrates heterogeneous thickness distributions correlated with former Varsican blocks (Andrieu et al., 2016 ; Andrieu 2016). This pattern suggests that although no significant tectonic effects are visible, large-scale and crustal parameters control subsidence; probably in relation to (i) the neo-Tethys opening in the Tethyan domain (to the south of the Paris Basin) and (ii) the North sea-doming in the Atlantic domain, north of the Paris Basin.

6.3.1.2 The Dogger Ramp – Regional reservoir

During the Dogger (Mid-Jurassic), the Paris Basin was located at subtropical latitudes and covered by an epicontinental sea connected to the Tethys to the southeast and the Atlantic to the southwest. The

The PilotSTRATEGY project has received funding from the European Union's Horizon 2020 research and innovation programme under grant agreement No. 101022664

contemporary Armorican and London-Brabant uplifts and exposed massifs significantly restricted its connection with the North Atlantic. There was polyphase rifting during the same period.

The early to late Bajocian is characterized by a carbonate-production crisis (REF) concomitant with deposition of open-marine marls marking a major flooding event across the Bajocian platforms. During the Bathonian, carbonate production began again and carbonate ramps developed around and within the Paris Basin. The Early Bathonian records the first stage of development of this ramp, with deposition of argillaceous limestone and associated in our study to the general prograding stage of the ramp. The Middle Bathonian and Late Bathonian corresponds to the main and long-lasting establishment of the ramp.

6.3.2 Sedimentological and Structural context review of the Dogger platform in the AOI

6.3.2.1 Structural review

Large scale structure mapping from the literature and interpretation of 3D seismic data indicate the absence of visible (i.e. with significant offset) structural features in the existing data. Maps provided by Baptistes (2016) show a magnetic anomaly, which could be associated to structural feature that includes basement. Following this interpretation, the restricted area of interest (3D seismic area) is bounded by two anomalies in the south and north. A structure map at the top of the Dogger reservoir (Delmas et al., 2002) does not display any faults. Subsequently, these anomalies are not associated with potential faults affecting the reservoir section. This is confirmed by the analysis of the 3D seismic cube where the presence of a potential fault at depth, with a N60°E trend, is likely sealed by Triassic sediments.

In the extended area of interest, 8 faults will be integrated into the static model. These faults are interpreted and retrieved from Delmas et al. (2002). The orientation of these faults are comparable to general trends observed in the Paris Basin. The location and offset of the faults are shown in Figure 6-7.

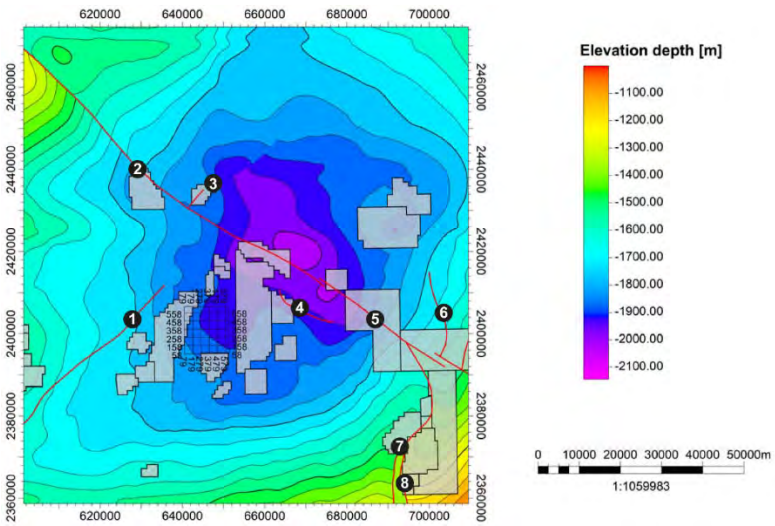

Figure 6-7: Maps showing main structural accident integrated in the static model of the extended AOI. Base map corresponds to depth map of the Bt10 horizon, interpolated from well log markers.

6.3.2.2 Sedimentological characteristics of the Dogger in the AOI

Lithostratigraphy in the Dogger is mostly defined by vertical facies variations, except with the Comblanchien Formation, which is in places the lateral equivalent of the Oolithe Blanche Formation

(White Oolite Fm). Five lithostratigraphic formations make up the Dogger platform. In stratigraphic order (oldest first), these formations are:

- ***Marnes à Ostrea acuminata* Formation**. Bajocian age, these marls represent the deepest depositional environment identified in the study area (Upper offshore).

- ***Oolithe Blanche* Formation.** Linked to a high-energy inner ramp depositional environment, this formation is mainly composed of grain-supported limestone (grainstone, packstone) with abundant ooids, pelloids and bioclastic debris from bivalves, echinoderms, bryozoans and gastropods. It makes the core of the target reservoir and represents outer ramp, shoal and back-shoal depositional environments.

- ***Calcaire du Comblanchien* Formation.** Mainly composed of oncoidal packstone, wackstone and mudstone, this formation indicates the onset of the lagoonal environment. The top of this formation is the maximum regressive surface of the Bajocian-Callovian cycle. It is the lateral equivalent of the Oolithe Blanche Formation, and as regression culminates with this unit, it locally rests upon the Oolithe Blanche Fm.

- ***Dalle Nacrée* Formation**. This last grainy formation is associated to the transgressive stage of the Callovian-Oxfordian cycle. It corresponds to the deposition the early stages of a bioclastic isolated ramp that developed during the Early Callovian in the study area. As with the Oolithe Blanche formation, the main depositional environments are shoal and back-shoal deposits.

- ***Callovian marls* Formation**. The last lithostratigraphic formation associated with the Dogger platform, these marls are offshore deposits (Upper and Lower) and seal the underlying formations.

Core description identified 37 sedimentological facies grouped into 17 facies associations. From the texture, mineralogy, fauna distribution and sedimentological structures of these lead to the definition of seven depositional environments, from distal to proximal: i) Upper offshore; ii) Lower offshore ; iii) Outer ramp; iv) Shoal ; v) Back-shoal; vi) tide-dominated lagoon; and vii) lagoon.

6.3.3 Storage Stratigraphy

The storage complex is defined as the following lithostratigraphic units (youngest at the top):

1. Oxfordian Limestone (Caprock-2)
2. Callovo-Oxfordian Marls (Caprock-1)
3. Dalle Nacrée Formation (Reservoir-2)
4. Calcaire du Comblanchien Formation (Comblanchien) (Semi-Permable1)
5. Oolithe Blanche Formation (Reservoir-1)

The Oolithe Blanche Formation is associated to the onset of an oolitic ramp developed during the Aalenian-Toarcian stage, associated with widespread subsidence and tectonic quiescence. The architecture of the reservoir is consequently controlled by eustatic variations in global sea-level and associated Maximum Flooding Surfaces. Detailed sequence stratigraphic analysis has been performed in this study, focussed on the CLF-1 well, which is located in the area of the seismic cube. Hence we

The PilotSTRATEGY project has received funding from the European Union's Horizon 2020 research and innovation programme under grant agreement No. 101022664

propose a sequence stratigraphic framework at different scale with i) a second, ii) a third order and high frequency cycles.

To reach the best balance between an accurate but complex representation of the reservoir architecture and a best static model for dynamic simulation, we decided that the reservoir and seismic interpretation will be done at the third order scale. Figure 6-8 indicates the names of horizons used for seismic data interpretation. In stratigraphic order these horizons correspond to:

1. **Bj1** – Bottom of the storage complex
2. **Bt10** – Maximum Flooding Surface which divides prograding and aggrading reservoir stages
3. **Sb-Comb** – Sequence Boundary, which indicates vertical facies variation between HST and LST. It also defines the bottom of semi-permeable reservoir
4. **Ca24** – Maximum Regressive Surface of the Bajocian-Bathonian cycle. This horizon indicate the vertical facies variation between Comblanchien lagoonal facies (LST) and Dalle Nacrèe oolitic facies (TST)
5. **Ca26** – Not associated to a specific sequence stratigraphic surface, this horizons is the top of reservoir facies of the Dalle Nacrée formation (Reservoir 2)
6. **Top_Oxfordian_Lower** – Not associated to a sequence boundary, this horizon is the vertical facies variation between Callovo-Oxfordian Marls and Oxfordian Limestone.
7. **Top_Oxfordian_Upper** – Maximum Regressive Surface of the Callovian-Oxfordian Cycle, This horizon defines the top of the Caprock 2 and the storage complex.

The PilotSTRATEGY project has received funding from the European Union's Horizon 2020 research and innovation programme under grant agreement No. 101022664

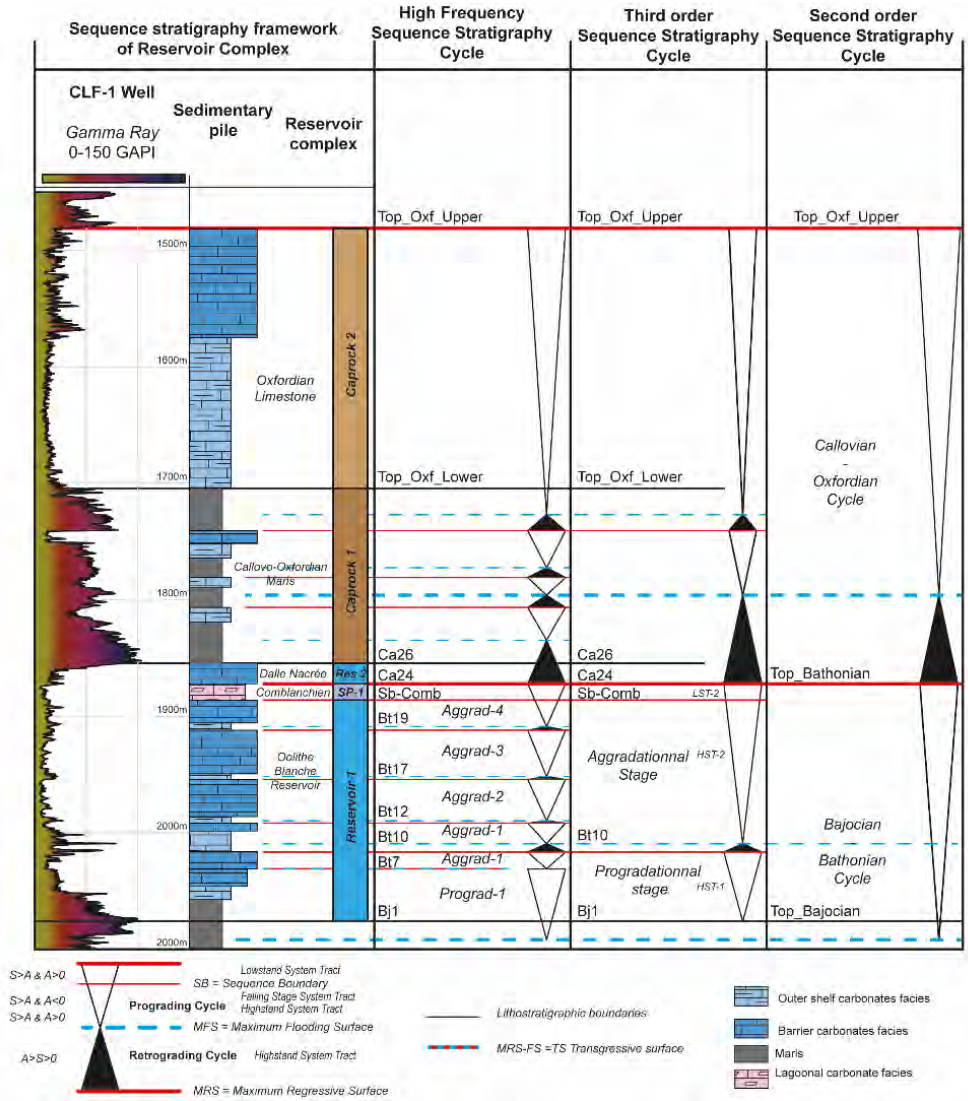

Figure 6-8: Sequence stratigraphic delimitation of the reservoir complex.

7. Storage Complex Characterisation

7.1 Storage Complex Characterisation (Portugal)

The characterization of the storage complex was done based on the seismic surveys calibrated using wellbore data, also used to perform part of the petrophysical characterization of the units. Six horizons were mapped in the seismic dataset, individualizing the main tectono-stratigraphic units of the storage complex (Figure 7-1). The interpreted seismic horizons correspond to the Top Alcobaça Formation (~145 Ma – secondary reservoir), Top Torres Vedras Group (~100 Ma – primary reservoir), Top Cacém Formation (~93 Ma – primary seal), Top Aveiro Group (~68 Ma – secondary seal), and Top Espadarte Formation (50 Ma – secondary seal).

The PilotSTRATEGY project has received funding from the European Union's Horizon 2020 research and innovation programme under grant agreement No. 101022664

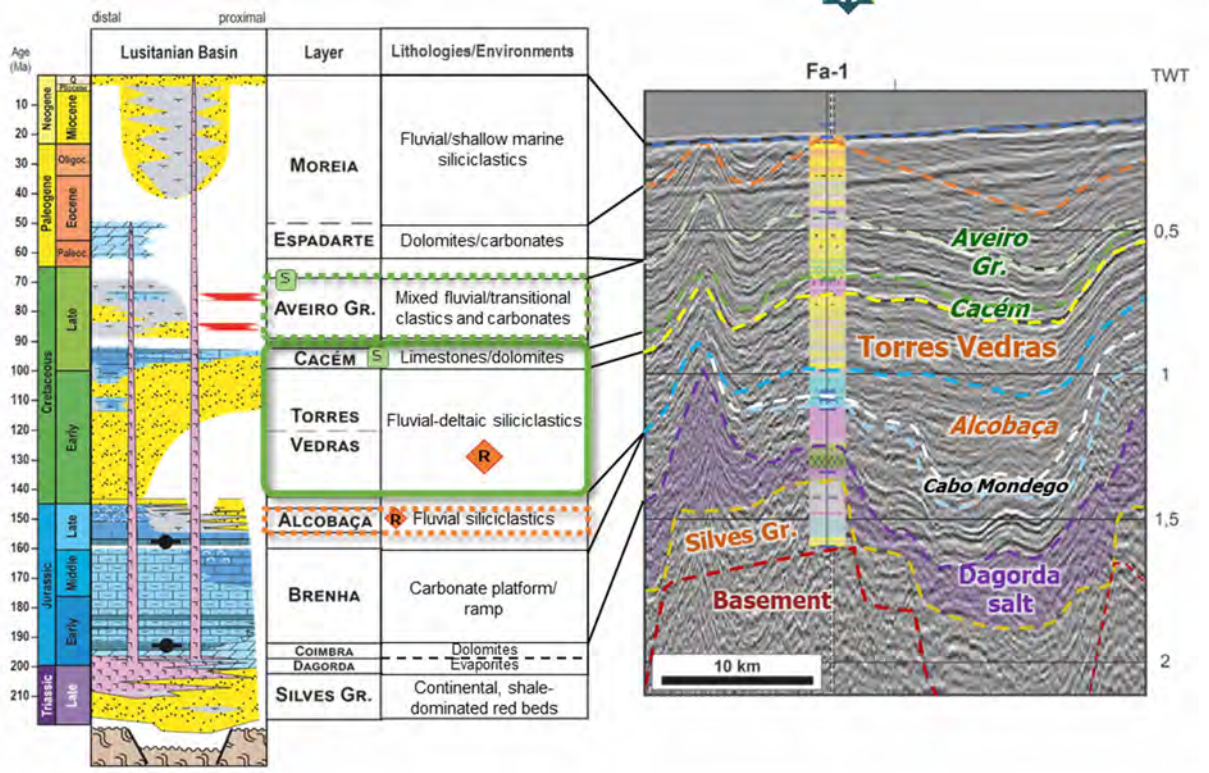

Figure 7-1: Lithostratigraphic chart of the Lusitanian Basin, its main tectono-stratigraphic units and a seismic screenshot with the main horizons mapped (Seabed, Top Espadarte, Top Aveiro Group, Top Cacém Formation, Top Torres Vedras Group, and Top Alcobaça Formation).

Several syncline and anticline structures were identified for the top of the TVG (the reservoir target) of several dimensions and located at variable depths (Figure 7-2). Although some of the structures present in the studied area have interesting dimensions for storage, they were disregarded due to the lack of guarantee of CO_2 containment or for being shallower than the required depth to ensure the CO_2 in the supercritical state.

Fault interpretation identified a total of 24 faults in the whole studied area (Figure 7-2). Faults strikes cluster around N-S and NW-SE directions, with exception of a couple of faults that strike W-E. Most of the interpreted faults are normal faults, with some reverse faults associated to salt halokinesis. The throws of the faults frequently have several hundreds of meters but throws of dozen to few hundred meters are also common. This structural framework is responsible for the development of the structural highs of the area, and the grabens and half-grabens also present.

The PilotSTRATEGY project has received funding from the European Union's Horizon 2020 research and innovation programme under grant agreement No. 101022664

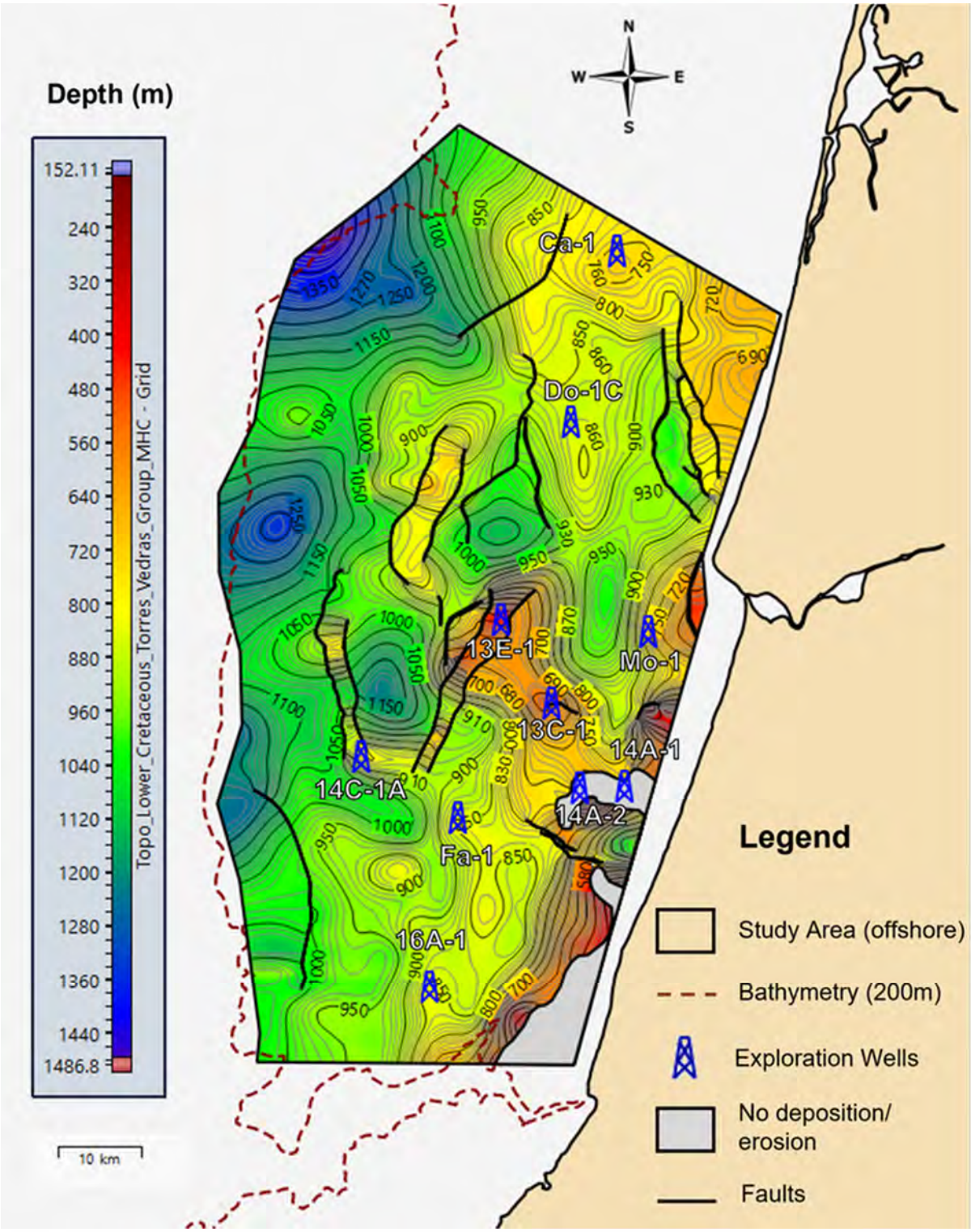

Figure 7-2: Structural map (in Depth) of the reservoir top (Torres Vedras Group) in the offshore study area. Isolines of 10 meters.

The PilotSTRATEGY project has received funding from the European Union's Horizon 2020 research and innovation programme under grant agreement No. 101022664

Analysis of vertical wells provided information of sedimentological and petrophysical characteristics of the storage complex. Despite the limited data acquired during drilling and the poor borehole quality some porosity determinations were done. Using effective porosity cut-offs of >8% for the reservoir formations and <2% for the seal formations, TVG have net-to gross ratios between 11% and 82%, with average porosities between 19% and 23%. The underlying upper Jurassic potential reservoir (Alcobaça Formation) was found in a single well and has a net-to gross ratio of 99% and an average porosity of 18%. However, these values should be considered with caution due the limited available data. Net-to-gross ratios for the primary and secondary seals ranges between 11% and 52% for the Cacém Fm (CF primary seal) and 5% and 78% for the Aveiro group (secondary seal).

Figure 7-3 shows an NNE-SSW seismic section crossing the Ca-1, Do-1C and 13E-1 wells, highlighting the main structural features. As observed, the main reservoir from TVG is laterally continuous and is thinning (shale-out) towards the Ca-1 well (NNE direction), which represents a stratigraphic trap. This characteristic helped to define the P10 outline of the Q4-TV1 structure, highlighted as the main prospect to focus further on. This package is mainly composed by siliciclastic sediments, primarily sandstones, and encompasses intra-reservoir claystones, as observed in the gamma-ray logs. The CF seal is composed by limestones, marls and clays, and is continuous and homogenous over the area of interest, showing strong amplitudes in the seismic section and low inferred porosity (low gamma-ray values). This gamma-ray trend is observed in all well correlations, in which the lower part of CF shows a higher gamma-ray values (corroborated in the Do-1 well report) and the upper section of CF shows slightly lower gamma-ray values and lower porosity, which is supported in literature and well reports by the limestone/dolomite-rich facies of this unit.

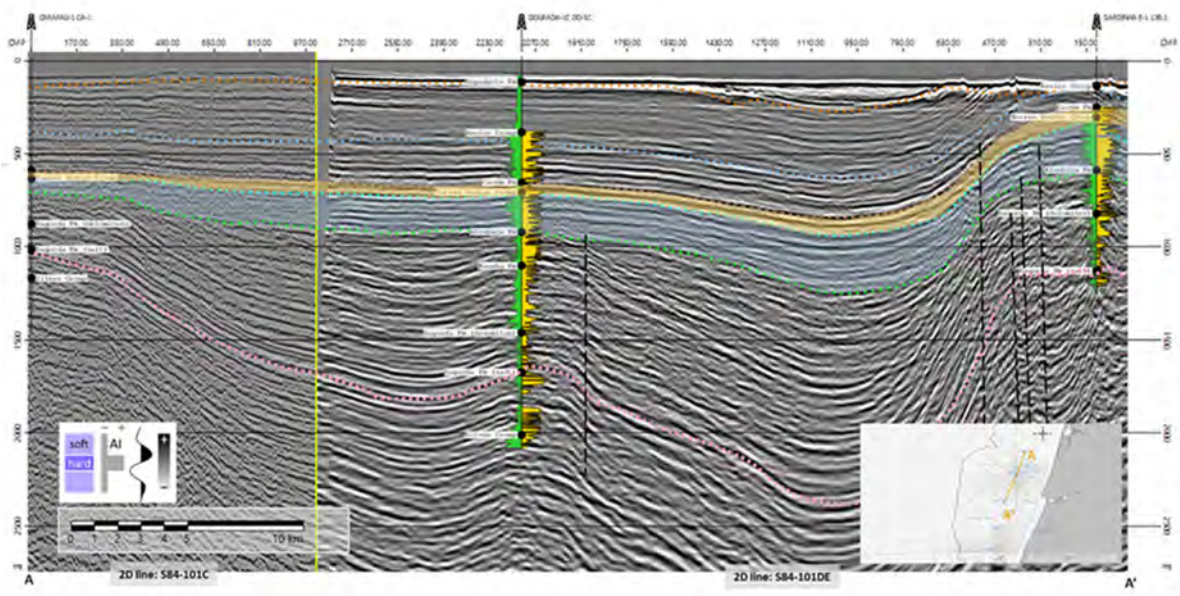

Figure 7-3: NNE-SSW seismic section crossing the wells Ca-1 (left), Do-1C (middle) and 13E-1 (right) and showing the Gamma-ray (GR) log in green and the effective porosity log (PHIE) in yellow.

As the selected study area is located offshore, there is scarce information for geological characterization apart from the available direct (wells) and indirect (seismic) geophysical data. However, there are outcrop analogues of the TVG reservoir, in which several depositional patterns typical of fluvial-deltaic-shoreline environments can be observed. Some of these include well-rounded, well sorted, quartz-rich sandstones within channel deposits, delta-front/mouth bar deposits,

The PilotSTRATEGY project has received funding from the European Union's Horizon 2020 research and innovation programme under grant agreement No. 101022664

as well as distributary-channels and interbedded floodplain silts and claystones. The lithological complexity, interbedding and thickness variations generally found in wells and in seismic data is also perceived, in a smaller scale, in outcrops.

Samples were collected at outcrop for petrographic, mineralogic, geomechanical and petrophysical analyses. The reservoir samples from the TVG are mainly sandstones, with variable grain sizes, ranging from fine- to coarse-grained sandstones with variable sorting. The grains are mainly quartz, although feldspar grains and lithoclasts are often found. Most of the samples have a calcitic cement; siliceous cement, kaolinite rich cement and iron oxy/hydroxides cement are also common. Types of cement tend to be heterogeneously distributed both laterally and vertically through the reservoir rocks. Quartz is the main mineralogical constituent while orthoclase, magnesian calcite, kaolinite, microcline, dolomite, and micas are also common constituents of these sandstones. The sandstones from the Upper Jurassic Alcobaça Formation are medium- to coarse-grained sandstones, poorly sorted with sub-angular grains (very similar to the Cretaceous samples) with a carbonate cement.

Geomechanical tests were conducted in the outcrop samples, given the total absence of cores, and while it is not intended that the samples are fully representative of the conditions at the expected reservoir depth, the results are nevertheless reported here for the primary seal, as the TVG samples are too loose to be tested. Geomechanical tests and determination of petrophysical (porosity, permeability, formation factor) and thermal (conductivity, capacity, diffusion) parameters through laboratory tests were also conducted for the Upper Jurassic Alcobaça Formation and are detailed in the annex.

Cretaceous primary seal is mainly constituted by carbonate rocks. Limestone and dolomite are the most common lithologies, although some claystone and interbedded thin layers of sandstone are present in the primary seal formation. Seal lithotypes collect at the outcrops have diverse textural characteristics that can be summarized as follows: i) wackestone with abundant bioclasts of gastropod and lamellibranch with calcite as the solely mineralogical component; ii) dolomite with minor amounts of detrital quartz and K-felspar and diagenetic calcite; iii) micritic limestone (only calcite was revealed by the X-ray diffraction) with bioclasts and profuse stylolithic surfaces, frequently open in the collected samples; iv) microsparitic limestone with abundant bioclasts and some intraclasts and quartz grains dispersed throughout the sample.

Cretaceous primary seal CF presents an average dynamic elastic modulus of 2.55 GPa. Tensile strength has an average value of 1.08 MPa while the uniaxial compressive strength averages 30.05 GPa. The elasticity modulus of the primary seal averages 17.28 GPa. Thermal conductivity, volumetric thermal capacity, and thermal diffusion were also determined for the CF seal samples: a) thermal conductivity has an average of 2.39 W/mk (minimum of 1.68 W/mk, maximum of 3.59 W/mk); b) volumetric thermal capacity ranges between 1.74 and 2.67 $(J/m^3,K) \times 10^6$ with an average of 2.10 $(J/m^3,K) \times 10^6$ and; c) thermal diffusion averages 1.11 $(m^2/s) \times 10^{-6}$ ranging between 0.83 and 1.55 $(m^2/s) \times 10^{-6}$.

Primary reservoir overburden thickness (primary + secondary seals) shows a thickening trend from east to west, towards the present-day continental shelf-break (200m bathymetric isoline). It is also noticeable several places with thin strata dispersed across the study area, associated with punctual salt diapirism. Apart from these locations, the average estimated overburden of ~650m to >1100 m associated with the regional geothermal gradient (~30ºC/km) suggests there is conditions to preserve CO_2 in the supercritical phase.

The PilotSTRATEGY project has received funding from the European Union's Horizon 2020 research and innovation programme under grant agreement No. 101022664

The criteria to select potential structures as candidates for CO_2 storage was the presence of a structural component, such as 4-way, 3-way, or 2-way structural closures (these last two bounded by faults and/or salt diapir lithological contacts). After identifying several structures with potential size to serve as storage sites, the prospect Q4-TV1, preferentially oriented N-S, located in the northern study area, close to the Do-1C well, was selected (Figure 8).

This structure lies in the northern flank of the broad anticlinal structure that was penetrated by the Do-1C well, and the trap type consists in a four-way dip closure with a lateral extension of about 25 km^2 (in the P50 scenario). Despite the large extension of the prospect, its lateral closure is relatively flat and subtle, with a gross thickness of about 30 m.

An alternative scenario of the structure's extent is given by the P10 outline (Figure 7-4), presenting a similar spatial orientation as the P50 scenario, but with a larger extent (250 km^2) and gross thickness of about 70 m. In this case, the trapping configuration is more akin to a 2-way dip closure, since the prospect is partially bounded to the east and west by N-S oriented faults, while the south and northern limits are open-type boundaries.

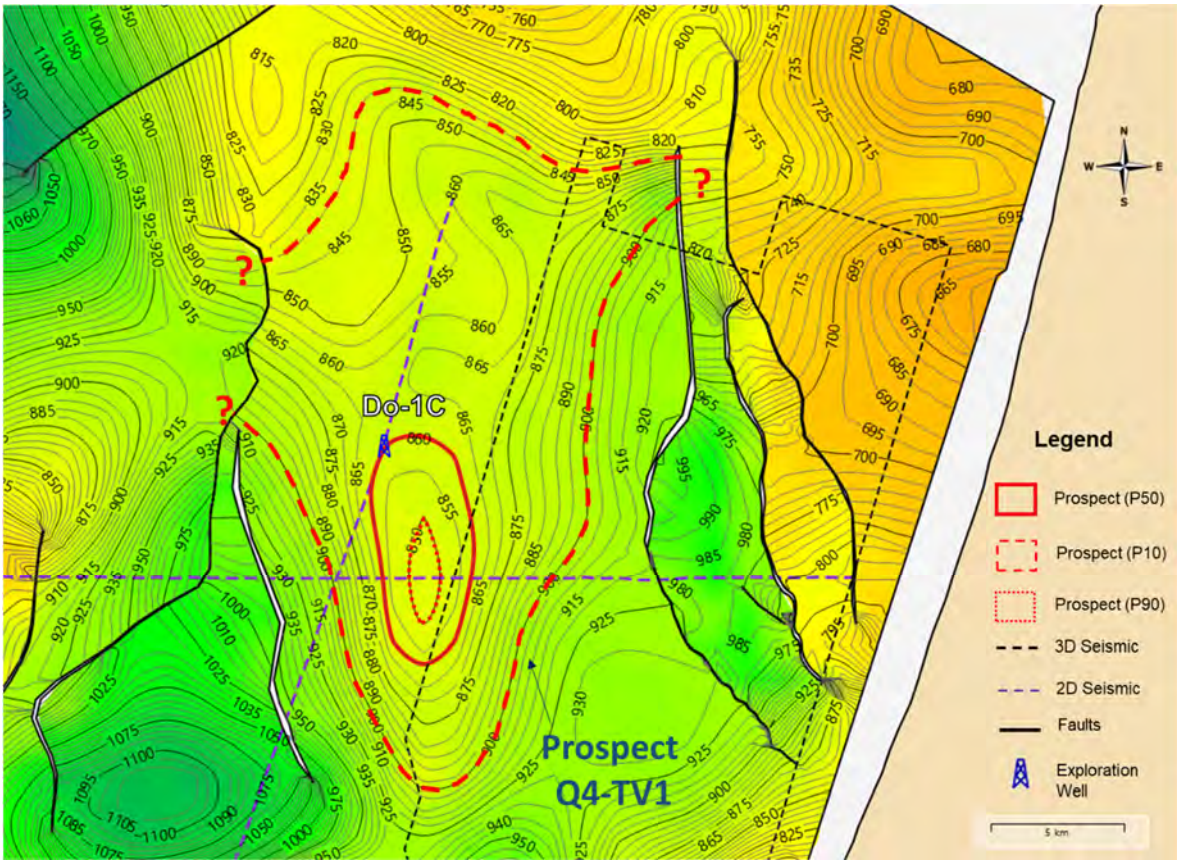

Figure 7-4: Location and outline definition of the Q4-TV1 prospect showing overlying the depth structural map of the Top Torres Vedras Group.

The PilotSTRATEGY project has received funding from the European Union's Horizon 2020 research and innovation programme under grant agreement No. 101022664

7.2 Storage Complex Characterization (Spain)

7.2.1 Horizons and Faults interpretation in the area of interest (Spain)

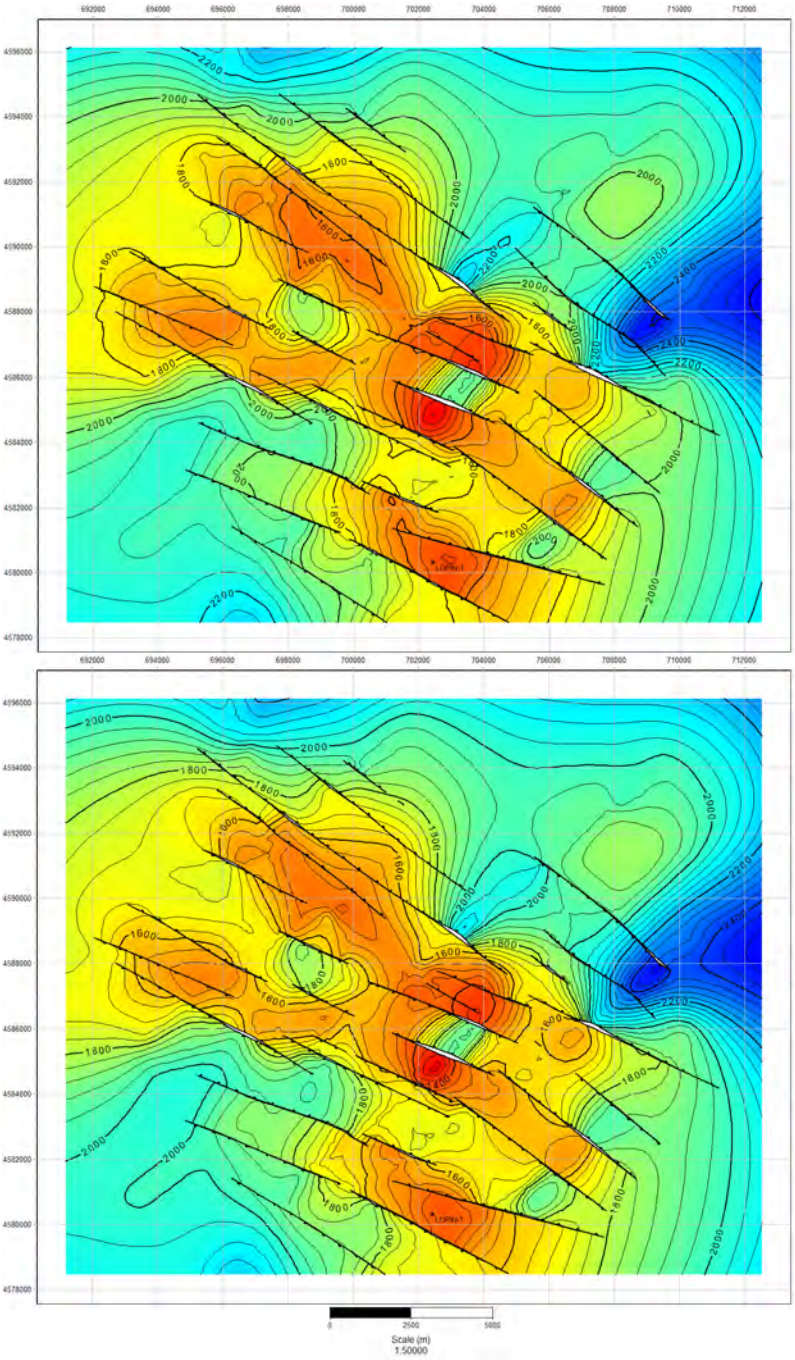

*Figure 7-5 Isobath map of the top of: **A**. basement (Paleozoic) rocks; **B**. Buntsandstein facies. Depths below mean sea level.*

Seven main seismic units are differentiated (**Erreur ! Source du renvoi introuvable.**). From top to bottom: (1) Cenozoic deposits, (2) Jurassic (-Cretaceous) deposits, (3) Hettangian limestones (Imón Fm), (4) Upper Triassic evaporites and siltstones (Keuper facies), (5) Middle Triassic rocks (Muschelkalk facies) comprising M3, M2 and M1, (6) Lower Triassic rocks (Buntsandstein facies), and (7) Paleozoic basement rocks

Figure 7-5 shows the orientation of the normal faults interpreted from the analysis of all seismic lines. The fault pattern shows a set of normal faults which delineate a series of three horsts and four grabens with the same orientation. These faults are not continuous through the study area and display segments between approximately 2000 and 5000 meters long (Figure 7-5).

The throw of the faults varies between few tens of meters to about 500 m. The distance between them is usually around 2 km and does not exceed 2.5 km in a NE-SW trending.

In **Erreur ! Source du renvoi introuvable.** there is a basal succession of Paleozoic basement rocks, Buntsandstein facies and M1 dolostones affected by a series of normal faults forming several horsts and grabens. Above this, the Middle Triassic evaporites (M2) act as a decoupling level above which the normal faulting is not observed. The M2 is overlain by the M3 and Keuper (Keuper

The PilotSTRATEGY project has received funding from the European Union's Horizon 2020 research and innovation programme under grant agreement No. 101022664

isobaths map in Figure 7-7) facies together with the Jurassic-(Cretaceous) rocks. At the top of the profile, Cenozoic strata overlap a roughly horizontal unconformity eroding the underlying Mesozoic rocks. The SW part of ZA-07 seismic profile (Figure 7-6) is characterized by reverse faults detached on the M2 evaporitic facies affecting the overlying Mesozoic deposits (**Erreur ! Source du renvoi introuvable.**).

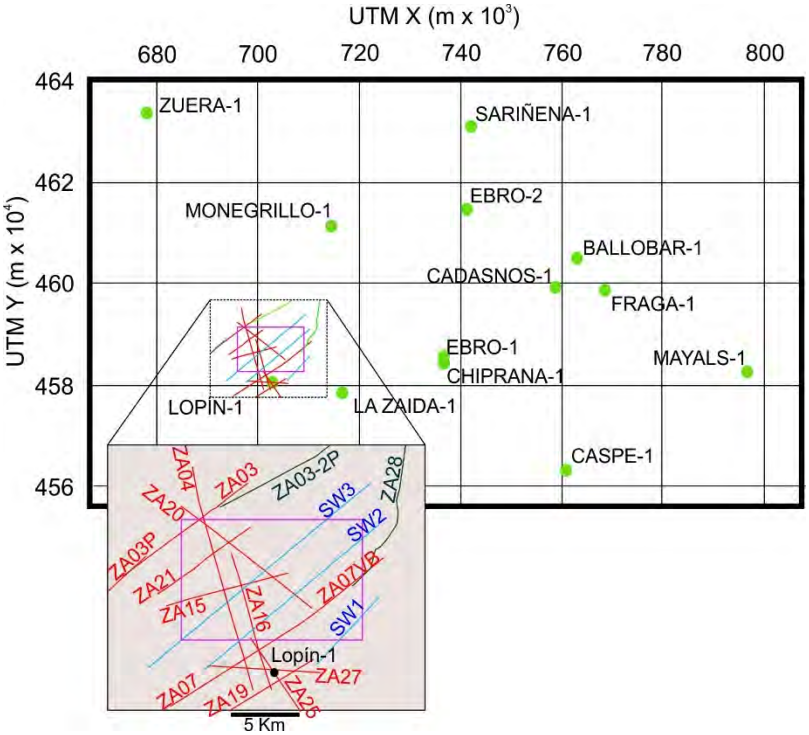

Figure 7-6 Map of the study area showing the cross sections derived from the reinterpretation of vintage seismic sections (in red) and cross-sections created specifically to constrain the SE end of the model (in blue). In green, vintage seismic sections, not interpreted because they are located outside the area of interest (purple box). Green dots mark the former wells locations.

7.2.2 Geophysical Models Implementation

Passive Seismic

Passive seismic H/V method provided information about the base of the Cenozoic and an impedance contrast within the Jurassic sequence. The autocorrelation results have imaged the main impedance contrasts and help to constrain the depth of top bedrock. Passive seismic methods have provided constraints for the interpretation of seismic reflection sections and gravimetric models.

Gravity Modelling

The PilotSTRATEGY project has received funding from the European Union's Horizon 2020 research and innovation programme under grant agreement No. 101022664

The gravimetric modelling of the geological cross-sections derived from the interpretation of the seismic lines and three new auxiliary geological cross-sections. Overall, **gravity modelling supports the interpretation of the Lopín structure as a succession of horsts and grabens where the faults that delimit those structures only affect the basement, Buntsandstein Facies and M1**. It is possible to conclude that all the faults have a high dip and moderate throw (in general, about 300 m or less).

7.2.3 Trap characterization

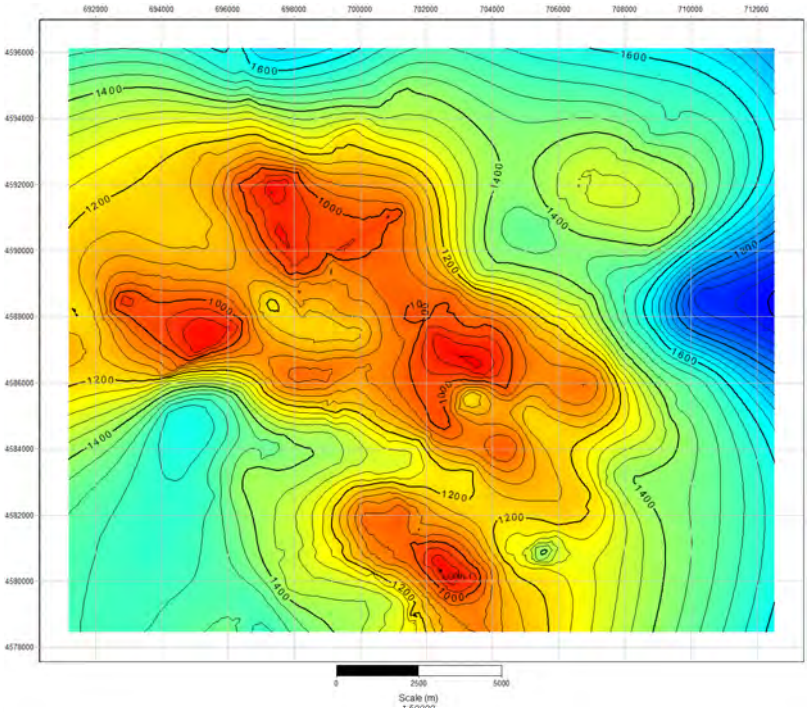

Figure 7-7 Isobath map of the top of Keuper. Depth below mean sea level.

In the 3D model the isobaths maps show the depths of the different horizons, reflecting the structure of the underlying basement, and how the fault network affects some of the layers (Figure 7-5). From the top Buntsandstein isobaths map, a structure can be defined following a closure isobath at about 1650m depth-bmsl (Figure 7-7).

The PilotSTRATEGY project has received funding from the European Union's Horizon 2020 research and innovation programme under grant agreement No. 101022664

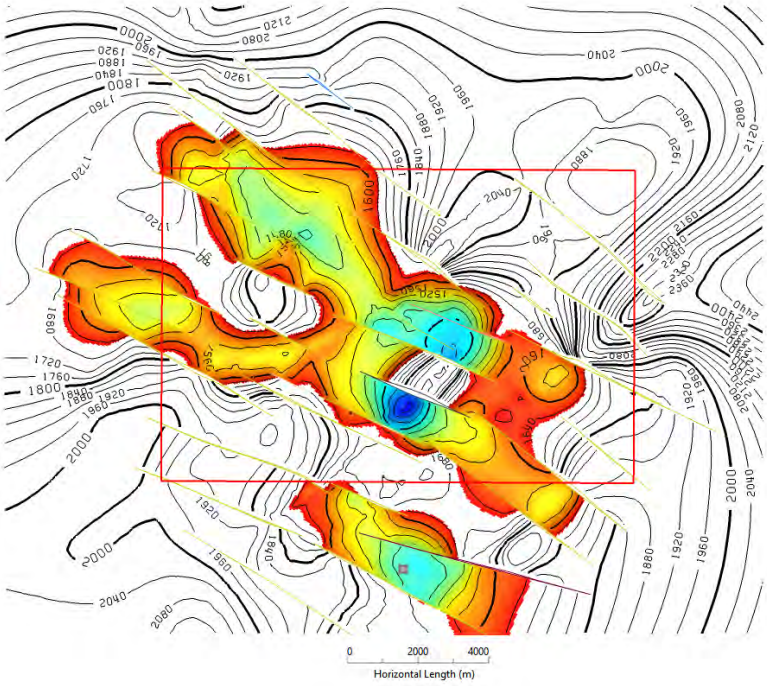

Figure 7-8 Isobaths of the top of the Buntsandstein fm. showing the structure with the probable closure for containment, at about 1650m depth (bmsl). The red box limits the area of interest proposed initially. The smaller structure at the south corresponds to the one explored in the 80's and drilled with the Lopín-1 well (grey point). Red colors are deeper than bluish ones.

The trap consists of a basement NW-SE horst. The current faults can actually connect the Buntsandstein formation with above Muschelkalk formations (M1 and M3). The main regional sealing formation is the Keuper which is not affected by the reservoir faults in this area. In conclusion the reservoir bounded by a series of stepping normal faults and gentle dip-closings. The sealing formations are the shaly/evaporitic formations (Rané Fm, Muschelkalk M2 and, above all, Keuper deposits).

7.2.4 Log analysis and Petrophysics

Comprehensive description of methodologies, log data, petrophysics results are located in Spain Annex section.

7.2.4.1 Reservoir Pressure and Temperature Assessment

Existing wells reports and well log header data were used to estimate reservoir temperature and pressure.

Temperature

The temperatures gradients estimated in the near boreholes are considered to be normal gradients, the wells Ebro-2, Ebro-1, Lopín-1, Caspe-1 Sariñena-1 and Chiprana-1 have temperature gradients about 28-32 °C/km, and the wells Monegrillo-1, Mayals-1 and Cadasnos-1 have gradients about 36-40 °C/km.

Pressures

The rest of the studied wells show pressures above the fresh water hydrostatic pressure. Specifically, the closest wells are summarized at the table. The pressures measured with DST (Drill Stem Test) in

The PilotSTRATEGY project has received funding from the European Union's Horizon 2020 research and innovation programme under grant agreement No. 101022664

Cadasnos-1 (37km E from Lopín) and Sariñena-1 (30mm NE from Lopín) are consistent with a fresh water hydrostatic pressure which could indicate communication of the reservoir with surface water inputs.

Wells	Formation pressure at Bundsandstein (bar)	Depth top Bundsandstein (m below sealevel)
Monegrillo-1	162	909
Chiprana-1	217	1392
Ebro-1	205 (from mud density data)	1341

7.2.4.2 Log analysis

In the logs the Buntsandstein has been split in three parts: basal conglomerates, middle sandstone sequences (Unit B1) and shaly top formation (Unit B2).

Buntsandstein Basal Conglomerates

This formation directly overlays an erosive unconformity over Paleozoic rocks. In the well logs it is characterized by an increase in electrical resistivity, density and a decrease in slowness (interval transit time; Figure 7-9). The gamma ray (GR) curves show a diverse shale volume (Vsh) between wells, most likely related to the distance to the source area.

Porosities calculated in Ebro-1 (well locations in Figure 7-6) are plotted in Figure 7-9. The porosities calculated with different methods varies in this formation from an average of 3% in Ballobar-1 to 10% in Caspe-1 and Fraga-1 wells. Ebro-1 well (closer to the study area than the other analysed wells) shows average calculated porosities of 5%. Wells Fraga-1 and Caspe-1 show low Vsh values (5-7%) and in the rest of wells it varies between 16 to 50%.

Buntsandstein Sandstones (Unit B1)

In this formation interval transit time (sonic log) and formation density show some peaks that could indicate more cemented sandstones (Figure 7-9). At the time of writing (July 2023) we are awaiting permeability analysis on new samples. No permeabilities were analysed in this report.

In the Ebro-1 borehole, porosities seem to increase from bottom to top, in contrast Vsh values decrease (Figure 7-9). The bottom section shows a small discrepancy between Vsh values from GR-Index and neutron porosity / bulk density calculations. The B1 calculated porosity from nearby wells are: Caspe-1 and Fraga-1 have averaged porosities around 16 – 22 %, and Ebro-1, Ebro-2 and Ballobar-1 have rather constant porosity of about 10 % in average, similar to samples obtained from field analogues and the Chiprana-1 borehole.

In Ebro-1 we could have Vsh 29% (Neuton / Density logs) or Vsh 15% (Gamma-ray logs) averaged depending on the appraisal method selected. GRi-Vsh average values have been compared: Ebro-1, Ebro-2, Ballobar-1 and Fraga-1 show around 12-15%, while Caspe-1 is 7%.

The PilotSTRATEGY project has received funding from the European Union's Horizon 2020 research and innovation programme under grant agreement No. 101022664

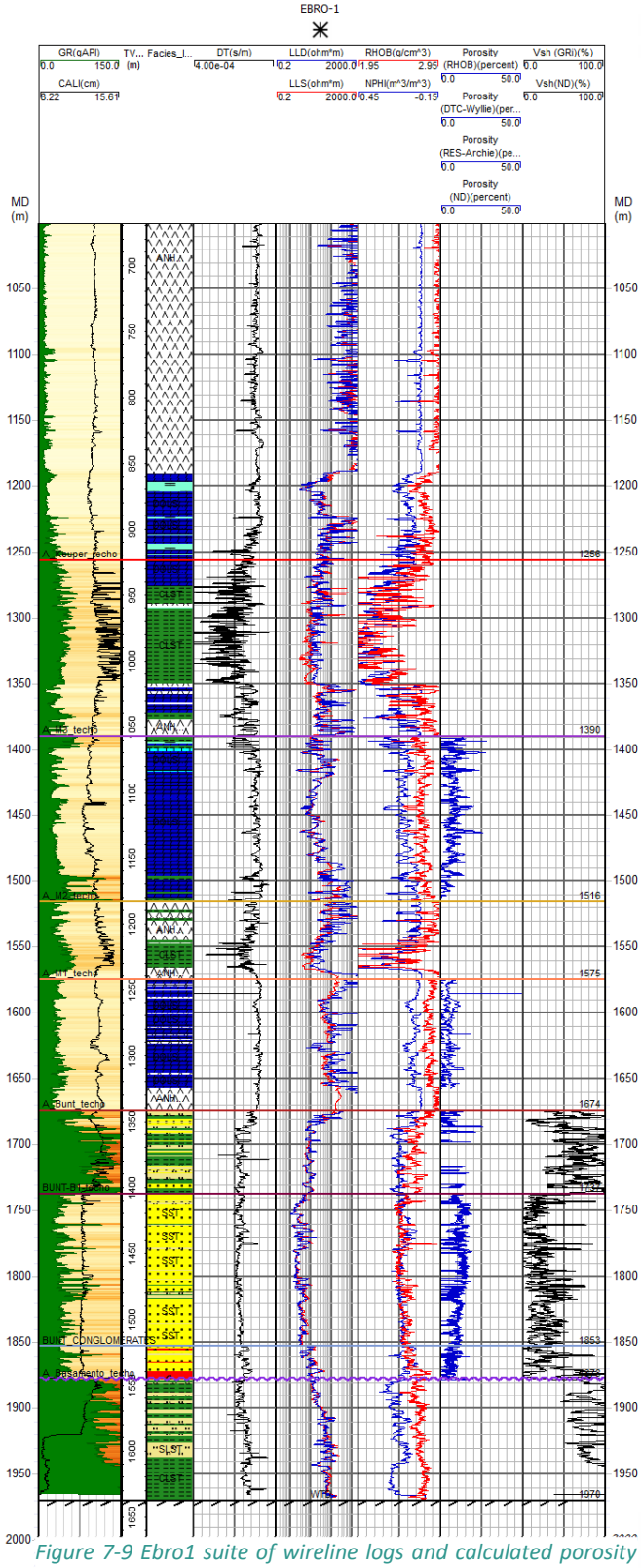

Figure 7-9 Ebro1 suite of wireline logs and calculated porosity and Vsh in Triassic formations.

Buntsandstein Sandstones and Shales (Unit B2)

This formation overlays the main reservoir. Compared with unit B1 it displays an increase in electrical resistivities and density. Sonic transit time logs show little to no change.

There may be well washouts, due to the shaly levels collapse (Figure 7-9). The calculated porosities in sandstones are: Ballobar-1, Fraga-1, Ebro-2 and Ebro-1 between 3 to 10% average; Caspe-1 has a higher average of 20%. The Vsh values for the whole formation are high, in the 5 analysed wells (Ballobar-1, Fraga-1, Caspe-1, Ebro-1 and Ebro-2) it varies between 60 to 81% average.

Muschelkalk M1 & M3

The Muschelkalk in the area has been divided in three members, called M1, M2 and M3 (from bottom to top). M1 and M3 are thick dolomitic formations with some intercalations of anhydrites or salts, and / or marls / limestones (Figure 7-9). Mud losses are commonly reported at the base of the M3 formation during drilling, indicating that these formations have some effective porosity (possibly fractures?). Porosity calculations for these two formations in the Ebro-1 well, which is closest to the area of interest are 2 to 4% average in M1 and 6% average in M3.

Muschelkalk M2

This formation consists of anhydrites, salts and shales. It is considered to be a seal formation (Figure 7-9).

Keuper

This is the main regional seal formation of the area. In the Lopín-1 well, from bottom to top, there are shales with some thick levels of salts, thick level of shales with some thin anhydrites and finally anhydrites with some dolomitic intercalations (Figure 7-9).

7.2.5 Stratigraphic well correlation

Well correlations point out to useful trends in the reservoir geology (Figure 7-10, Figure 7-11 and Figure 7-13). The interpolation of the Total Vertical Thickness of the Conglomeratic facies points to a source area located to the SW of the basin (Figure 7-10). The Total Vertical Thickness of the B1 formation (main reservoir) increases eastward, notably Caspe-1 and Ballobar-1 have a much thicker B1 formations than other wells (Figure 7-11). The B2 formation shows a much more complex thickness distribution, which may be linked to the paleo-geography (?).

The PilotSTRATEGY project has received funding from the European Union's Horizon 2020 research and innovation programme under grant agreement No. 101022664

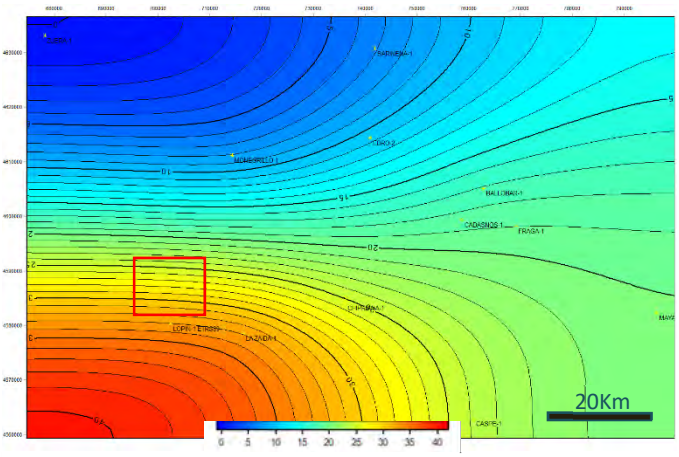

Figure 7-10 Buntsandstein basal conglomerates thickness (True Vertical Thickness-TVT meters) interpolated (Discrete-Smooth-Interpolation-DSI). Red Box= Area of Interest

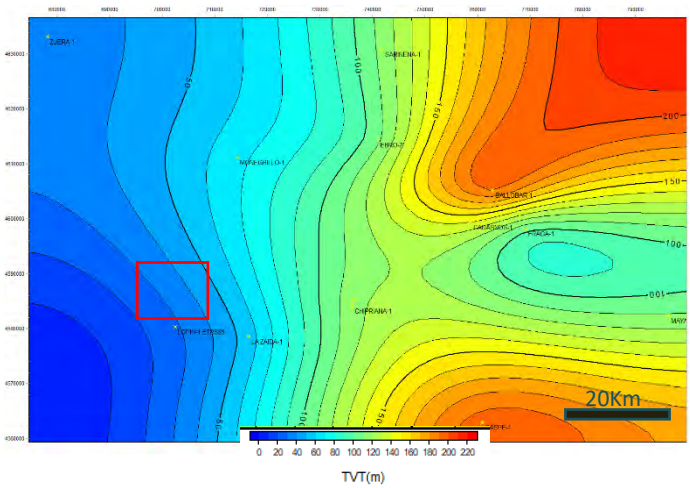

Figure 7-11 Buntsandstein Sandstone (B1) TVT interpolated using DSI. The Buntsandstein thickness in this area increases slightly eastwards, but the eastern-most wells show huge increases. Red box=AOI.

7.2.6 Reservoir Facies

7.2.6.1 Reservoir Facies

The Permian unit (basement) is a series of polymictic conglomerates, with abundant sub-angular Paleozoic quartzites and with some sand intercalations, which are structured in more or less horizontal strata from 0.5 to 2 m thick, quite well sorted. Coarse sandy strata with cross-bedding may be interbedded. They are interpreted as gravel bars, from braided alluvial systems, in some cases passing laterally to sand bars.

The Triassic series are compounded of three Germanic facies: Buntsandstein, Muschelkalk and Keuper. The Buntsandstein facies are composed of the three formations: Aranda, Carcalejos and Rané (Figure 6-4). In this case, Aranda and Carcalejos formations correspond to units B-1 and B-2, respectively, as they are usually named in the oil and gas industry in this area (Aurell et al., 2001. In the well logs analysis Rané formation is not defined (Figure 6-5), never the less B-2 unit gradually pass upwards to Rané formation.

The PilotSTRATEGY project has received funding from the European Union's Horizon 2020 research and innovation programme under grant agreement No. 101022664

Unit B1

The lower section of the B1-Unit is a succession of red conglomerates up to 1 to 5 m thickness with fining-upward cycles. The conglomerate is matrix-supported and predominantly contains quartzite pebbles.

At the bottom and top of Unit B1, red sandstones stratum thinning trends are recognized, fining upwards from medium to fine grain size. The base is slightly channeled. They are organized in tabular strata with an average thickness of 1.5 m. It is made-up of sub-rounded to sub-angular quartz, with less abundant feldspar and clays (Figure 7-12 a and c). Laterally and vertically these pass into fine-grained red sandstones (Figure 7-14).

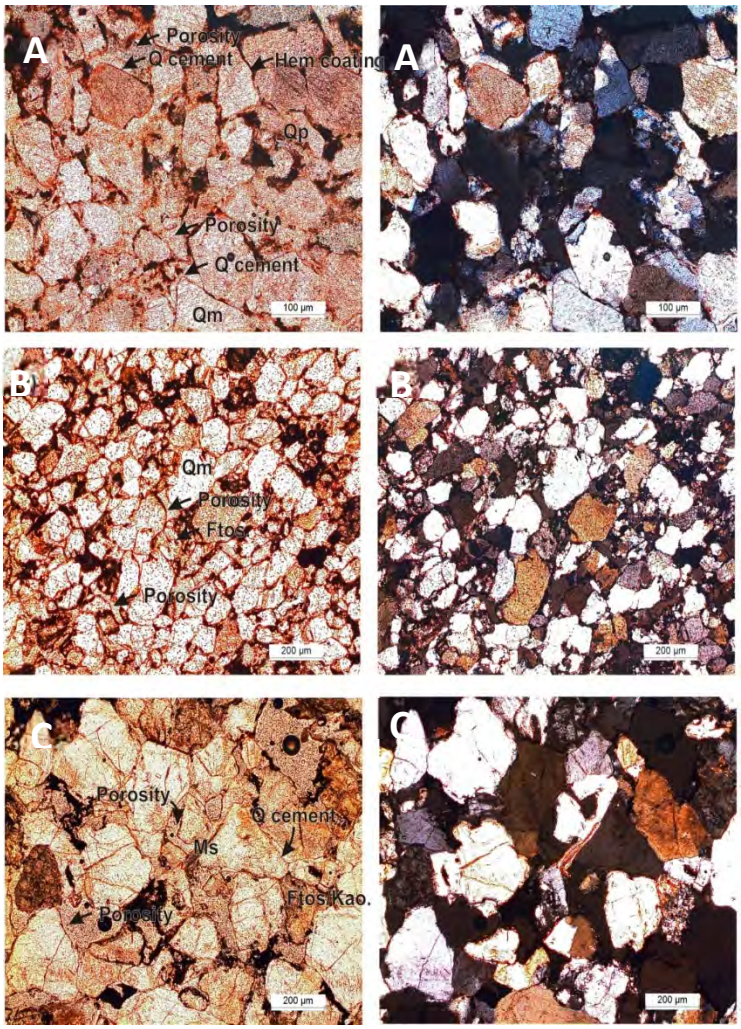

*Figure 7-12 Representative microphotographs of thin sections (parallel and crossed nicols). **A**. Cross.bedding sandstone, bottom of Unit B1; **B.** Cross.bedding sandstone, top of Unit B1; and **C**. Cross bedding sandstone, top of Unit B2.*

Unit B2

The boundary is marked by an increase in floodplain facies resulting in isolated sandstone beds and partly amalgamated complexes, but also single-storey bodies. The section of this unit is recognised by

The PilotSTRATEGY project has received funding from the European Union's Horizon 2020 research and innovation programme under grant agreement No. 101022664

tabular, sheetlike, pink to red sandstone bodies with a thickness ranging between 2 and 5 m and extending laterally for 100 – 200 m. Grain size ranges from medium to coarse sand, with fining upward sequences (Figure 7-12c). Alternating with the red sandstone bodies there is very fine sand to silt that reach up to 20 m in thickness. These beds are dark red in colour, finely laminated and commonly include a high mica content. The top of these silts are frequently recognised by red muddy/silty palaeosols.

Petrology of the Units B1 and B2.

The detrital mineralogy of Unit B1 is dominated by monocrystalline and polycrystalline quartz. Unit B1 samples are >75% quartz (quartz arenites). While in the detrital mineralogy the Unit B2 samples are mainly compound of monocrystalline quartz and muscovite (Figure 7-12c). Feldspar is the second most abundant detrital component. Fe-oxide cements represent the major grain coating phases. On average, the three sample sets bear authigenic phases that include illite, syntaxial quartz overgrowths and kaolinite.

7.2.6.2 Reservoir Architecture

Reservoir architecture was reconstructed using field analogues and the Chiprana-1 core (Figure 7-14). In general, the Buntsandstein facies is of fluvio-lacustrine origin, with main fairways to the NE, and the main sediment supply from the SW (Arche et al., 2004). At the end, the entire basin was flooded by the Proto-Tethyan Sea from the East, resulting in the deposition of claystones and dolostones in a brackish to marine coastal plain (Rané and Muschelkalk Formations).

7.2.6.3 Reservoir Properties

The optical porosity is intergranular and some is secondary from feldspar leaching. Porosity is mainly controlled by grain size (with a wide variability), clay content and quartz cements presence (more quartz cements equates to more porosity). Porosity is, however, very variable. The vertical to horizontal permeability (k_v/k_h) ratio is in general very low; the highest is located in the braided channel-fills (0.01). In contrast, ephemeral channel-fills and sheetflood sandstones have k_v/k_h ratios of 0.001. Sandbody continuity is higher at the bottom and top of Unit B1. The upper sandbodies of B2 are more isolated and would be expected to have along-channel linear fluid flow.

7.2.7 Seal Facies

7.2.7.1 Stratigraphy

The fluvial Röt facies or Rané Formation (Arche et al., 2004) is the potential seal. Red sandstones and siltstones change upwards into very fine to fine grained sandstone with mud and siltstone, with some salt. Shales tend to be thicker towards the top. Bed thickness varies from 5 to 10 cm and sandstone content decreases towards the top. Analogue fields show the top formation is composed of laminated fine mudstone alternating with shales and tepee structures. This transition zone from continental to marine sedimentation also includes minor gypsum horizons. The thickness of this heterolithic unit reaches 15–40 m.

7.2.7.2 Seal Properties

From XRD analysis the Röt facies or Rané Formation is composed of quartz and phyllosilicates. In field samples, anhydrite appears as a trace mineral replace by calcite or dolomite, but analysis carried out in the Monegrillo-1 borehole, to the north of the Lopín structure, indicate common anhydrite.

The PilotSTRATEGY project has received funding from the European Union's Horizon 2020 research and innovation programme under grant agreement No. 101022664

Likewise, electrofacies analysis (Rueda, 2022) shows that the gamma ray log has serrated curves and varied geometries. In the case of Chiprana-1, Caspe-1 and Ebro-2, it is cylindrical, indicating shales with anhydrite and sandstone intercalations.

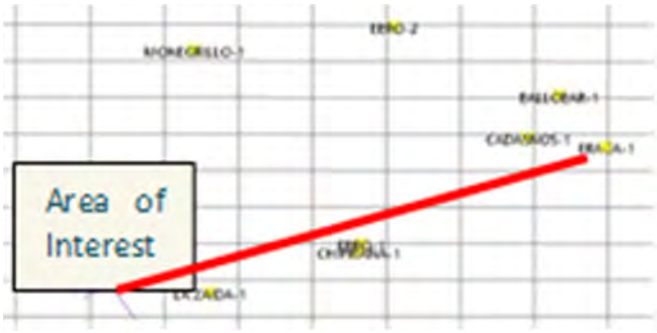

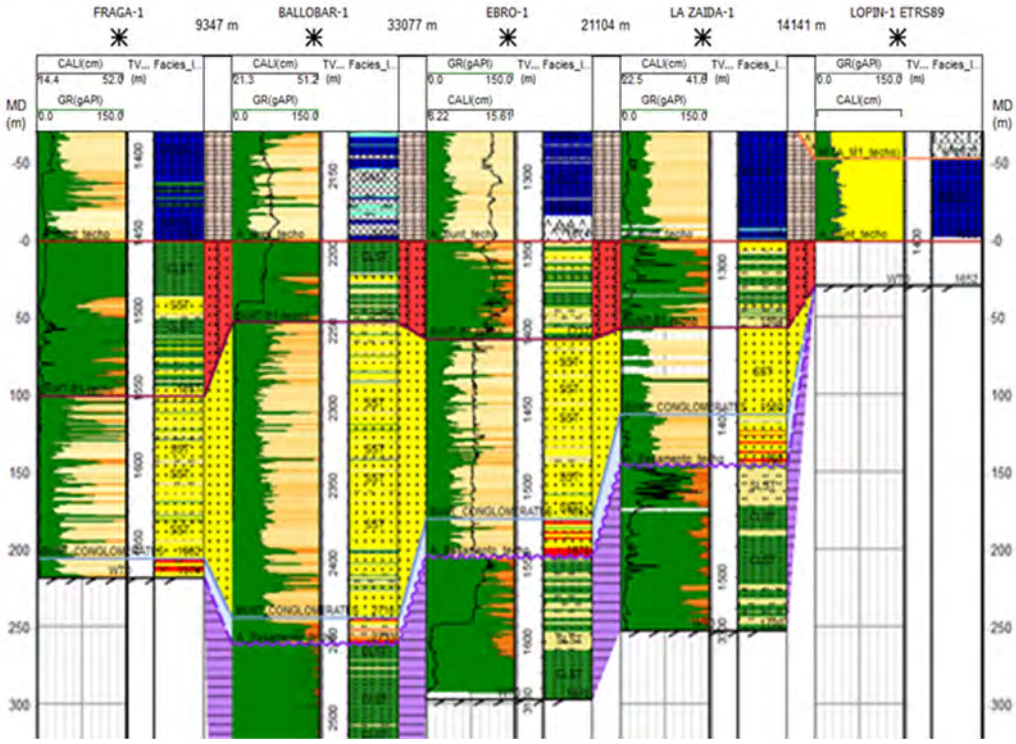

Figure 7-13: (this and next page) Formations correlation ENE-WSW and SE-NW, top of Buntsandstein flatten, note the increase in thickness to E and SE, as well as a slight increase in the Vsh (lower GR values) to the NE in the Buntsandstein formations (yellow). Caspe-1 shows a very thick Buntsandstein formation (next page).

The PilotSTRATEGY project has received funding from the European Union's Horizon 2020 research and innovation programme under grant agreement No. 101022664

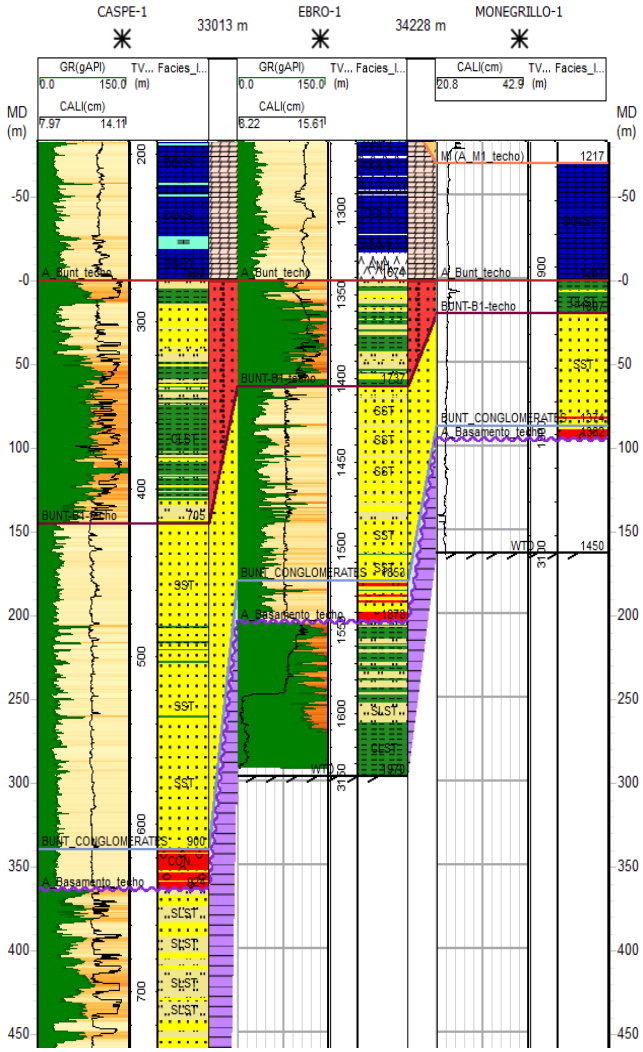
CASPE-1
33013 m
EBRO-1
34228 m
MONEGRILLO-1
MD (m)
GR(gAPI)
CALI(cm)
A_Bunt_techo
BUNT-B1-techo
BUNT_CONGLOMERATES
A_Basamento_techo
M1(A_M1_techo)
WTD

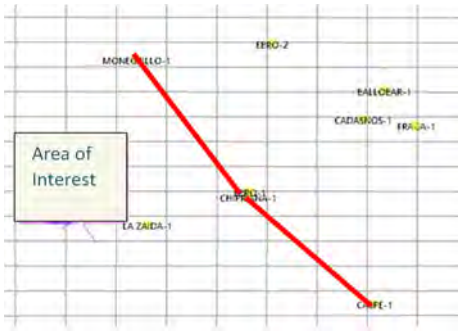
MONEGRILLO-1
EBRO-2
BALLOBAR-1
CADASROS-1
ERAGA-1
Area of Interest
LA ZAIDA-1
CASPE-1

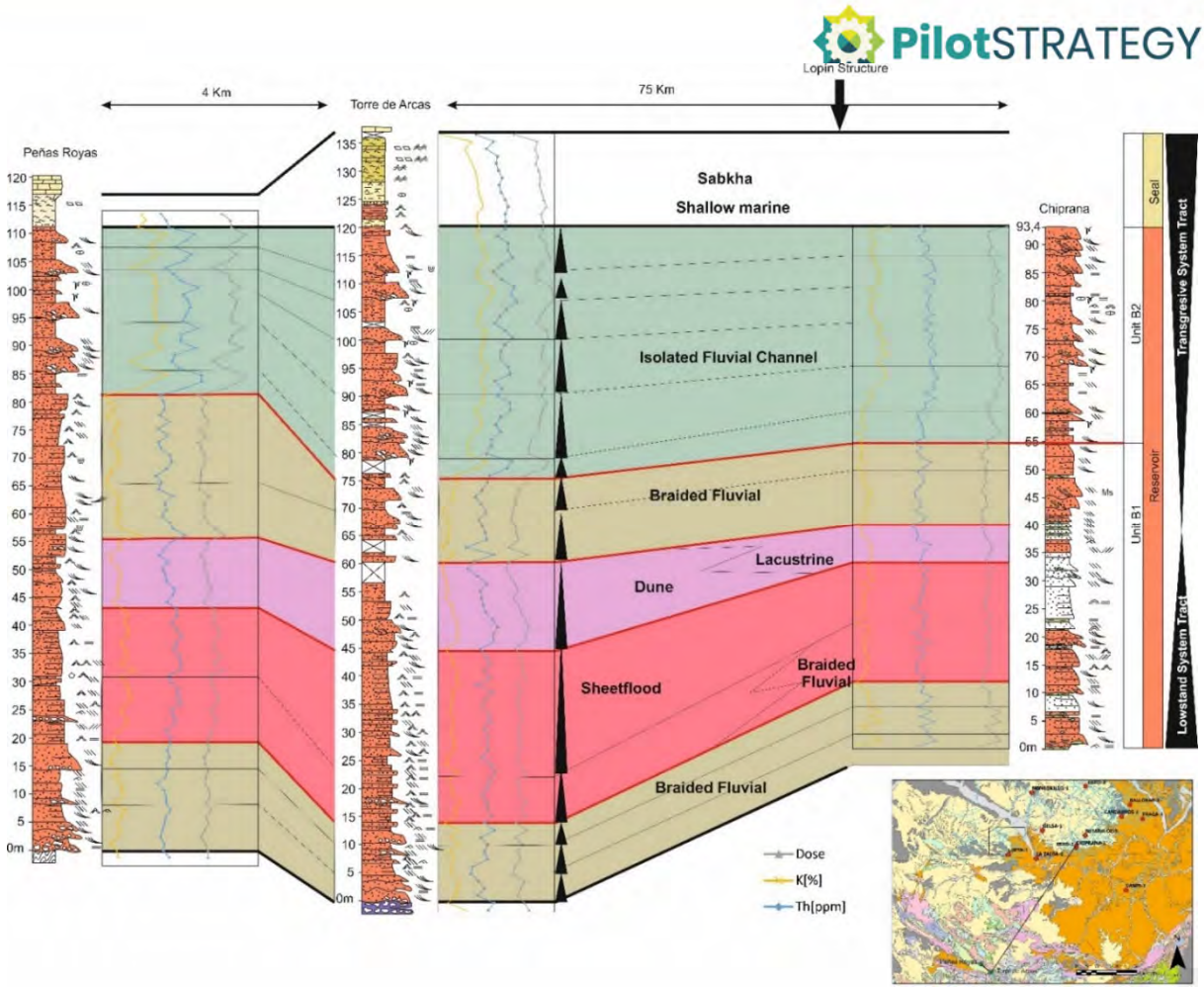

Figure 7-14: *Stratigraphic correlation*

7.3 Storage Complex Characterization (France)

7.3.1 Horizons and fault interpretation in the area of interest

Seven horizons have been interpreted which delimit six seismic units (Figure 7-15). There are no major unconformities in the area however the single sequence boundary (Sb-Comb see previous section) is the lateral equivalent of an unconformity in the easternmost Paris Basin, although it conformable in the study area (a correlative conformity surface). Consequently, seismic interpretation is based on a stratigraphic framework defined along wells. Particularly the Clos Fontaine well (CLF-1), a unique well in the study area with both a velocity-depth relationship and checkshot data. The seismic units are here described from top to bottom.

- **Unit I – Caprock 2 (Top_Oxf_Upper to Top_Oxf_Lower)**

This first seismic-unit corresponds to the second unit defined as caprock (Figure 6-8). The unit is bounded by the horizons Top_Oxf_Upper at the top and the Top_Oxf_Lower horizons at the bottom. It shows an homogeneous thickness distribution between 106 and 128 ms. After time / depth conversion, this thickness corresponds to 246 to 297 meters with a total volume estimation of 30 Km^3, and a projected surface of 110 Km^2 (Figure 3-17).

- **Unit II – Caprock 1 (Top_Oxf_Lower to Ca26)**

This second units is identified as the first caprock interval located above the reservoir section (Figure 6-8). The top of the unit is bounded by the horizon Top_Oxf_Lower, which corresponds in the area to a major vertical facies variation from marls to tight limestone, at the boundary between Caprock 1 and Caprock 2. The bottom of the unit is the Ca26 horizon, which is the transition between the reservoir facies of the Dalle Nacrée Formation and the Callovian caprock. The unit is isopachous with an absence of strong thickness variations (55-75 ms corresponding to 100 -130 m). The projected surface of the unit is 110 km^2. As observed on seismic lines, the unit does not show variations in amplitude and has a tabular geometry.

The combination of seismic units I and II corresponds to the full caprock of the storage complex, an interval of marls and tight limestones (offshore mudstones). Thickness varies between 366 and 413 m, which is approximately twice as thick as the reservoir itself.

- **Unit III – Reservoir 2 (Ca26 to Ca24)**

This unit represents the top reservoir interval defined in the storage complex. It is associated with the Dalle Nacrée Formation, which is isolated oolitic shoals deposited during a transgressive stage. The Horizon Ca26 delimits the top of the unit and its bottom corresponds to the horizon Ca24. This seismic unit is isopachous but only 6 to 10ms thick, corresponding to 12-20 m. The top of the reservoir is located between 1763 and 1682 m below sea level. Attention was paid to the quantification of uncertainties in these estimates because the seismic resolution is only 4 ms. Amplitude variations and internal geometry of the unit cannot be distinguished because of the low resolution and thickness of the unit itself.

- **Unit IV – Semi-permeable 1 (Ca24 to Sb-Comb)**

Associated to the Calcaire du Comblanchien formation, this semi-permeable unit is important to characterise for static and dynamic modelling. Top and bottom of this seismic unit is respectively

The PilotSTRATEGY project has received funding from the European Union's Horizon 2020 research and innovation programme under grant agreement No. 101022664

horizons Ca24 and Sb-Comb. As with previous seismic unitsFigure 3-18, this unit has thickness varying from only 6 to 10 ms (11 to 25 m). As previously mentioned with the Reservoir 2 unit, these thickness variations are close to the seismic resolution of 4ms. Due to the low thickness, it is not possible to specify internal geometry and amplitudes characteristics of the unit.

Unit V – Reservoir 1 (Sb-Comb to Bj1)

This last unit is the main reservoir target, the Oolithe Blanche Formation. In detail, this reservoir section is divided into two intervals with a first one denominated by a prograding system tract and bounded by Bj1 (bottom) and Bt10 (top) horizons. The second interval corresponds to the aggrading system tract, bounded by the Bt10 and S-Comb horizons. Distinguishing these units is not possible on the 3D seismic data, but the 2 units will be used as internal architecture during static modelling, based on well correlations. Processed thickness map indicate a potential thickening to the South East. This thickness variation ranges between 80 and 60 ms (133 to 211 m). The top and bottom of the seismic unit are conformable and do not show seismic toplap or onlap. A slight fanning geometry could be interpreted in the seismic unit only seen using extreme vertical exaggeration.

The PilotSTRATEGY project has received funding from the European Union's Horizon 2020 research and innovation programme under grant agreement No. 101022664

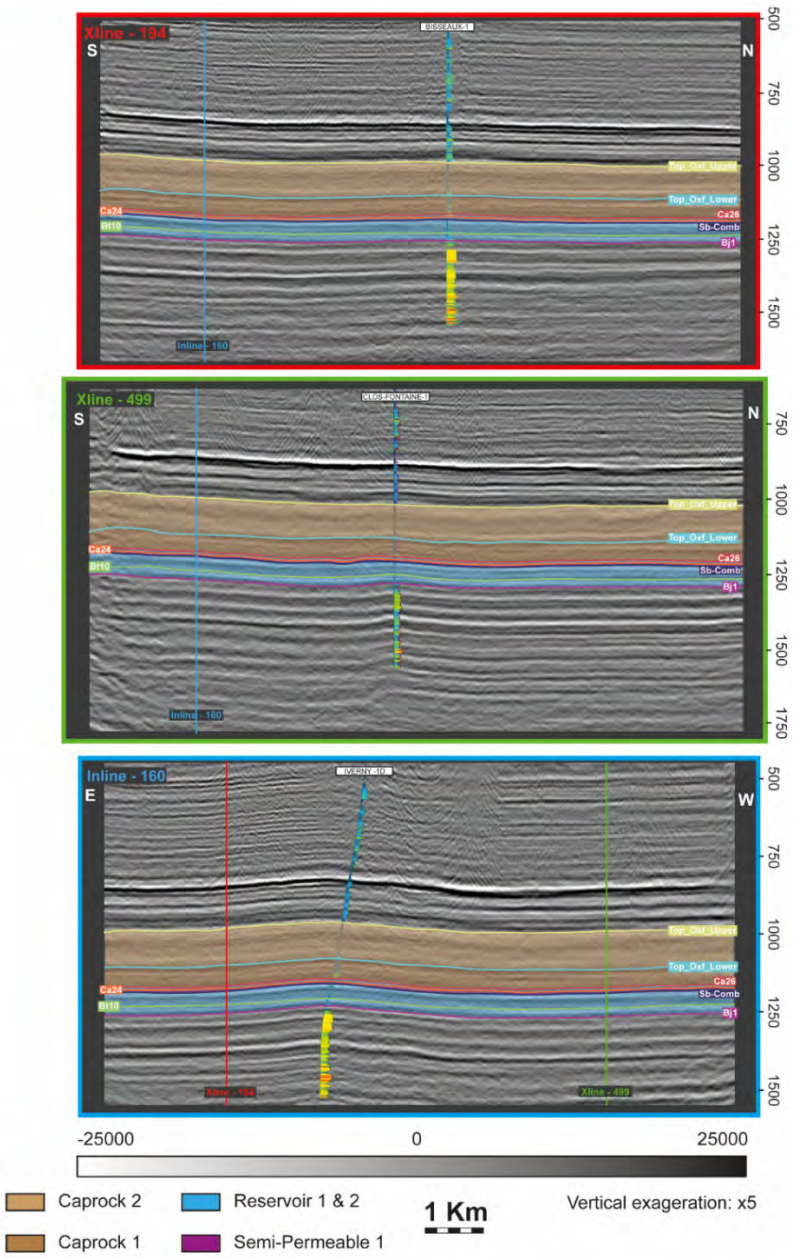

Figure 7-15: Seismic interpretation of storage complex horizons and distribution of caprock and reservoir intervals along three seismic lines. The locations of the seismic lines are shown on Figure 5-4. Vertical scale is in Two Way Time (ms)

The PilotSTRATEGY project has received funding from the European Union's Horizon 2020 research and innovation programme under grant agreement No. 101022664

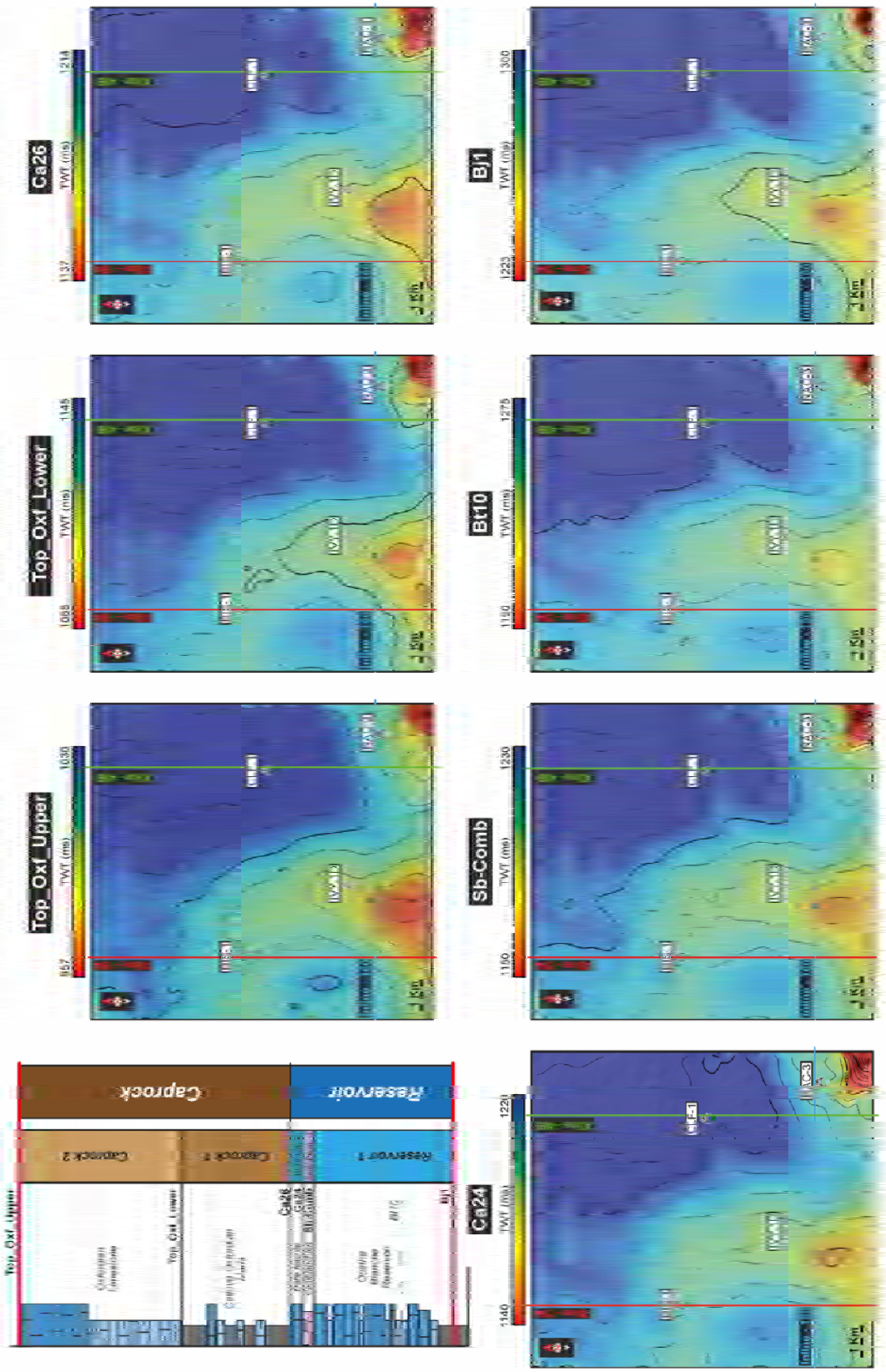

Figure 7-16: Isochron maps of storage complex horizons. Maps in Two Way Time (twt – ms).

The PilotSTRATEGY project has received funding from the European Union's Horizon 2020 research and innovation programme under grant agreement No. 101022664

7.3.2 Characterization of trap(s)

Seismic interpretation and isochron / isochore maps indicate two geological structures in the restricted AOI. Analysis of isochron maps of all horizons lead to the identification of two main structures called the Charmotte and Clos-Fontaines folds.

7.3.2.1 The Charmotte fold

The Charmotte fold is visible in the southern part of the area and it affects the entire sedimentary pile. This structure dips to the north and the fold crest is convex to the west. As shown on *Figure 7-17*, the Charmotte anticline is 4 km wide and flattens to the north with a width of 3.7 km. From its apex to its end, the anticline length is 7.5 km. This structure has been explored in the past as proved by wells BIS-1 and IVY-1D. This important structure is the structural trap of the southern Charmotte oil reservoir exploited by Vermilion Energy.

The PilotSTRATEGY project has received funding from the European Union's Horizon 2020 research and innovation programme under grant agreement No. 101022664

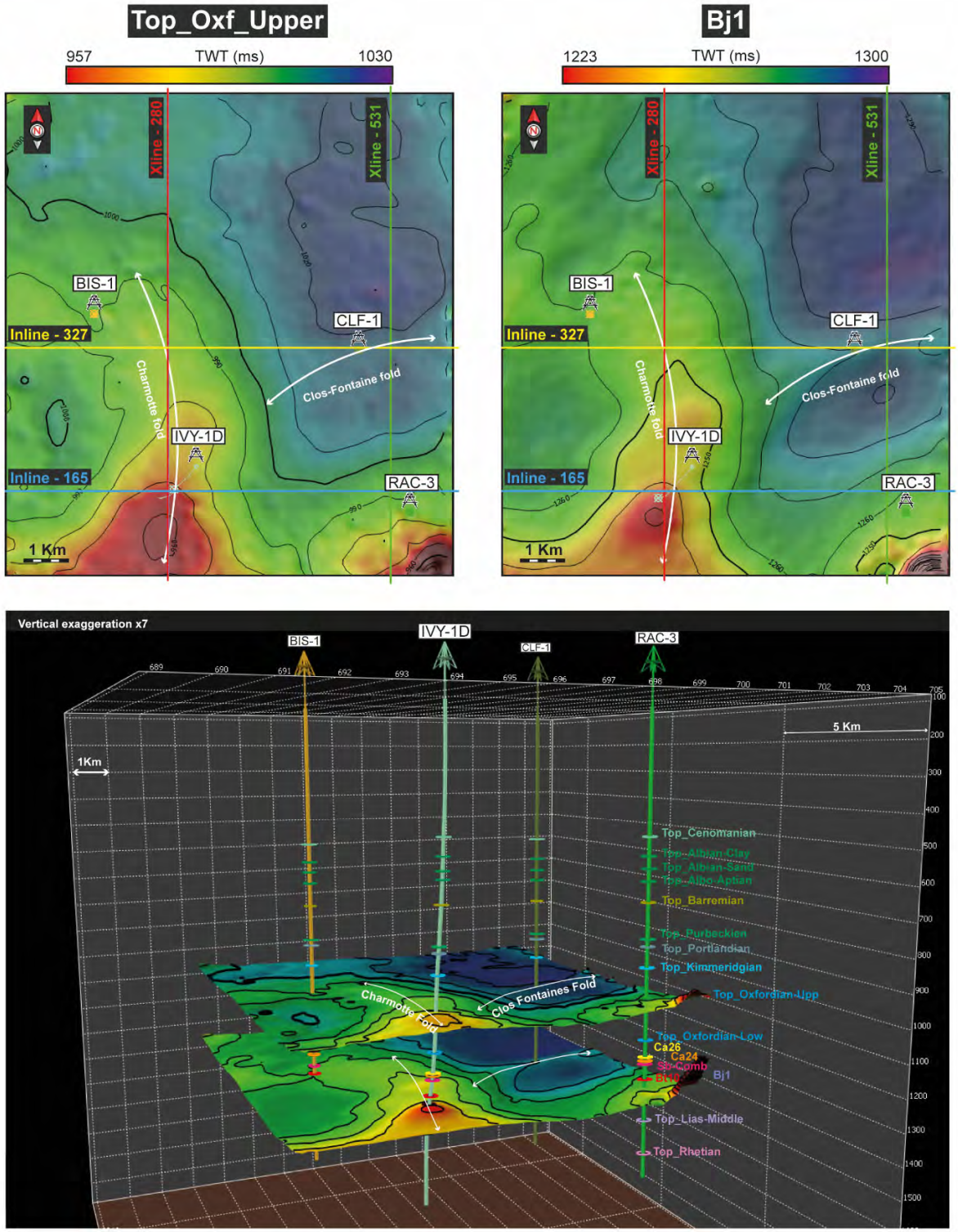

Figure 7-17: Map and 3D view of the Charmotte and Clos Fontaine folds

The PilotSTRATEGY project has received funding from the European Union's Horizon 2020 research and innovation programme under grant agreement No. 101022664

7.3.2.2 The Clos-Fontaine fold

The second structure, which we have named the Clos-Fontaine anticline, corresponds to the small anticline visible on time maps from Top_Oxfordian-Low to Top_Rhetian (*Figure 7-17*). This small structure has a N45°E direction with a deepening to the East-North-East. This small structure affects only the base of the sedimentary pile, which includes the reservoir complex. Its width is between 1.8 km and 500m and its length reaches 3 to 4 km. On seismic data, a fault is observed at the edge of this structure, which mostly impacts Triassic sedimentary units.

7.3.3 Log analysis and Petrophysics

7.3.3.1 Qualitative study – depositional environment determination

A qualitative study has been conducted on all well logs used in the study, from both the extended and the restricted area. It relies on electro-facies classification stemming for a combination of wireline attributes, especially the gamma ray, density, sonic, neutron and resistivity logs. It remains a qualitative approach in the sense that classification is 'hand-made' and does not rely on automatic and quantified analysis. Furthermore, it does not account for high resolution variations. However, it permits a fast and relative reliable interpretation of the reservoir units as it is consistent with cores description (Figure 7-18). It must be noticed that a condensed facies was identified typical of hard-ground texture (high gamma ray and density values).

Depositional environment from sedimentological description	Depositional environment interpreted on well logs
Upper offshore	Offshore upper
Lower offshore	Offshore lower
Outer ramp	Tight limestone
	Outer shoal
Shoal / Middle ramp	Shoal
Back-shoal	
Tide-dominated lagoon	Lagoon
Lagoon	
Condensed	

Figure 7-18: Table resuming relationship between depositional environments interpreted though sedimentological facies from core and well logs data.

47 wells in the extended AOI has been interpreted. Figure 7-19 shows an example of this interpretation along the CLF-1 well. Depositional environment, sequence stratigraphic scheme and vertical facies variation are clearly linked. Oolitic shoal deposits are the most encountered "facies" within reservoir complex with an average of 40% abundance. Next in abundance are offshore (upper / lower) and outer ramp domains. Lagoons only presents 8% of the occurrences.

The PilotSTRATEGY project has received funding from the European Union's Horizon 2020 research and innovation programme under grant agreement No. 101022664

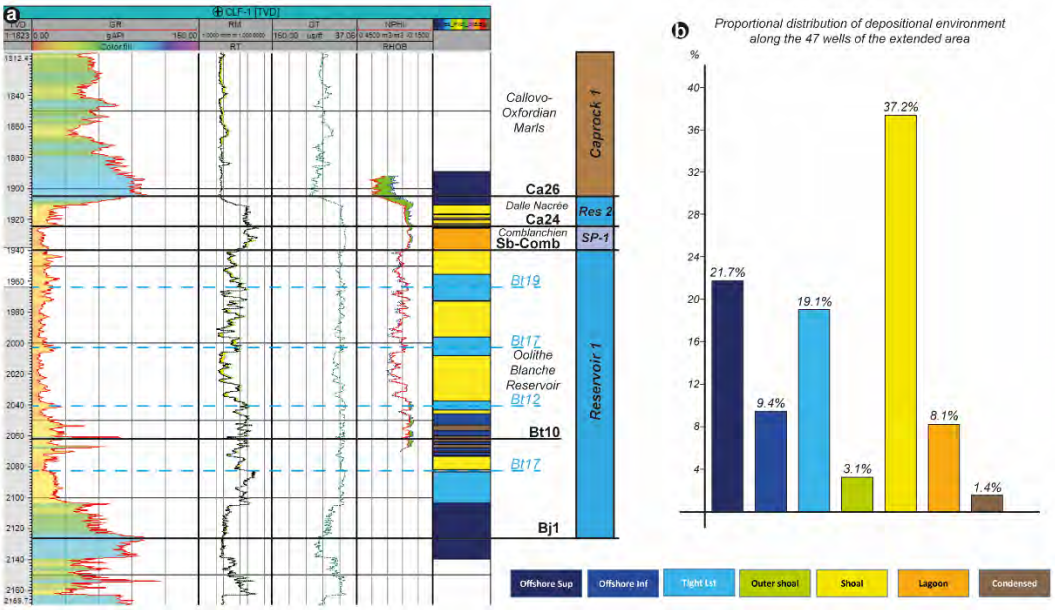

Figure 7-19: a. Example of qualitative depositional environment interpretation along CLF-1 well. b. Histogram showing the proportional distribution of depositional environment along the 47 wells of the extended AOI.

7.3.4 Quantitative analysis – Rock-type classification

As a second approach, a rock-type (RT) analyse was conducted on the wireline logs. As observed during the sedimentary analysis, reservoir properties in the Dogger ramp are mostly driven by ooids versus bioclast distribution plus diagenesis. Consequently, the RT study only focuses on the classification from poor to the best reservoir qualities.

Four specific cross plots has been used: (i) sonic vs. neutron porosity ; (ii) acoustic impedance vs. neutron porosity ; (iii) gamma ray vs. neutron porosity ; and (iv) density vs. neutron porosity. Neutron Porosity has been systematically used in cross plots since it is a direct reservoir investigation tool and is calibrated for (calcite) limestone by default. A third dimension was adding by colouring the plotted points according to the gamma ray value. This colour permits a rapid identification of effective porosity versus total porosity which reaches its maximum within argillaceous sediments of the offshore facies.

Analysis of the different cross plots classifies the Dogger into five to six group of points that we call EF1 to EF5 (or EF6) from the least to most porous RT (Figure 7-20). It is noteworthy that EF1, which we consider to be marl facies, is always high porosity and high gamma ray value. After plotting the rock types on logs and comparing with effective porosity and reservoir layers, it appears that most of the cross plots give similar results and fit with effective porosity trends. This is explained by the common use of the Neutron Porosity as an axis for every cross plot. However, some limits could already be considered for acoustic impedance and gamma ray cross plots which do not fit perfectly with effective porosity logs.

To improve this first raw classification, a similar study was undertaken using only log intervals where sedimentary description has been conducted.

The PilotSTRATEGY project has received funding from the European Union's Horizon 2020 research and innovation programme under grant agreement No. 101022664

This approach reveals that the RT groups defined by the density versus neutron porosity cross plot have the best fit with reservoir facies. Electro-facies comparison indicates that EF1 to EF5 correspond to marls, bioclastic packstone, oolitic or bioclastic wackstone / grainstone, oo-bioclastic grainstone, and very-fine grainstone respectively. The last electro-facies (EF6) is not identified in core because it is only found in the deeper (uncored) part of the reservoir. Unfortunately, this facies is likely to represent the most suitable reservoir intervals. This is probably a similar facies to one already described but with less cementation due to diagenesis.

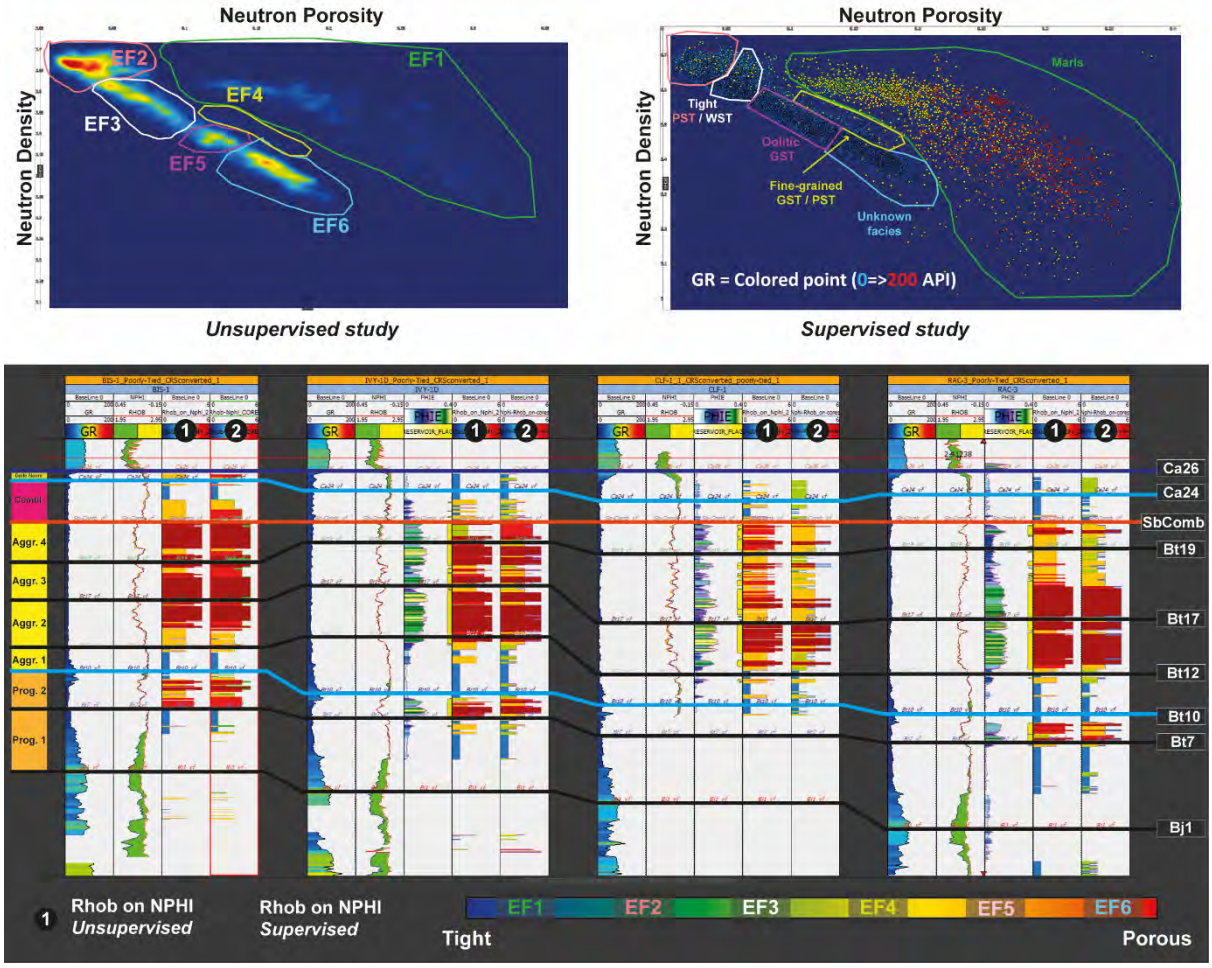

Figure 7-20: vertical plot of different rock-type classification

7.3.5 Well-Seismic stratigraphic correlation

All horizons interpreted on the seismic data correspond to specific markers identified in wells. They mark specific offsets of the wireline logs and maximum or minimum values for certain logs (e.g. gamma ray, sonic). Rapid offsets are likely to represent abrupt facies or lithology variations and to bound depositional sequences and/or lithostratigraphic units (e.g Sb-Comb). These markers not only represent sudden offset within the geophysical signal; they point to key inflexion points in the signal representing the progress of a progradational or retrogradational trend, i.e. respectively a maximum regressive surface and a maximum flooding surface.

This interpretation, followed by correlation between wells has been done on the 47 wells present in the extended area. This identification and well log correlation has been interpreted thought the full

sedimentary pile and the specific markers within the storage complex. The table presented in Annex (France) Appendix 5 describes all the markers, their corresponding horizons and their link to the storage complex of the studied area.

7.3.6 The reservoir properties of individual facies

An important dataset of plug data is available, together with petrophysical analysis in the literature about both geothermal and CCS prospects. We generated porosity-permeability cross-plots to determine the porosity – permeability (Ø/k) relationships. A first approach consists in producing an average Ø/k law for each depositional environment identified from well data. A second one stems for Ø/k law for each rock-type identified.

7.3.6.1 Reservoir Properties by depositional environments

In the 372 meters cores described and sampled for reservoir properties characterisation, only four depositional environment have been defined using well log data. These depositional environments are lower and upper offshore, shoal and lagoonal environments. The lower offshore cannot been sampled and plugged for reservoir properties characterisation because of the rheology of the marls. Consequently, only lagoon, shoal and upper offshore has been sampled. The outer ramp system (tight limestone and outer shoal environment) and condensed interval has not been sampled.

7.3.6.1.1 Upper offshore depositional environment

Only three samples are available from this environment. Consequently, no reliable Ø/k law is possible. A single value will be applied to this facies, of low porosity and very low permeability values. (Ø = 5% and k ~ 1.5 µD).

7.3.6.1.2 Shoal depositional environment

The oolitic shoal environment has been sampled 104 times. Porosity measurements indicate a mean around 10 % with a standard deviation of 5.3 %. Permeability measurements indicate a 51.3 md mean with a standard deviation of 80.55 mD. Maximum measured value correspond to 1.8 D. These 104 Ø/k couples do not follow the published correlations by Catinat et al. (2023) which are from a similar depositional environment in the central Paris Basin. Furthermore, it does not follow analyses presented in PilotSTRATEGY deliverable 2.3. This is mostly explained by the sampled interval which is more affected by diagenetic cement which partly blocked porosity.

7.3.6.1.3 Lagoonal depositional environment

The lagoon environment has been sampled 55 times. Porosity measurements indicate a mean around 6% with a standard deviation of 2.8%. Permeability values indicate a very low permeability with 4.7mD has a mean with a standard deviation calculated at 6.8 mD. Maximum measured value correspond to 66 mD. The 55 couples display similar Ø/k relationship than those of shoal depositional environments.

Cross-plot comparison and Ø/k laws obtained and compared to data from the literature indicate that results obtained in this study are not comparable. This might be explained by the high number of rock-types within a single depositional environment (Figure 7-21). To improve these Ø/k law, we propose to work at the rock-type scale.

The PilotSTRATEGY project has received funding from the European Union's Horizon 2020 research and innovation programme under grant agreement No. 101022664

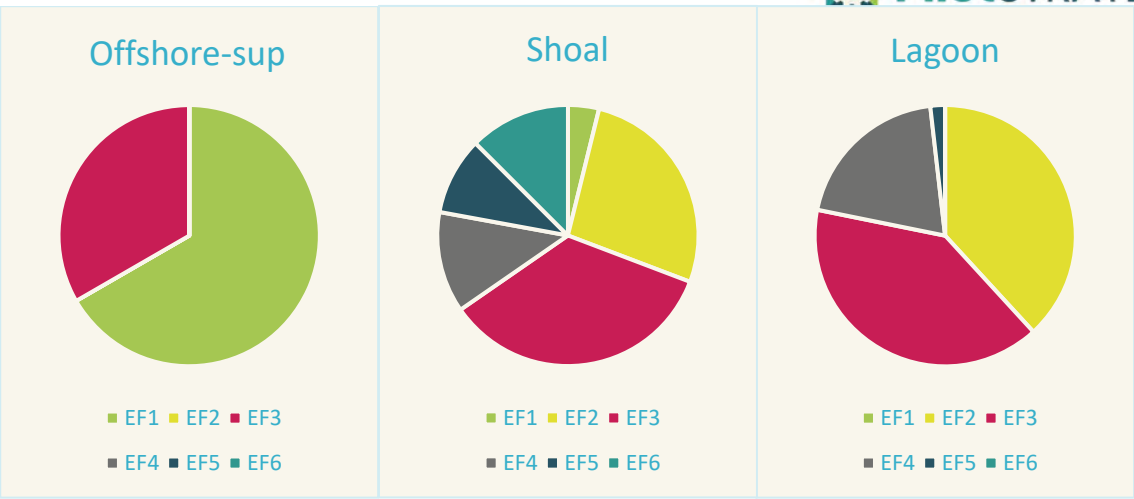

Figure 7-21: Rock-types for the different environmental deposits

7.3.6.2 Reservoir properties by calibrated rock-type

Six different Rock-Types (RT) have been identified (Figure 7-22). A database of 371 porosity and permeability measurements were plotted according to each RT.

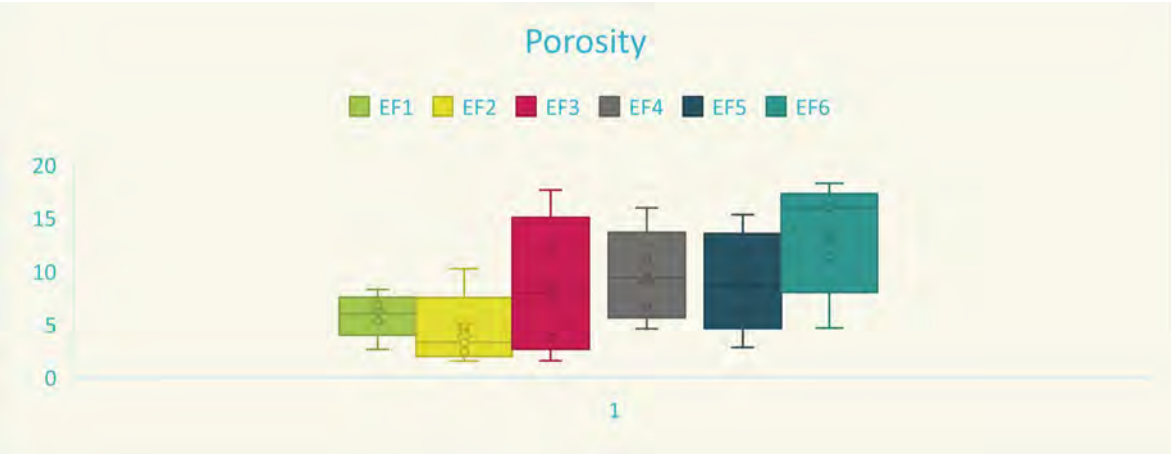

Figure 7-22: Calibrated rock-type with porosity data

7.3.6.2.1 Rock-type EF1 and EF2

Respectively identified 24 and 162 times, Rock-Types EF1 and EF2 correspond to marly / argillaceous limestone facies, generally associated to offshore and lower shoreface environments. These RT can be found marginally within shoal and lagoon environments. They are non-porous facies. Median porosity correspond to 5.9 % for EF1 and 4.2 for EF2. The median permeability measured correspond to 1.2 mD for EF1 and 15.4 mD for EF2. A porosity-permeability relationship is proposed for each RT.

7.3.6.2.2 Rock-type EF3

Rock type EF3 is characterised by 122 plug measurements. This RT is associated with cemented facies to facies displaying good porosity. Median porosity is 4.2 % with a standard deviation of 4.4 %. The average porosity measured is 15 mD with a standard deviation of 66 mD. A porosity-permeability relationship is proposed:

$$k = 1125.3 \times \theta^{2.2861}$$

The PilotSTRATEGY project has received funding from the European Union's Horizon 2020 research and innovation programme under grant agreement No. 101022664

7.3.6.2.3 Rock-type EF4

Rock type EF4 is identified 28 times in the database. This rock is associated with slightly tight facies compare to EF5 and EF6. Typically, these RT represents very fine-grained grainstone observed in the Iverny-1D core. It has a good porosity with an average of 9.6%. The average permeability measured is 24 mD with a 34mD standard deviation. The equation below represent porosity-permeability relationship obtained for the rock-type EF4:

$$k = 4524.1 \times \theta^{3.0227}$$

7.3.6.2.4 Rock-types EF5 and EF6

Rock types EF5 and EF6 represent the best reservoir properties. They are oolitic / oo-bioclastic grainstones with good macroporosity, and dissolution vugs. These rock types are represented by 15 measures for EF5 and 19 measures for EF6. The average measured porosity is 9.2% and 13% with a standard deviation at 3.4 and 3.7 respectively. The average permeability measured is 256 and 40 mD respectively. The equations presented below represent porosity-permeability relationships:

$$EF5: \quad k = 545565 \times \theta^{4.4662}$$

$$EF6: \quad k = 1628.7 \times \theta^{2.3747}$$

The equation for the porosity-permeability relationship for rock-type EF5 follows the equation proposed in PilotSTRATEGY deliverable 2.6. This is mostly due to the sampling strategy, which was focussed on reservoir facies in cores. Unfortunately, the EF6 facies was not sampled.

7.3.6.3 Seal Facies properties

The general architecture, framework and distribution of the seal has already been presented in previous sections of this report. The seal is a thick succession of Callovian to Oxfordian marly deposits. As presented before, the two units are generally isopach and their thickness range respectively between 100 to 130 meter and 246 to 297 meters.

Unfortunately, poor information exists on the seal facies. First, cores were rarely acquired on it since Oil & Gas exploration targeted the underlying reservoir. Consequently, we cannot measure an accurate data for seal properties. In PilotSTRATEGY deliverable D2.6 samples were only analysed from the transition between the reservoir and the overlying seal.

The pore size distributions measured by mercury injection indicate that the samples are essentially composed of micro-porosity (pore entry size < 2 µm); they have a low porosity and low to very law permeability (up to 7 nD). The measured entry pressure values are relatively small (1 bar) when the permeability is of the order of 1 µD and much larger (44 bars) when the permeability is very small (10 nD).

The PilotSTRATEGY project has received funding from the European Union's Horizon 2020 research and innovation programme under grant agreement No. 101022664

8. Depositional Environments and Geological Conceptual Model

8.1 Depositional Environments and Geological Conceptual Model (Portugal)

This Early Cretaceous interval corresponds to deposition of shallow marine to fluvial sandstones in the Northern Lusitanian Basin (TVG), followed by an erosional event just before lithospheric breakup (paleoenvironmental maps that describe the evolution of this sedimentation phase are provided in the annex).

As crustal stretching progressed throughout the Early Cretaceous, a basinward migration of the rift locus was recorded (Murillas et al., 1990; Alves et al., 2009), mostly due to continental crust thinning and rupture in the Upper Barremian, followed by exhumation and thinning of the upper mantle until the Aptian-Albian boundary (Pinheiro et al., 1996). This later rift stage ultimately led to the lithospheric breakup and the onset of seafloor spreading between the WIM and the Canadian Grand Banks since the Late Aptian (Pinheiro et al., 1996; Dinis et al., 2008).

Some of the wells located on top of interpreted salt diapirs record a fair amount of the TVG interval. This can indicate that some diapirs should not have been present at the timing of deposition, and probably have been developed later, during the Miocene inversion phase.

Thickness variations of the TVG (from well data and 2D and 3D seismic reflection) data give valuable insights into sedimentary thickness variations and the impact of diapirism in sedimentary pathways definition and eventual bypassing (Figure 8-2). This sketch of the depositional environment also accounts for the total reservoir thickness found in each well, leading to the schematic drawing of the most likely sedimentary routes and bypass, as well as suggesting the presence of sub-basins locally created due to salt withdrawal. Despite presenting notable thickness, petrophysical interpretation in the wells show substantial claystone intercalations, probably reflecting the proximity to open marine sedimentation, and do not display the best reservoir facies in the area.

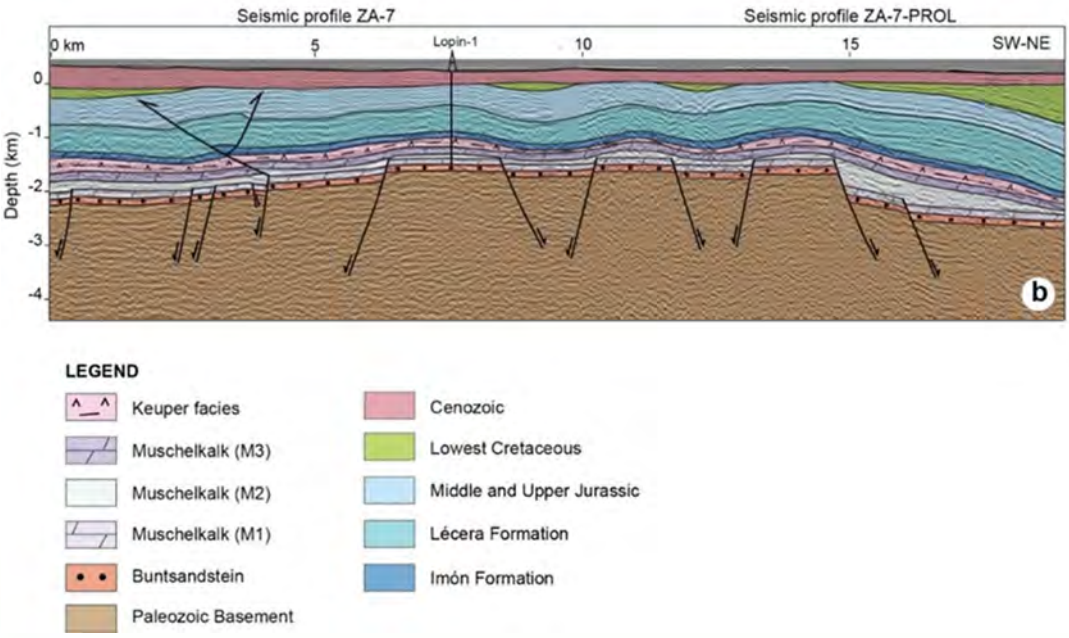

The PilotSTRATEGY project has received funding from the European Union's Horizon 2020 research and innovation programme under grant agreement No. 101022664

Figure 8-1: Geological and structural interpretation on top of depth-converted seismic profiles with no vertical exaggeration: ZA-07 and ZA-7-PROL (ZA-07-VB in the Figure 7-6*). Includes the projection of Lopín-1 borehole. Modified from Ayala et al. (2022).*

In the southwest portion of the study area, two wells (Fa-1, 16A-1) show particularly thick intervals (441 to 498 meters), in a basin-ward area where no salt diapirs are interpreted. This map also allows to show the relationship between salt diapirism, timing of emplacement, and sedimentation during the Early Cretaceous. Despite generally observing 300 to 500 meters of gross-thickness, it is also possible to observe the absence of the Torres Vedras unit in the Espadarte wells (14A-1, 14A-2), and negligible in MRW-5 (drilled onshore). This can be interpreted as the result of salt ascent and erosion during the Miocene tectonic inversion phase, which acted locally, as indicated by strong thickness variations (sometimes hundreds of meters) in wells located close by.

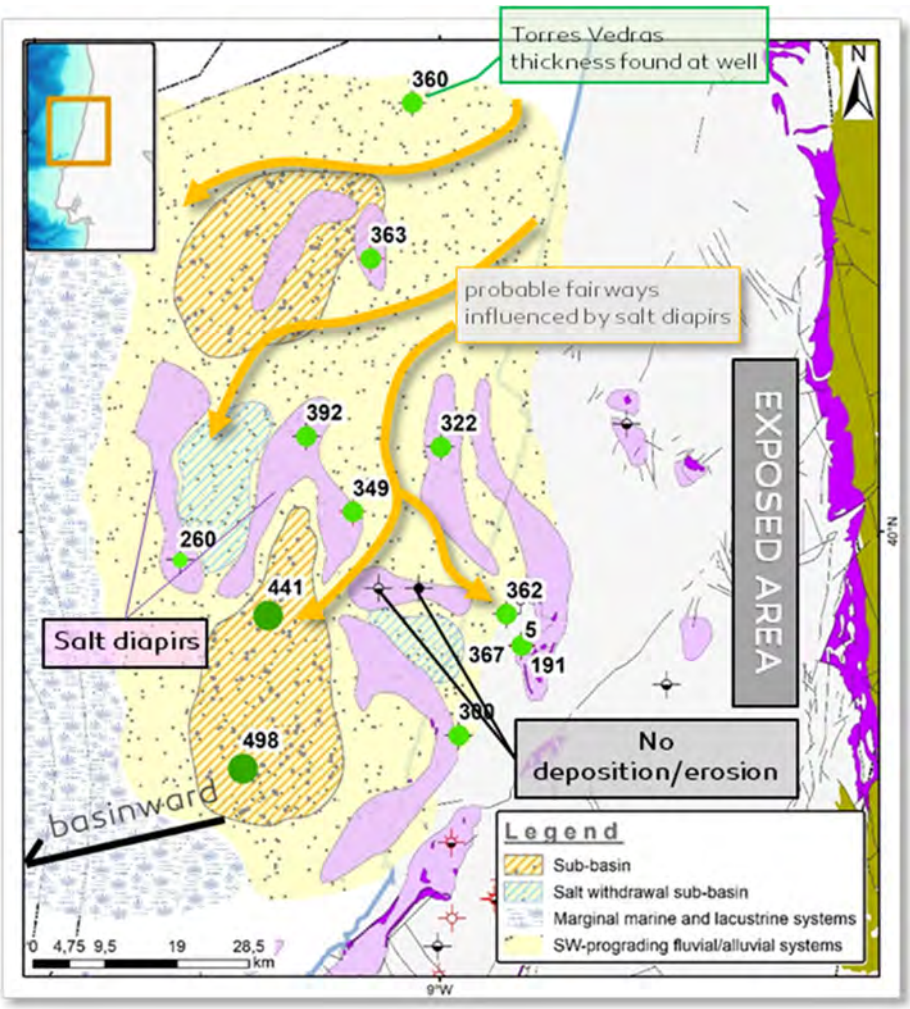

Figure 8-2: Paleoenvironmental sketch map at the Albian age (modified from Alves et al., 2002; Rey et al., 2006) that includes the interpreted sub-basins and salt diapirs in the study area, as well as the main sedimentary flow directions. Map also illustrates the indication of total thickness of Torres Vedras Group reservoir found in each well.

The PilotSTRATEGY project has received funding from the European Union's Horizon 2020 research and innovation programme under grant agreement No. 101022664

As a conclusion, the conceptual geological model of the target storage complex selected for modelling purposes in WP3 is composed by:

- Overburden – the main units that composed the overburden are 1) the Espadarte Formation, which is composed by dolomites and an alternation of clay and fine-coarse sandstones, deposited in a fluvial/lacustrine marine environment; and 2) **the Aveiro Group**, which is a **potential secondary seal** composed by alternating sands and claystones;
- Primary seal – the Upper Cretaceous **Cacém Formation**, (Figure 8-3b) a thick sealing layer conformably sitting combines in the topmost part limestone and dolomite, and marls and clays at the base;
- Main reservoir – the Lower Cretaceous section (Figure 8-3a), designated as **Torres Vedras Group**, mainly composed sandstones deposited in a fluvial environment with interbedded sealing clays. The sedimentary fairways are mildly influenced by salt tectonics, and based on the seismic interpretation, reservoir depth at the Q4-TV1 prospect is estimated to be at ~860m (P50 in **Erreur ! Source du renvoi introuvable.**).

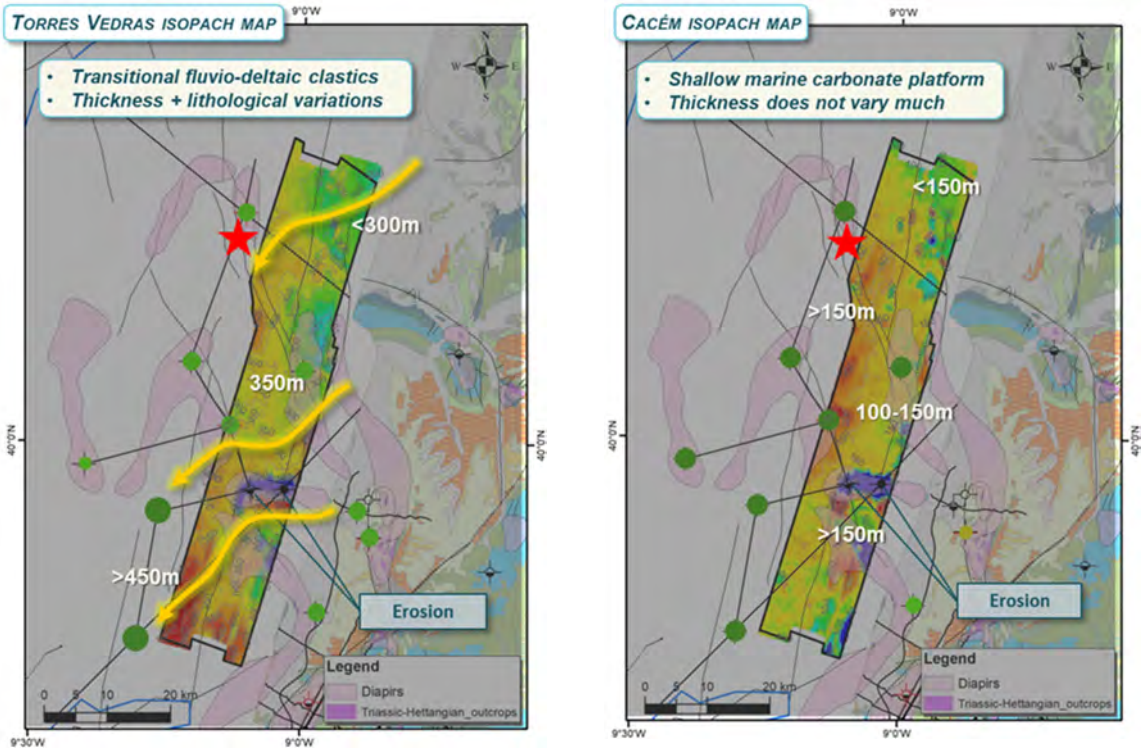

(a) (b)

Figure 8-3: (a) Simplified sedimentary fairways for the Torres Vedras Group; (b) Cacém Formation consists of a carbonate platform with no significant thickness difference. Prospect Q4-TV1 location is identified with a red star.

The PilotSTRATEGY project has received funding from the European Union's Horizon 2020 research and innovation programme under grant agreement No. 101022664

8.2 Depositional environments and geological conceptual model (Spain)

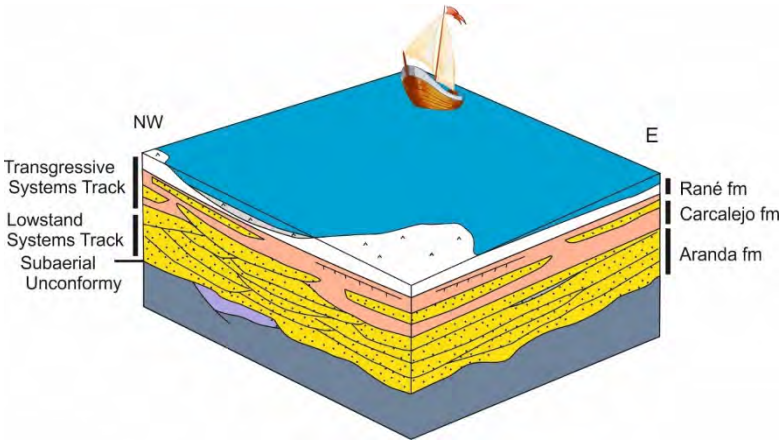

Figure 8-4 Representative stacking model of Buntsandstein facies. It shows the progressive transgressive from the east to west.

The Bundsandstein facies are composed of, from bottom to top: Aranda Formation or Unit B1, which corresponds with fluvial braided systems; Carcalejo Formation or Unit B2 which represents isolated fluvial systems with flood plain; and Rané Formation which represents the transition to sabkha lake facies (Figure 8-4).

Unit B1 is formed by the following facies associations:
Channel fill deposits: ≈1.5-m thick, fine to medium grained, typically scour-based and fine-upwards. They have an extension of several hundred meters to several kilometres. There are mainly two main subunits of channel facies: the base and the top. The top subunit has a much larger grain size, with the appearance of muscovite and the polycrystalline quartz gradually vanishing, likely due to a change in the sands source. It is frequent the presence of crevasse splay deposits.

Sheetflood deposits: ≈10m thick, low angle and planar laminated, fine-grained, presence of current-ripples, dewatering structures, rare burrows and root traces. It is the most common environment in field outcrops, but in the Chiprana-1 wellbore they pass laterally to shallow lacustrine green marls.

Aeolian Deposits: <2m intervals, well-sorted, fine-grained sandstones, grading laterally and vertically to sheetflood deposits.

Lacustrine deposits: heterolithic, abundant wave-ripples, mud-cracks, and locally root traces.

Unit B2 is formed by the following facies associations:
Channel fill deposits: ≈2 – 5 m thick, with cross stratification, fine to coarse grained, some intraclasts, typically scour-based and fining-upwards. They have a lateral extent of several hundred meters.
Floodplain deposits: <10m thick siltstones and very fine to fine grained sandstones: planar, ripple and wave-ripple laminations, root traces. Carbonate paleosols may be developed.

The Rané Formation or seal is composed of:
Lacustrine coastal deposits: heterolithic, abundant wave-ripples, root traces, mud-cracks and evaporites. In analogue fields it is composed of dolomite and carbonate with tepee structure.

The PilotSTRATEGY project has received funding from the European Union's Horizon 2020 research and innovation programme under grant agreement No. 101022664

8.3 Depositional environments and conceptual geological model (France)

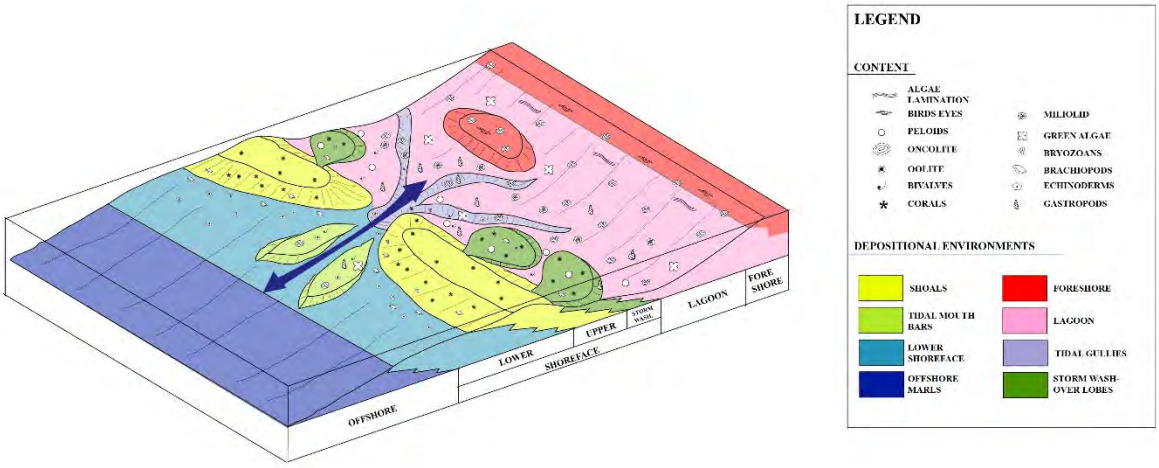

Figure 8-5: *Conceptual depositional model for the Dogger carbonate ramp*

This conceptual geological model for the depositional of the Dogger units (Figure 8-5) is a typical carbonate ramp profile with the development of shallow oolite-dominated barrier in the mid-ramp position. This latter separates an open-marine domain dominated by fair-weather and storm waves (respectively lower shoreface and offshore) from a restricted lagoon. The distal depositional section (blue colours in *Figure 8-5*) includes sediments ranging from marly mudstone to wackstone attesting to depositional process dominated by fair-weather settling (offshore marls) and storms (mudstone-wackstone with bioclast alignment). The fauna is typical of open-marine conditions with corals, bryozoans, brachiopods and crinoids.

The mid-ramp shoreface environment (yellow colour in Figure 8-5) corresponds to oolites and bioclast shoals organized in grainstone-packstones. They display mega-ripples and fauna association with brachiopods, corals, bryozoans, and crinoids. When storm currents are strong-enough, part of these shoals is reworked landward as storm wash-over deposits (green colour in *Figure 8-5*). These have fan-like geometries with a fauna dominated by open-marine species and a minor proportion of more restricted fauna and biogenic elements (pellets, green algae and oncolites) with grainstone to packstone textures).

The inner-ramp is lagoon-type deposits (pink colour in *Figure 8-5*characterized by muddy textures (wackstone-mudstone) rich in green algae, miliolids (foraminitera), gastropods and oncolites. Very locally, oncolites-rich grainstone to rudstone attests to shoal to foreshore depositional environments (red colour in *Figure 8-5*). Some grainy facies (grainstone to packstone) display both inner-ramp and outer-marine fauna (miliolids and oncolites as opposed to crinoids and bryozoans) which are likely to be tide-dominated facies interpreted as mouth-bars in shoreface position and gullies in the lagoon.

The PilotSTRATEGY project has received funding from the European Union's Horizon 2020 research and innovation programme under grant agreement No. 101022664

4. References

Ábalos, B., Carreras, J., Druguet, E., Escuder, J., Gómez-Pugnaire, M.T., Lorenzo Álvare, S., Quesada, C., Rodríguez-Fernández, R. and Gil-Ibarguchi J. I. 2002. Variscan and Pre-Variscan tectonics. In: Gibbons W, Moreno T (eds) The Geology of Spain. Geological Society, London, Special Publications, 155-183, http://doi.org/10.1144/GOSPP.9

Alves, T., Cunha, T.A., 2018 – A phase of transient subsidence, sediment bypass and deposition of regressive–transgressive cycles during the breakup of Iberia and Newfoundland. Earth and Planetary Science Letters, 484, p. 168–183

Alves, T., Gawthorpe, R.L., Hunt, D.H., & Monteiro, J.H., 2003 – Cenozoic tectono-sedimentary evolution of the western Iberian margin, Mar. Geol., 195, p. 75–108

Alves, T., Gawthorpe, R.L., Hunt, D.W., & Monteiro, J.H., 2002 – Jurassic tectono-sedimentary evolution of the Northern Lusitanian Basin (offshore Portugal). Marine and Petroleum Geology, 19, p. 727-754

Alves, T., Moita, C., Cunha, T., Ullnaess, M., Myklebust, R., Monteiro, J.H., and Manuppella, G., 2009 – Diachronous evolution of Late Jurassic-Cretaceous continental rifting in the northeast Atlantic (west Iberian margin). Tectonics, 28, TC4003, doi:10.1029/2008TC002337

Andrieu, S, 2016, Lien entre diagenèse des discontinuités, faciès sédimentaire et stratigraphie séquentielle: exemple de la plateforme carbonatée de l'ouest de la France (Aalénien-Oxfordien). Université Paris Saclay.

Andrieu, S, Brigaud, B., Barbarand, J., Lasseur, E. and Saucède, T., 2016, Disentangling the control of tectonics, eustasy, trophic conditions and climate on shallow-marine carbonate production during the Aalenian–Oxfordian interval: From the western France platform to the western Tethyan domain. Sedimentary Geology 345, 54 84. https://doi.org/10.1016/j.sedgeo.2016.09.005.

Angrand, P., Mouthereau, F., Masini, E., Asti, R. 2020. A reconstruction of Iberia accounting for Western Tethys–North Atlantic kinematics since the late-Permian–Triassic. *Solid Earth*, *11*(4), 1313-1332.

Arche, A., Gómez, J. L., Marzo, M., & Vargas, H., 2004. The siliciclastic Permian-Triassic deposits in Central and northeastern Iberian Peninsula (Iberian, Ebro and Catalan basins): a proposal for correlation. Geologica Acta, 305-305.

Archie, G.E. 1942. The Electrical Resistivity as an Aid in Determining Some Reservoir Characteristics. J. Pel. Tech. (Jan) 5, No. I.

Arenillas, A., Mediato, J. F., García Crespo, J., Nita, R., Molinero, R., Gª Lobón, J.L., Heredia, N, Marín, C., López, F.L., Pueyo, E.L., Martínez-Orio, R., et al. 2014. Atlas de estructuras del subsuelo susceptibles de almacenamiento geológico de CO2 en España. ISBN: 978-84-7840-935-8; 211 pp.

Arlegui, L. and Simón, J.L. 2001. Geometry and distribution of regional joint sets in a non-homogeneous stress field: case study in the Ebro basin (Spain). J. Struct. Geol. 23, 297–313.

The PilotSTRATEGY project has received funding from the European Union's Horizon 2020 research and innovation programme under grant agreement No. 101022664

Arribas, J., 1984. Sedimentología y diagénesis del Buntsandstein y Muschelkalk de la Rama Aragonesa de la Cordillera Ibérica (provincias de Soria Zaragoza). Tesis Doctoral. Universidad Complutense de Madrid. 354 pp.

Arribas, J., 1985. Base litoestratigráfica de las facies Buntsandstein y Muschelkalk en la Rama Aragonesa de la Cordillera Ibérica (Zona Norte). Estudios Geológicos 41, 47-57

Aurell, M., Bádenas, B., Casas, A., & Alberto, S., 2001. La Geología del Parque Cultural del Río Martín. Asociación Parque Cultural del río Martín.

Ayala, C., Torné, M. and Pous, J., 2003, The lithosphere-asthenosphere boundary in the western Mediterranean from 3D joint gravity and geoid modelling: tectonic implications. Earth and Planetary Science Letters, 209, 3-4, pp 275-290

Ayala, C., Rubio, F. M. and Rey-Moral, C. 2011. Caracterización microgravimétrica de la estructura geológica seleccionada para Planta de Desarrollo Tecnológico de Almacenamiento Geológico de CO2 en Hontomín (Burgos). [Confidential]. Fondo documental del IGME, Código 64091. 44 pp.

Ayala, C., Benjumea, B., Mediato, J. F., García-Crespo, J., Clariana, P., Soto, R., Rubio, F., Rey-Moral, C., Pueyo, E. L., Martín-León, J., García, A. G., Fernández-Canteli, P., Martínez-Orio, R. 2022. DeveLopíng a new innovative methodology to integrate geophysical techniques into characterization of potential CO 2 storage sites: Lopín structure (southern Ebro Basin, Spain). *Geological Society, London, Special Publications*, 528 (1). https://doi.org/10.1144/SP528-2022-70

Azerêdo, A.C., Duarte, L.V., Henriques, M.H., & Manuppella, G., 2003 – Da dinâmica continental no Triásico aos mares do Jurássico Inferior e Médio. Cadern. Geol. Portugal, Instituto Geológico e Mineiro, Lisboa, 43 p.

Baptiste, J, 2016, Cartographie structurale et lithologique du substratum du Bassin parisien et sa place dans la chaîne varisque de l'Europe de l'Ouest: approches combinées géophysiques, pétrophysiques, géochronologiques et modélisations 2D.

Baranov, V., & Naudy, H., 1964 – Numerical calculation of the formula of reduction to the magnetic pole. Geophysics, 29(1), 67-79.

Benjumea, B., Garcia-Crespo, J., Mediato, J.F., Rey-Moral, C., Ayala, C., Rubio, F., Soto, R., Clariana, P., Pueyo, E.L., Fernández-Canteli, P., 2022 - Passive Seismic Methods as Support for the Interpretation of Legacy Seismic Profiles: CO_2 Storage, 83rd EAGE Annual Conference & Exhibition; 2022 https://doi.org/10.3997/2214-4609.202210533

Benjumea, B., Macau, A., Gabàs, A., Bellmunt, F., Figueras, S. and Cirés, J. 2011. Integrated geophysical profiles and H/V microtremor measurements for subsoil characterization. Near Surface Geophysics, 9 (5), 413-425, DOI: https://doi.org/10.3997/1873-0604.2011021

Bonnefoy-Claudet, S., Cotton, F., & Bard, P. Y. 2006. The nature of noise wavefield and its applications for site effects studies: A literature review. Earth-Science Reviews, 79(3-4), 205-227.

Brigaud, B., Durlet, C., Deconinck, J.F., Vincent, B., Puceat, E., Thierry, J. and Trouiller, A., 2009, Facies and climate/environmental changes recorded on a carbonate ramp: a sedimentological and geochemical approach on Middle Jurassic carbonates (Paris Basin, France). Sediment Geology 222, 181–206.

The PilotSTRATEGY project has received funding from the European Union's Horizon 2020 research and innovation programme under grant agreement No. 101022664

Brocher, T. M. 2005. Empirical relations between elastic wavespeeds and density in the Earth's crust. *Bulletin of the seismological Society of America*, 95 (6), 2081-2092, DOI:10.1785/0120050077

Brosse, E., Badinier, G., Blanchard, F., Caspard, E., Collin. P.Y. et al., 2010, Selection and characterization of geological sites able to host a pilot-scale CO2 storage in the Paris Basin (PICOREF). Oil Gas Sci Technol 65, 375–403.

Butillé, M., Ferrer, O., Granado, P., Roca, E., Muñoz, J.A., Ballesteros, J.C., Gimenez, A., Vallejo, R.A., González, P., 2012. Evidencias de deformaciones salinas en las sucesiones mesozoicas del sector sur de la Cuenca del Ebro, 13. Geotemas, p. 176.

Casacão, J., Silva, F., Rocha, J., Almeida, J. and Santos, M., 2023 – Aspects of salt diapirism and structural evolution of Mesozoic–Cenozoic basins at the West Iberian margin. *AAPG Bulletin*, Volume 107(1), pp. 49–85. https://doi.org/10.1306/08072221100

Casas-Sainz, A.M. and Faccenna, C. 2001. Tertiary compressional deformation of the Iberian plate. Terra Nova 13, 281–288.

Colomer i Guilera, V., Navarro-Juli, J.J., Hernández-Samaniego, A., Ramírez-Merino, J.I. 1994. Mapa Geológico de España E. 1:50.000, Hoja 412 (Pina de Ebro), 2ª Serie MAGNA. Instituto Geológico y Minero de España, Madrid.

Cortés, A.L. and Casas, A.M. 1996. Deformación Alpina del zócalo y cobertera en el borde norte de la Cubeta de Azuara (Cordillera Ibérica). Revista de la Sociedad Geológica de España, 9 (1-2), 55-66.

Cortés, A.L. and Casas, A.M. 1999. Estructura y cinemática de los pliegues y cabalgamientos de Belchite-Sierra de Arcos (Cordillera Ibérica). Cuadernos de Geología Ibérica, número 25, 213-227.

Cortés, A.L.; Liesa, C.L., Soria, A.R., Meléndez, A. 1999. Role of extensional structures in the location of folds and thrusts during tectonic inversion (Northern Iberian Chain). Geodinámica Acta, 12(2) 113-132.

Cuevas-Martínez, J.L. 2022. La Formación Caspe: análisis sedimentológico y estratigráfico de los depósitos fluviales del Oligoceno – Mioceno inferior del SE de la Cuenca del Ebro. Tesis doctoral, Universitat de Barcelona, 273pp.

Davison, I. & Barreto, P., 2020 – Deformation and sedimentation processes, and hydrocarbon accumulations on upturned salt diapir flanks in the Lusitanian Basin, Portugal. Petroleum Geoscience, 27, p. 138

Delmas, J., Brosse, E., and Houel, P., 2010, Petrophysical properties of the middle Jurassic carbonates in the PICOREF sector (South Champagne, Paris Basin, France). Oil & Gas Science and Technology – Revue de l'Institut Français du Pétrole 65, 405-34.

Delmas, J., Houel, P., and Vially, R., 2002, Paris Basin, Petroleum Potential. IFP Regional Report, 2002.

Díez, J. B., Bourquin, S., Broutin, J., & Ferrer, J., 2007. The Iberian Permian Triassic 'Buntsandstein' of the Aragonian Branch of the Iberian Range (Spain) in the West-European sequence stratigraphical framework: a combined palynological and sedimentological approach. Bulletin de la Société Géologique de France, 178(3), 179-195.

The PilotSTRATEGY project has received funding from the European Union's Horizon 2020 research and innovation programme under grant agreement No. 101022664

Dinis, J.L., Rey, J., Cunha, P.P., Callapez, P., and Pena dos Reis, R., 2008 – Stratigraphy and allogenic controls of the western Portugal Cretaceous: an updated synthesis. Cretaceous Research, v. 29 (5-6), p. 772-780

Durlet, C., and Thierry, J., 2000, Modalites sequentielles de la transgression aalenobajocienne sur le sud est du Bassin parisien. Bull Soc Geol France 171, 327–339.

Gabàs, A., Macau, A., Benjumea, B., Queralt, P., Ledo, J., Figueras, S. and Marcuello, A. 2016. Joint audio-magnetotelluric and passive seismic imaging of the Cerdanya Basin. Surveys in Geophysics, 37 (5), 897-921. DOI:10.1007/s10712-016-9372-4

García Lobón, J.L., Reguera, M.I., Martín León, J., Rey Moral, C. and Berrezueta, E.R. 2010. Plan de selección y caracterización de áreas y estructuras favorables para el almacenamiento geológico de CO2 en España: Resumen ejecutivo. IGME, 76 pp.

García-Quintana, A., 1977. Jurásico terminal y Cretácico inferior en la región central de la provincia de Valencia y noreste de la provincia de Albacete. *Seminario de Estratigrafía*. Serie Monográficas, 1, 1-334.

Gaumet, F., 1997, Fondements géologiques pour la modélisation stratigraphique des systèmes carbonatés: le jurassique moyen de l'Angleterre à la Méditerranée.

Gaumet, F., Garcia, J.P., Dromart, G. and Sambet, G., 1996, Stratigraphic control upon depositional facies, geometries and profiles across the Bathonian-Callovian carbonate platform in Burgundy. Bull Soc Geol France 167, 409–421.

Gaumet, F., Garcia, J.P., Dromart, G. and Allemand, P., 2001, Middle Jurassic production rates and "patchy" architectures of the carbonate systems along the north-western Tethyan margin (Paris Basin to Sub-alpine Basin). Geol Mediterr XXVIII 1–2, 79–83.

Girard, A. J., & Shragge, J. 2020. Automated processing strategies for ambient seismic data. Geophysical Prospecting, 68, 293-312.Romero, P., & Schimmel, M. [2018]. Mapping the basement of the Ebro Basin in Spain with seismic ambient noise autocorrelations. Journal of Geophysical Research: Solid Earth, 123, 5052–5067.

Gomez, J.J., Goy, A. and Barron, E. 2007. Events around the Triassic-Jurassic boundary in northern and eastern Spain. A review. *Palaeogeography, Palaeoclimatology, Palaeoecology*, 244, 89-110, DOI:10.1016/j.palaeo.2006.06.025

González, A. 1989. Análisis Tectosedimentario Del Terciario Del Borde SE de La Depresión Del Ebro (Sector Bajoaragonés) y Cubetas Ibéricas Marginales. Tesis doctoral, Universidad de Zaragoza, 507 pp.

Greenberg, M. L. and Castagna, J. P. 1992. Shear-wave velocity estimation in porous rocks: theoretical formulation, preliminary verification and applications1. *Geophysical prospecting*, 40 (2), 195-209, DOI/10.1111/j.1365-2478. 1992.tb00371.x

Guillocheau, F., Robin, C., Allemand, P., Bourquin, S., Brault, N., Dromart, G., Friedenberg, R., et al., 2000, Meso-Cenozoic geodynamic evolution of the Paris Basin: 3D stratigraphic constraints ». Geodinamica Acta 13, 189 245. https://doi.org/10.1080/09853111.2000.11105372

Guimerà, J. 2018. Structure of an intraplate fold-and-thrust belt- The Iberian Chain. A synthesis. Geologica Acta, 16, 427–438, doi: 10.1344/GeologicaActa2018.16.4.6.

The PilotSTRATEGY project has received funding from the European Union's Horizon 2020 research and innovation programme under grant agreement No. 101022664

Guimerá, J. and Álvaro, M., 1990. Structure et évolution de la compression alpine dans la Chaîne Ibérique et la Chaîne Côtière Catalane (Espagne). Bull. Soc. Géol. Fr. 8 (VI), 339–348.

Gunn, P. J., Fitzgerald, D., Yassi, N., & Dart, P., 1997 – New algorithms for visually enhancing airborne geophysical data. Exploration Geophysics, 28(2), 220-224.

Hernández-Samaniego, A. and Ramírez-Merino, J.I. 1993. Mapa Geológico de España E. 1:50.000, Hoja 441 (Hijar), 2ª Serie MAGNA. Instituto Geológico y Minero de España, Madrid.

Horner, D. R., 1951. Pressure build-up in wells, Proc. Third World Petroleum Congress, 34, 316, The Hague.

Iaffa, D. N., Sàbat, F., Bello, D., Ferrer, O., Mon, R., Gutierrez, A. A. 2011. Tectonic inversion in a segmented foreland basin from extensional to piggy back settings: The Tucumán basin in NW Argentina. Journal of South American Earth Sciences, 31(4), 457-474.

Ibs-von Seht, M. and Wohlenberg, J. 1999. Microtremor measurements used to map thickness of soft sediments. Bulletin of the Seismological Society of America 89 (1), 250–259, https://doi.org/10.1785/BSSA0890010250

Isles, D. J., & Rankin, L. R., 2013 – Geological interpretation of aeromagnetic data. Society of Exploration Geophysicists and Australian Society of Exploration Geophysicists.

ITGE, 1990. Documentos sobre la Geología del subsuelo de España. Tomo VI: Ebro-Pirineos. ITGE, Madrid.

Izquierdo-Llavall, E.; Ayala, C.; Rodríguez Pintó, A.; Pueyo, E.L.; Oliva-Urcia, B.; Casas, A.M.; Rubio, F.M.; García Crespo, J.; Llorente Delgado, J.M.; González Durán, A.; Suárez, I.; Rey Moral, C.; Mediato Arribas, J.F.; Pérez Ortiz, I. 2015. Informe de la investigación del reservorio potencial de CO2 "Zona de Enlace" (Cordilleras Ibérica y Costero Catalanas), 229 pp. Instituto para la Reestructuración de las Comarcas Mineras (Ministerio de Industria).

Izquierdo-Llavall, E., Ayala, C., Pueyo, E.L., Casas, A.M., Oliva-Urcia, B., Rubio, F., Rodríguez-Pintó, A., Rey-Moral., C., Mediato, J.F. and García-Crespo, J. 2019. Basement-cover relationships and their along-strikechanges in the Linking Zone (Iberian Range, Spain): a combined structural and gravimetric study. Tectonics, 38, 2934-2960, DOI: 10.1029/2018TC005422

Jurado, M.J., 1990. El Triásico y Liásico basal evaporíticos del subsuelo de la cuenca del Ebro. In: Ortí, F., Salvany, J.M. (Eds.), Formaciones evaporíticas de la Cuenca del Ebro y cadenas periféricas y de la zona de Levante. Enresa, pp. 21–28.

King, M. T., Welford, J. K., Tugend, J. 2023. The role of the Ebro Block on the deformation experienced within the Pyrenean realm: Insights from deformable plate tectonic models. *Journal of Geodynamics*, *155*, 101962.

Klimowitz, J., 1992. Estratigrafía y disposición estructural del Terciario Inferior en el subsuelo del Sector Central de la Cuenca del Ebro. Acta Geol. Hisp. 27 (1–2), 117–125.

Konno, K. & Ohmachi, T., 1998. Ground-motion characteristics estimated from spectral ratio between horizontal and vertical components of microtremor, Bull. seism. Soc. Am., 88, 228–241.

The PilotSTRATEGY project has received funding from the European Union's Horizon 2020 research and innovation programme under grant agreement No. 101022664

Kullberg, J. C., Rocha, R. B., Soares, A. F., Rey, J., Terrinha, P., Azerêdo, A.C., Callapez, P., Duarte, L. V., Kullberg, M. C., Martins, L., Miranda, R., Alves, C., Mata, J., Madeira, J., Mateus, O., Moreira, M. & Nogueira, C. R., 2013 – A Bacia Lusitaniana: Estratigrafia, Paleogeografia e Tectónica. In: Dias, R., Araújo, A., Terrinha, P. & Kullberg, J. C. (eds.) Geologia de Portugal. Lisboa: Escolar Editora, 2, p. 317-368

Lanaja, J. M., 1987. Contribución de la exploración petrolífera al conocimiento de la Geología de España. Instituto Geológico y Minero de España Ed., 465 pp., 17 mapas.

Leinfelder, R. R. & Wilson, R. C. L., 1998 – Third-order sequences in an Upper Jurassic rift-related second-order sequence, central Lusitanian Basin, Portugal. P. C. Graciansky, J. Hardenbol, T. Jacquin, P. R. Vail, SEPM Special Publication, 60, p. 507-525

Letouzey, J., Werner, P., Marty, A. 1990. Fault reactivation and structural inversion. Backarc and intraplate compressive deformations. Example of the eastern Sunda shelf (Indonesia). Tectonophysics, 183(1-4), 341-362.

Li, X., 2006 – Understanding 3D analytic signal amplitude. Geophysics, 71(2), L13-L16.

López-Gómez, J., Alonso-Azcárate, J., Arche, A., Arribas, J., Fernández Barrenechea, J., Borruel-Abadía, V. (…) Ángela Suárez-Rodríguez, A., Tubía, J.M., Ubide, T., Valero Garcés, B., Vargas, H. and César Viseras, C. 2019. Permian-Triassic Rifting Stage. The Geology of Iberia: A Geodynamic Approach, C. Quesada and J. T. Oliveira (eds.), Regional Geology Reviews, 29-112 https://doi.org/10.1007/978-3-030-11295-0_3

Lumley, D., Shragge, J., Issa, N, Kamei, R., Potter, T., Miyoshi, T., Pevzner, R., Bona, A., Tertyshnikov, K., Langhi, L., Sarout, J., 2014 – Feasibility and design of robust passive seismic monitoring arrays for CO_2 geosequestration, ANLEC Project 7-0212-0203

Mas, P., Calcagno, P., Caritg-Monnot, S., Beccaletto, L., Capar, L., and Hamm, V., A 3D geomodel of the deep aquifers in the Orléans area of the southern Paris Basin (France). Scientific Data 9, 781. https://doi.org/10.1038/s41597-022-01876-4.

Maxwell. S.C, Fabriol, H., 2004 – Passive Seismic Imaging of CO_2 Sequestration at Weyburn, SEG Int'l Exposition and 74th Annual Meeting

Mediato, J. F., García-crespo, J., Izquierdo, E., García-lobón, J. L., Ayala, C., Pueyo, E. L. & Molinero, R. 2017. Three-dimensional reconstruction of the Caspe geological structure (Spain) for evaluation as a potential CO 2 storage site. Energy Procedia, 00, 14–18.

Miranda, R., Valadares, V., Terrinha, P., Mata, J., Azevedo, M. D. R., Gaspar, M., Kullberg, J. C. & Ribeiro, C., 2009 – Age Constrains on the Late Cretaceous Alkaline Magmatism on the West Iberian Margin. Cretaceous Research, 30, p. 575-586

Mitchum, R. M., Vail, P. R. and Sangree, J. B., 1977a, Seismic stratigraphy and global changes of sea-level — Part 6: Stratigraphic interpretation of seismic reflection patterns in depositional sequences, in Payton C. E., ed., Seismic stratigraphy — Applications to hydrocarbon exploration: AAPG Memoir 26, 117–133.

Mitchum R. M. Vail P. R. Thompson S., 1977b, Seismic stratigraphy and global changes of sea-level — Part 2: The depositional sequence as a basic unit for stratigraphic analysis, in Payton C. E., ed., Seismic stratigraphy — Applications to hydrocarbon exploration: AAPG Memoir 26, 53–62.

Murillas, J., Mougenot, D., Boulot, G., Comas, M.C., Banda, E., and Mauffret, A., 1990 – Structure and evolution of the Galicia Interior Basin (Atlantic western Iberian continental margin). Tectonophysics, 184, p. 297-319

Nakamura, Y., 2000. Clear identification of fundamental idea of Nakamura's technique and its applications, Proceedings of the 12th World Conference on Earthquake Engineering, Auckland, New Zealand.

Oliveira, J.T., Pereira, E., Ramalho, M., Antunes, M.T., Monteiro, J.H. (coords.), 1992 – Carta Geológica de Portugal, escala 1:500 000, Lisboa, Serviços Geológicos de Portugal

Oliveira, K. M. L., de Castro, D. L., Branco, R. M. G. C., de Oliveira, D. C., Alvite, E. N., Jucá, C. C., & Branco, J. L. C. (2018). Architectural framework of the NW border of the onshore Potiguar Basin (NE Brazil): An aeromagnetic and gravity based approach. Journal of South American Earth Sciences, 88, 700-714.

Ortí, F., Pérez-López, A. and Salvany, J. A. 2017. Triassic evaporitic of Iberia: Sedimentological and palaeogeographical implications for the western Neotethys evolution during the Middle Triassic-Earliest Jurassic. *Palaeogeography, Palaeoclimatology, Palaeoecology*, 471, 157–180, https://doi.org/10.1016/j.palaeo.2017.01.025

Palain, C., 1976 – Une série détritique terrígene, les "Grés de Silves": Trias et Lias inférieur du Portugal. Mem. Serv. Geol. Portugal. N.S., Lisboa, 25, 377 p.

Pardo, A., Arenas, C., González, A., Luzón, A., Muñoz, A., Pérez, A., Perez-Rivarés, F.J., Vázquez-Urbez, M. y Villena, J. 2004: La Cuenca del Ebro. En: Geología de España. (J.A. Vera ed.). SGE-IGME, Madrid, 533-542

Pena dos Reis, R., 2000 – Morfologias de talude instável em contexto de rifting. Exemplo do Jurássico superior da Bacia Lusitânica. Ciências da Terra (UNL), 5, p. 65–68

Pereira, P., Ribeiro, C., Carneiro, J., 2022 – Identification and characterization of geological formations with CO2 storage potential in Portugal, Petroleum Geoscience

Pereira, R., Rosas, F., Mata, J., Represas, P., Escada, C., and Silva, B., 2020 – Interplay of tectonics and magmatism during post-rift inversion on the central West Iberian Margin (Estremadura Spur). Basin Research, vol. 33-2, p. 1497-1519

Pinheiro, L.M., Wilson, R.C.L., Reis, R.P., Whitmarsh, R.B. & Ribeiro, A., 1996 – The western Iberian margin: A geophysical and geological overview. Proceedings of the Ocean Drilling Program Scientific Results, 149, p. 3-23

Pueyo, E. L., Izquierdo-Llavall, E., Rodríguez-Pintó, A., Rey-Moral, C., Oliva-Urcia, B., Casas, A. M., ... & Rubio, F. M. 2016. Petrophysical properties in the Iberian Range and surrounding areas (NE Spain): 1-density. *Journal of Maps*, *12*(5), 836-844

Purser, B.H., 1972, Subdivision et interpretation des sequences carbonatees. Mem BRGM 77, 679–698.

The PilotSTRATEGY project has received funding from the European Union's Horizon 2020 research and innovation programme under grant agreement No. 101022664

Purser, B.H., 1975, Sedimentation et diagenese precoce des series carbonatees du Jurassique moyen de Bourgogne. Unpublished PhD Thesis, Orsay, p 450.

Purser, B.H., 1978, Early diagenesis and the preservation of porosity in Jurassic limestones. J Petrol Geol 1, 83–94.

Purser, B.H., 1989, Plates-formes carbonatees exemple du Jurassique moyen du Bassin de Paris, Dynamique et methodes d'etude des bassins sedimentaires. Technip 145–164.

Quirantes, J., 1978. Estudio sedimentológico y estratigráfico del Terciario Continental de los Monegros. Publicación 681. Institución Fernando el católico (CSIC), Diputación de Zaragoza, 207 p.

Ramírez-Merino, J.I. 1991. Mapa Geológico de España E. 1:50.000, Hoja 413 (Gelsa), 2ª Serie MAGNA. Instituto Geológico y Minero de España, Madrid.

Rasmussen, E. S., Lomholt, S., Andersen, C. & Vejbæk, O. V., 1998 – Aspects of the structural evolution of the Lusitanian Basin in Portugal and the shelf and slope area offshore Portugal. Tectonophysics, Elsevier 300, p. 199-225

Raymer, L.L., Hunt, E.R., and Gardner J.S., 1980. An Improved Sonic Transit Time-To-Porosity Transform. Paper presented at the SPWLA 21st Annual Logging Symposium, Lafayette, Louisiana, July 1980

Reid, A. B., Allsop, J. M., Granser, H., Millett, A. T., & Somerton, I. W., 1990 – Magnetic interpretation in three dimensions using Euler deconvolution. Geophysics, 55(1), 80-91.

Reid, A. B., Ebbing, J., & Webb, S. J., 2014 – Avoidable Euler Errors–the use and abuse of Euler deconvolution applied to potential fields. Geophysical Prospecting, 62(5), 1162-1168.

Rey, J., Dinis, L., Callapez, P., and Cunha, P.P., 2006 – Da rotura continental à margem passiva, Composição e evolução do Cretácico de Portugal. Cadernos de Geologia de Portugal, Inst. Geol. e Mineiro – INETI, 75 p.

Ribeiro, A., Kullberg, M. C., Kullberg, J. C., Manuppella, G., & Philipps, S., 1990 – A review of Alpine tectonics in Portugal: Foreland detachment in basement and cover rocks. Tectonophysics, 184, p. 357-366

Roest, W. R., Verhoef, J., & Pilkington, M., 1992 – Magnetic interpretation using the 3-D analytic signal. Geophysics, 57(1), 116-125.

Romero, P. and Schimmel, M. 2018. Mapping the basement of the Ebro Basin in Spain with seismic ambient noise autocorrelations. Journal of Geophysical Research: Solid Earth, 123, 5052–5067.

Rueda Fort, M., 2022. Caracterización a partir de diagrafía del posible almacén de CO2 de Lopín. Trabajo Fin de Master, Universidad Complutense de Madrid, 57 pp

Ruiz, V. and Lendínez, A. 1986. Mapa Geológico de España E. 1:50.000, Hoja 440 (Belchite), 2ª Serie MAGNA. Instituto Geológico y Minero de España, Madrid.

Salas, R., Guimera, J., Mas, R., Martín-Closas, C., Meléndez, A., Alonso, A., 2001. Evolution of the Mesozoic Central Iberian Rift System and its cainozoic inversion (Iberian Chain). In: Ziegler, P.A., Cavazza, W., Robertson, A.H.F., Crasquin-Soleau, S. (Eds.), Peri-Thetys Memoir 6: Peri-Thetyan Rift/Wrench Basins and Passive Margins. Mem. Mus. Nac. Hist. Nat., vol. 186, pp. 145–185.

The PilotSTRATEGY project has received funding from the European Union's Horizon 2020 research and innovation programme under grant agreement No. 101022664

Schimmel M., 1999, Phase cross-correlations: design, comparisons and applications, Bull. Seismol. Soc. Am., 89, 1366-1378.

Schimmel, M., & Gallart, J. 2007. Frequency-dependent phase coherence for noise suppression in seismic array data. Journal of Geophysical Research, 112, B04303. https://doi.org/10.1029/2006JB004680.

Schlumberger, 2009, "Log interpretation Charts", Schlumberger, p279

Soares, A.F., Kullberg, J.F., Bordalo da Rocha, R. & Callapez, P.M., 2012 – Tectono-sedimentary model for the evolution of the Silves Group (Triassic, Lusitanian basin, Portugal). Bull. Soc. géol. France, t. 183, no 3, pp. 203-216.

Soares, D.M., Alves, T.M., and Terrinha, P., 2012 – The breakup sequence and associated lithospheric breakup surface: Their significance in the context of rifted continental margins (West Iberia and Newfoundland margins, North Atlantic). Earth and Planet. Sci. Lett., 355-356, p. 311-326.

Sopeña, A., López-Gómez, J., Arche, A., Pérez-Arlucea, M., Ramos, A., Virgili, C., Hernando, S., 1988. Permian and Triassic Rift basins of the Iberian Peninsula. In: Manspeizer, W. (Ed.), Triassic-Jurassic Rifting. Continental Breakup and the Origin of the Atlantic Ocean and Passive Margins. Elsevier, Amsterdam, pp. 757–786

Soto, R., Casas-Sainz, A. M., & Del Río, P. 2007. Geometry of half-grabens containing a mid-level viscous décollement. *Basin Research*, *19*(3), 437-450

Soto, R., Larrasoaña, J. C., Arlegui, L. E., Beamud, E., Oliva-Urcia, B., Simón, J. L. 2009. Reliability of magnetic fabric of weakly deformed mudrocks as a palaeostress indicator in compressive settings. *Journal of Structural Geology*, *31*(5), 512-522

Soto, R., Juan C. Larrasoaña, J.C., Beamud, E., Garcés, M. 2016. Early–Middle Miocene subtle compressional deformation in the Ebro foreland basin (northern Spain); insights from magnetic fabrics. C. R. Geoscience 348, 213–223

Soto, R., Casas-Sainz, A. M., Oliva-Urcia, B., García-Lasanta, C., Izquierdo-Llavall, E., Moussaid, B., et al. 2019. Triassic stretching directions in Iberia and North Africa inferred from magnetic fabrics. *Terra Nova*, *31*(5), 465-478

Stapel, G., Cloetingh, S., and Pronk, B., 1996 – Quantitative subsidence analysis of the Mesozoic evolution of the Lusitanian Basin (western Iberian margin). Tectonophysics, 266 (1–4), p. 493–507

Sutgerand, F., Lawrance, D., Legrand, P., Wraith, E., 2022 – Seismic monitoring for subsurface uncertainties at the Endurance CO_2 store, The Leading Edge, 41; https://doi.org/10.1190/tle41040253.1

Talwani, M., Worzel, J. L., & Landisman, M. 1959. Rapid gravity computations for two-dimensional bodies with application to the Mendocino submarine fracture zone. Journal of geophysical research, 64(1), 49-59.

Talwani, M., and Heirtzler, J. R., 1964, Computation of magnetic anomalies caused by two-dimensional bodies of arbitrary shape, in Parks, G. A., Ed., Computers in the mineral industries, Part 1: Stanford Univ. Publ., Geological Sciences, 9, 464-480.

The PilotSTRATEGY project has received funding from the European Union's Horizon 2020 research and innovation programme under grant agreement No. 101022664

Terrinha, P. et al., 2019a – The Alpine Orogeny in the West and Southwest Iberia Margins. In: Quesada, C., Oliveira, J. (eds) The Geology of Iberia: A Geodynamic Approach. Regional Geology Reviews. Springer, Cham. https://doi.org/10.1007/978-3-030-11295-0_11

Terrinha, P. *et al.*, 2019b – Rifting of the Southwest and West Iberia Continental Margins. In: Quesada, C., Oliveira, J. (eds) The Geology of Iberia: A Geodynamic Approach. Regional Geology Reviews. Springer, Cham. https://doi.org/10.1007/978-3-030-11295-0_6

Tugend, J., Manatschal, G., Kusznir, N. J., Masini, E., Mohn, G., Thinon, I., 2014, Formation and deformation of hyperextended rift systems: Insights from rift domain mapping in the Bay of Biscay-Pyrenees. *Tectonics*, *33*(7), 1239-1276

Vail P. R., Mitchum R. M., Thompson S., 1977a, Seismic stratigraphy and global changes of sea level — Part 3: Relative changes of sea level from coastal onlap, in Payton C. E., ed., Seismic stratigraphy — Applications to hydrocarbon exploration: AAPG Memoir 26, 63–81.

Vail P. R., Todd R. G., Sangree J. B., 1977b, Seismic stratigraphy and global changes of sea level — Part 5: Chronostratigraphic significance of seismic reflections, in Payton C. E., ed., Seismic stratigraphy — Applications to hydrocarbon exploration: AAPG Memoir 26, 99 –116.

Vera, J.A. 2004. Geología de España. Sociedad Geológica de España-Instituto Geológico y Minero de España, 884 p. Madrid.

Villa, E., Escuder, J. & Ginkel, A. C. 1996. Fusulináceos y edad de los afloramientos carboníferos de Puig Moreno (Cordillera Ibérica, Teruel, España). Spanish Journal of Palaeontology, 11, 207–215.

Villena, J., González, A., Muñoz, J. A., Pardo, G. & Pérez, A. 1992. Síntesis estratigráfica del Terciario del borde Sur de la Cuenca del Ebro: unidades genéticas. Acta geológica hispánica, 27, 225–245.

Wathelet, M., Chatelain, J.-L., Cornou, C., Di Giulio, G., Guillier, B., Ohrnberger, M. and Savvaidis, A. 2020. Geopsy: A User-Friendly Open-Source Tool Set for Ambient Vibration Processing. *Seismological Research Letters*, 91(3), 1878--1889, doi: 10.1785/0220190360.

Wilson, R. C. L., Hiscott, R. N., Willis, M. G., & Gradstein, F. M., 1989 – The Lusitanian basin of west-central Portugal: Mesozoic and Tertiary tectonic, stratigraphy, and subsidence history. In Extensional Tectonics and Stratigraphy of the North Atlantic Margins, edited by A. J. Tankard and H. R. Balkwill, AAPG Mem., 40, p. 341 – 361

Witt, W.G., 1977, Stratigraphy of the Lusitanian Basin: Shell Prospex Portuguesa (unpublished report), 61 p.

Won, I. J., and Bevis, M., 1987, Computing the gravitational and magnetic anomalies due to a polygon: Algorithms and Fortran subroutines, Geophysics, 52, 232-238.

Wyllie, M. R. J., Gregory, A. R., Gardner, G. H. F., 1958, An experimental investigation of factors affecting elastic wave velocities in porous media. Geophysics; 23, 459–493.

Zbyszewski, G., 1959 – Étude structurale de la vallée typhonique de Caldas da Rainha (Portugal). Mem. Serv. Geol. Portugal, 3, Lisboa, 184 p.

Zhao, C., Zheng, Y., Wang, Y., Zhao, L., 2022 – Seismic ambient noise auto-correlation imaging in a CO_2 storage area, Journal of Geophysics and Engineering, 19, 1134–1148

The PilotSTRATEGY project has received funding from the European Union's Horizon 2020 research and innovation programme under grant agreement No. 101022664

The PilotSTRATEGY project has received funding from the European Union's Horizon 2020 research and innovation programme under grant agreement No. 101022664